17th International Symposium on Advanced Technology (ISAT-17)

Engineering Innovation for Sustainable Future

November 13 – 15, 2018

Danang, Vietnam

Sponsored by
The University of Danang
University of Science and Technology

Co-Sponsored by
Kogakuin University, Japan
Southern Taiwan University of Science and Technology, Taiwan
University of the Philippines, Philippines

Welcome Message from the Rector of DUT

The University of Danang – University of Science and Technology (DUT) since its establishment in 1975, has always asserted its leading position in the system of higher education in Vietnam and in the region. DUT is not only the center of training highly-qualified human resources in science, technology, industrial management, but also the hub for scientific research and technology transfer of Central Vietnam, and of the whole country and region at large.

This year, our University is honored to host the 17th International Symposium on Advanced Technology (ISAT17) which is sponsored by The University of Danang – University of Science and Technology (DUT), Kogakuin University (KU), Southern Taiwan University of Science and Technology (STUST) and The University of the Philippines Los Baños (UPLB). I am extremely proud and happy to welcome you to the ISAT17. This symposium is held annually by the partnership universities to share the scientific research excellences and to foster the scientific cooperation between the member universities.

With the main theme of "Engineering Innovation for Sustainable Future" related to a various fields as: Bio-engineering and Biochemistry, Chemistry, ICT, IoT & Smart System, Energy, Advanced Materials, Civil Engineering, Robot, Education and Human Science, the ISAT17 will effectively contribute to the advancement of knowledge of Industry 4.0 and I firmly believe that this annual symposium is an important and valuable resource thanks to all of your helpful contributions. This is one of the most important events in DUT this year since this symposium will act as a motivation for lecturers, researchers, and scientists to publish their ideas and researchers in an international forum.

I would like to express my sincere thanks to the organizing committee members and my appreciation to the collaborative universities and wish you all an enjoyable stay in Danang city and a productive and fruitful symposium.

Sincerely Yours,

Doan Quang Vinh

Rector,

The University of Danang - University of Science and Technology

■ Organization

Symposium Chairperson	**Prof. Doan Quang Vinh** *Rector of DUT*
Co-Chairperson	**Prof. Mitsunobu Sato** *President of Kogakuin University*
	Prof. Deng-Maw Lu *President of Southern Taiwan University of Science and Technology*
	Prof. Fernando C. Sanchez, Jr. *Chancellor of University of Philipines Los Banos*
Vice-Chairperson	**Prof. Le Thi Kim Oanh** *Vice Rector of DUT*
	Prof. Ichiro Takano *Vice President of Kogakuin University*
	Prof. Min-Tsai Lai *Vice President of Southern Taiwan University of Science and Technology*

Advisory Board

Prof. Tran Van Nam	*Former President of The University of Danang*
Prof. Le Kim Hung	*UD - University of Science and Technology*
Prof. Vo Trung Hung	*The University of Danang*
Mr. Nguyen Quan Hoang	*General Director, Foster Electric Vietnam Group*

Organizing Committee

Chair:	**Prof. Le Thi Kim Oanh**	*UD - University of Science and Technology*
Member:	**Prof. Nguyen Huu Hieu**	*UD - University of Science and Technology*
	Dr. Phan Minh Duc	*UD - University of Science and Technology*
	Prof. Nguyen Dinh Lam	*UD - University of Science and Technology*

	Dr. Doan Anh Tuan	*UD - University of Science and Technology*
	Prof. Duong Viet Dung	*UD - University of Science and Technology*
	Dr. Pham Anh Duc	*UD - University of Science and Technology*
	Dr. Le Phuoc Cuong	*UD - University of Science and Technology*
	Mr. Hoang Quang Huy	*UD - University of Science and Technology*
	Dr. Yung-Peng Wang	*Southern Taiwan University of Science and Technology*
	Prof. Takashi Wantanabe	*Kogakuin University*
	Prof. Kazuyoshi Endo	*Kogakuin University*
	Prof. Yasutada Imamura	*Kogakuin University*

Program Committee

Chair:	**Prof. Nguyen Dinh Lam**	*UD - University of Science and Technology*
Member:	**Prof. Nguyen Thanh Binh**	*UD - University of Science and Technology*
	Dr. Nguyen Hong Ngoc	*UD - University of Science and Technology*
	Prof. Tran Quang Hung	*UD - University of Science and Technology*
	Dr. Le Anh Tuan	*UD - University of Science and Technology*
	Dr. Nguyen Hoang Mai	*UD - University of Science and Technology*
	Dr. Bui Minh Hien	*UD - University of Science and Technology*
	Dr. Pham Minh Tuan	*UD - University of Science and Technology*
	Prof. Toru Honda	*Kogakuin University*
	Prof.Shigehiro Hashimoto	*Kogakuin University*
	Prof. Yasushi Nozawa	*Kogakuin University*
	Prof. Noboru Sugamura	*Kogakuin University*

Secretariat

Chair:	**Dr. Pham Anh Duc**	*UD - University of Science and Technology*
Member:	**Mr. Nguyen N. H. Van**	*UD - University of Science and Technology*
	Ms. Hoang N. Dieu Trang	*UD - University of Science and Technology*
	Mr. Nguyen Thanh Cong	*UD - University of Science and Technology*
	Mr. Nguyen Hong Nguyen	*UD - University of Science and Technology*

■ Scope of the Symposium

Dear Colleagues,

The dates for the 17th International Symposium on Advanced Technology (ISAT-17) that organized by The University of Danang - University of Science and Technology have been set for November 13th-15th, 2018. The Internatiotal Advisory and Organizing Committees cordially invite you to attend the symposium and participate in its scientific and social programs. The theme of the ISAT-17 will be "*Engineering Innovation for Sustainable Future*".

Presentations will consist of three categories, several keynote lectures, oral presentations, and poster presentations. Prizes will be awarded for the best presentations, especially for students. The International Advisory and Organizing Committee hope all registrants will present a paper, but acceptance of papers will be at the discretion of the committee. The official language of the symposium will be English.

In the following pages, you will find details concerning the symposium. We are looking forward to meeting you in Danang, Vietnam!

■ Main Theme of ISAT-17

Topics of interest include but not limited to:

1. Biomedical Engineering and Biochemistry
2. Synthetic Organic Chemistry
3. Information and Communications Technology (ICT)
4. Internet of Things (IoT) and Smart System
5. Energy and Transportation
6. Advanced Functional Materials
7. Architecture and Civil Engineering
8. Intelligent Manufacture and Robot
9. Education and Human Science

■ Language

English will be the official language during the Conference.

■ Conference Venue

The Conference will be held at The University of Danang - University of Science and Technology, 54 Nguyen Luong Bang Street, Lien Chieu District, Danang City, Vietnam.

■ Conference Website

http://isat17.dut.udn.vn

■ Important Dates

❖ Important Deadlines

- Call for Papers: Now – Oct. 15th, 2018
- Deadline of Paper Abstract Submission: Oct. 15th, 2018
- Deadline of Registration: Oct. 30th, 2018
- Notification of Acceptance: Oct. 31st, 2018
- Full Paper Submission: October 30th, 2018

All papers must be submitted by email to isat17@dut.udn.vn

❖ ISAT Symposium: Nov. 13th-15th, 2018

November 13: Arrival; Welcoming participants

November 14: Keynote/Presentation/Poster session

November 15: Excursion

Program

■ General Program

Tuesday, November 13, 2018				
18:00	**Welcome Reception**			
Wednesday, November 14,2018				
08:00-08:30	**Registration**			
08:30-09:00	**Opening Ceremony** • Welcome speech by Prof. Doan Quang Vinh, Rector of DUT • Congratulatory Speech by the UD President • Speeches by representatives of co-organizers and sponsors			
09:00-09:40	**Keynote Speaker 1: Prof. Mitsunobu Sato** *(Kogakuin University)*		Chair: Prof. Hong-Ru Lin (STUST)	
09:40-10:20	**Keynote Speaker 2: Prof. Myra G. Borines** *(University of The Philippines Los Baños)*			
10:20-10:30	**Coffee Break**			
10:30-11:10	**Keynote Speaker3: Prof. Ming-Shyan Wang** *(Southern Taiwan University of Science and Technology)*		Chair: Prof. Le Kim Hung (DUT)	
11:10-11:50	**Keynote Speaker 4: Prof. Bui Thi Minh Tu** *(Danang University of Science and Technology)*			
12:00-13:00	**Lunch** (LRCC Building)			
13:00-14:40	**Mechanical Engineering**		**Chemical and Environmental Engineering**	
13:00-13:20	Prof. Kazuhiro Suga	Chair: Dr. Yung-Peng Wang	Prof. Tomohiro Yamaguchi	Chair: Prof. Nguyen Van Dung
13:20-13:40	Dr. Hoang Van Thanh		Prof. Hong-Ru Lin	
13:40-14:00	Dr. Vo Nhu Thanh		Prof. Shiro Seki	
14:00-14:20	Mr. Kazuya Takeda		Prof. Ting-Feng Wu	
14:20-14:40	Mr. Hiroaki Terakado		Dr. Dang Quang Hai	
14:40-15:00	**Break time**			
	Civil and Architecture		**Electrical and Electronic Engineering**	
15:00-15:20	Mr. Do Tich	Chair: Prof. Masaki Tamura	Prof. Chien-Min Chang	Chair: Prof. Le Kim Hung
15:20-15:40	Prof. Nguyen The Hung		Prof. Chao-Tang Yu	
15:40-16:00	Dr. Huynh Nhat To		Dr. Le Dinh Duong	
16:00-16:20	Prof. Nguyen The Hung		Mr. Ryosuke Nawa	
16:20-16:40	Ms. Erika Futami		Ms. Ayaka Fujima	
16:40-17:30	**Poster Presentations**			
17:30	**Closing Remarks**			
18:00	**Gala Dinner** (LRCC Building)			
Thursday, November 15, 2018				
08:00-12:00	**Field Trip** (Invite Only)			

No.	Title of Paper, Author and Affiliation	Presenter
Keynote Lecture		
1	**Water splitting by photovoltaic lithium-ion-battery fabricated with gel-type electrolyte -Toward the Hydrogen Society** Mitsunobu Sato	Prof. Mitsunobu Sato
2	**Opportunities and Prospects of Macroalgae-Based Biorefinery in the Philippines** Myra G. Borines	Prof. Myra G. Borines
3	**Sensorless Speed Control of Induction Motor Using Artificial Neural Network** Ming-Shyan Wang and Narongrit Pimkumwong	Prof. Ming-Shyan Wang
4	**A Solution for the Combination of Solar Power and Electricity for Normal Usage** Thi Minh Tu Bui, Van Thanh Vu	Prof. Thi Minh Tu Bui
Oral Presentation		
1	**Epitaxial Growth of Cu_3N Films on (0001) Al_2O_3 Substrates by Mist Chemical Vapor Deposition** T. Yamaguchi, H. Itoh, M. Takahashi, H. Nagai, T. Onuma, T. Honda and M. Sato	Tomohiro Yamaguchi
2	**Development of Supporting System for Safety and Efficient Orthodontic Treatment** Kazuhiro Suga	Kazuhiro Suga
3	**Smart Hydrogel for Biomedical Applications Through Injection** Hong-Ru Lin, Yan-Ting Chen, Yu-Chun Wu, Yiu-Jiuan Lin	Hong-Ru Lin
4	**Dynamics of a Droplet at Trap-Squeeze Transition in Contraction Microchannel** Van Thanh Hoang, Quang Bang Tao, Duc Binh Luu, Jang Min Park	Van Thanh Hoang
5	**Research and Development of Next-Generation Battery Systems: Lithium-Sulfur Batteries and All-Solid-State Batteries** Shiro Seki	Shiro Seki
6	**The Apoptotic Effects of Pomegranate Juice on Prostate Cancer DU145 Cells** Song-Tay Lee, Szu-Ting Chen, and Ting-Feng Wu	Ting-Feng Wu
7	**Adsorption and Rejection of HydrophoTobic Trace Organic Contaminants by Nanofiltration and Reverse Osmosis Membranes** Hai Quang Dang	Hai Quang Dang

8	**Combining Image Processing and Tactile Sensation Actuator for Improving Athletic Training in Squat Work Out** Vo Nhu Thanh	Vo Nhu Thanh
9	**A Novel Approach for Evaluating the Performance Efficiency of Power Plants** Nhat-To Huynh, Thi-Kim-Oanh Le	Nhat To Huynh
10	**Lead-Free Piezoceramics for Low Power Vibration Energy Harvesting Applications** Da-Huei Lee and Chien-Min Chang	Chien-Min Chang
11	**Waterproofing Underground Construction** Tich Do, Tin Do	Tich Do
12	**An Experiment Study on One-Dimensional Flow Under Influent of Vertical Velocity in the Bed** Phuc-Hau Huynh, The-Hung Nguyen, and Thi-Nam Nguyen	The-Hung Nguyen
13	**Flow Observation of Synthetic Jets Produced by Asymmetric Slot** Hiroaki Terakado, Ryota Kobayashi, Koichi Nishibe, and Kotaro Sato	Hiroaki Terakado
14	**A Dual Approach for Modeling Two-Dimensional Horizontal Flow** Tinh Ton That, The-Hung Nguyen, Dong-Anh Nguyen	The-Hung Nguyen
15	**Development of the Next-Generation Internet of Vehicles Communication System for Driving Safety (II)** Chao-Tang Yu, Liang-Bi Chen, Wei-Wen Hu, Wan-Jung Chang, Jing-Jou Tang, and Da-Huei Lee	Chao-Tang Yu
16	**A Wind Forecasting Approach for Power System Operations** Dinh Duong Le	Dinh Duong Le
17	**Fabrication of μ-LED Arrays Toward Future Realization of μ-LED Display** Ryosuke Nawa**,** Shouma Takeda, Yoshifumi Kamei, Takeyoshi Onuma, Tomohiro Yamaguchi, and Tohru Honda	Ryosuke Nawa
18	**Characteristics of Flow Generated by Annular Inlet Guide Vanes with Outlet Pipe** Kazuya Takeda, Kotaro Yamanaka, Kotaro Sato, Koichi Nishibe	Kazuya Takeda
19	**Toward Long Time Use of Stone-based Wall Panel in High-rise Building between Past and Future in Japan** Erika Futami, Masaki Tamura	Erika Futami
20	**Identifying Blur Car License Plate Numbers Using Machine Learning** Ayaka Fujima, Seiichi Gohshi	Ayaka Fujima

Poster Presentation

No	**Title of Paper** Author and Affiliation
1	**Inspection of Outer Wall Tiles in High-rise Building by Measuring Impact Response Value** Yuhei Oppata, Masaki Tamura
2	**Deterioration Evaluation of the Stucco Lath Ceilings in the Historic Building in Japan** Misako Hanza, Masaki Tamura, Kentaro Oka, and Osamu Goto
3	**Designing a Program to Forecast the Service Life of Mechanically Stabilized Earth Wall Used Steel Reinforcement** Truong-Linh Chau, Thu Ha Nguyen
4	**The Production of Peach-Flavored Yogurt Enriched in Isoflavones From Soymilk and Sweetened Condensed Milk** Thi Minh Hanh Truong, Thi Ngoc Thu Tran, Thi Dong Phuong Nguyen, Xuan Vung Bui, Thi Tuyet Anh Le
5	**Electrochemical Measurements for Rechargeable Batteries Single Positive Electrode Particle** Takahiro Saito, Tatsuya Nakamura, Shiro Seki
6	**Na Conductive Polymer/Inorganic Hybrid Electrolyte for High Performance-All-Solid-State Battery** Koji Hiraoka, Kato Masaki, Hidefumi Motobayashi, Hiroshi Kaneko, Yuzo Tasaki, Shiro Seki
7	**A Method Football Team Model Optimization and Application of the Optimization Control** Nguyen Hoang Mai
8	**Application of PGM Absorbent for Plating Wastewater Treatment** Le Thi Xuan Thuy, Nguyen Ngoc Huy, Le Thi Suong and Nguyen Thi Sao Mai
9	**Can Reaction-Transport Diagenetic Modelling Support Management Efforts? A Case Study in the Bay of Quinte (Lake Ontario), Canada** Phuong T.K. Doan
10	**Multi-Class Classification Model for Urban Land Cover** Trang Thi Phuong Pham
11	**Optimization of Mangiferin Extraction from Mango (Mangifera Indica L.) Leaves Using Ultrasound-Assisted Methodology** Truc Loan Nguyen, Trinh Pham
12	**A Study on Development of a Tangible Interface for an Introduction to Computer Programming Education Using QR Codes** Ryota Tominaga, and Hidetoshi Saito
13	**Analysis of Deep Ultraviolet Emission Properties in Rocksalt-structured MgxZn1-xO Films** Mizuki Ono, Kyohei Ishii, Kentaro Kaneko, Tomohiro Yamaguchi, Tohru Honda, Shizuo Fujita and Takeyoshi Onuma
14	**Growth and Characterization of Single Crystalline alpha-Ga2O3 Film on c-plane Sapphire Substrates by Mist CVD** Kenichiro Rikitake, Tomohiro Yamaguchi, Takeyoshi Onuma and Tohru Honda

15	**Geo-Chemical Environment Status in Suoi Ram Hamlet, Long Giao Commune, Cam My District, Dong Nai, Vietnam** Le Phuoc Cuong, Luong Van Tho, Tatjana Juzsakova and Ákos Rédey
16	**Aquaculture Water Quality Monitoring Based on Wireless Sensor Networks Using LoRA Technology** Quoc-Huy Le, Van-Tien Huynh, Thanh-Hieu Tran, Ngoc-Tan Huynh, Ngoc-Quoc Duong
17	**Development on Tire Performance Prediction Tool Based on Tire Mechanics** Shunya Hidano, Yukio Nakajima
18	**Performance Control by Guide Vanes for Axial-Flow Fan with a Blockage Disk** Sho Yamagiwa, Kotaro Sato, Koichi Nishibe, Donghyuk Kang
19	**Development of the Residual Ammonia Removal System for Installation on Vehicles** Ryutaro Hanazaki, Masahiro Inamoto, and Takashi Saika
20	**Development of a Hydrogen Generation System by Ammonia Decomposition** Masahiro Inamoto, Ryutaro Hanazaki, and Takashi Saika
21	**Study on the Effect of Road Roughness on Tire Wear** Kei Omura, Yukio Nakajima
22	**Aerodynamic Characteristics of Multicopter Hovering near a Boundary** Kazuki Konno, Kotoro Sato, Koichi Nishibe
23	**Behavior of Pulsating Jets near a Rigid Boundary** Daiki Yamaguchi, and Kotaro Sato
24	**Development of a Receptionist Robot: Mechanical and Control System Design** Danh Ngoc Nguyen, Hoang Trung Ngo, Ha Linh Le and Hoai Nam Le
25	**Characterization of Plain Journal Bearings Using an Original Test-Rig** Phuoc Vinh Dang, Thanh Nghi Ngo
26	**Prediction and Prevention of Pressure Ulcers in Patients Using Wheelchairs** He-Thong Bui, Quang-Bang Tao
27	**Construction of Disassemble Technology for Lithium Batteries Towards Material Investigation** Yusuke Ushioda, Yuki Ishino, and Shiro Seki
28	**Photoluminescence Measurements of GaInN Grown at Different Temperatures by RF-MBE** Ryosuke Yoshida, Yusuke Nakazima, Hiroki Hirukawa,Takeyoshi Onuma, Tomohiro Yamaguchi, and Tohru Honda
29	**Polyether/Li1.5Al0.5Ge1.5(PO4)3 Hybrid Electrolyte for High Performance All-solid-state Li Battery** Naamo Suzuki, Masaki Kato, Tatsuya Hayano, and Shiro Seki
30	**Proposal of Sulfolane Electrolyte with High Lithium Salt Composition for Realization of New Generation Batteries** Kohei Inaba, Keitaro Takahashi, Yuki Ishino, Yusuke Ushioda, Satoshi Katou, and Shiro Seki
31	**Study on Wavelength Matching for Optical Wireless Power Transmission for Visible Light** Hiroki Hirukawa, Tomohiro Yamaguchi, Takeyoshi Onuma, and Tohru Honda

32	**Accelerating Ipsec Communication Using Hardware & Software Co-Design Technique on the Xilinx Zynq-7000 ARM/FPGA Soc Platform** Viet-Thang Huynh, Hoang-Viet Ho*, and Nguyen-Hoang-Phuc Ly
33	**Implementing an Energy Efficient OpenFlow Switch on the Xilinx Virtex-6 FPGA ML605 Platform** Van-Cuong Nguyen*, Nguyen-Hoang-Phuc Ly *, and Hoang-Viet Ho
34	**Developing the Overturning Warning Systems for Motorcycles Travelling in Strong Wind Condition** Vu Anh Do, Trung Van Ngo, Hung Duy Vo *, Thuong Nhat Huynh Nguyen
35	**Research in Transmission of Sound in Human Body – Bone Conduction Devices** Vo Hoang Chuong, Pham Le Minh Hoang, Le Quang Dao and Ho Ba Trung
36	**Robotic Hand Controlled by Glove** Hoang-Khoi Dang, Minh-Vu Nguyen, Tuan-Anh Le, Duc-Huy Dang, Duc-Thinh Nguyen, Van-Lic Tran
37	**Design and Build a Self-study Space Management System for Smart Campus using Image Processing and LoRA Wireless Communication** Loc-Minh-Phuc Le, Van-Khoi Bui, Tan-Hien Van, Nguyen-Phu-Hien Pham, Thai-Hoang Nguyen*, Dinh-Thanh Ngo
38	**Self-Driving Car – Traffic Signs Recognition** Thi-Thanh-Hoa Tran, Duy-Hung Phan, Gia-Khang Tran, Quang-Huy Tran
39	**3D Printing Technology- A Model of Lattice Structure in CAD Environment** T.H. Tuan Tran, D. Kien Le, V. Than Le, D. Son Nguyen
40	**Development of Automatic Washing and Selecting Fruit System Applying Image Processing Technology** Vo Nhu Thanh, Pham Duy Thong
41	**Development of Restaurant Serving Robot Using Line Following Approach** Vo Nhu Thanh, Vuong Dinh Nhan
42	**Development of Vietnamese Banana Leaf Cake Maker Machine** Vo Nhu Thanh, Vo Minh Nhat

Keynote Lecture

Water splitting by photovoltaic lithium-ion-battery fabricated with gel-type electrolyte -Toward the Hydrogen Society-

Mitsunobu Sato[1), *]

[1)] Department of Applied Physics, School of Advanced Engineering, Kogakuin University, Tokyo, Japan
E-mail: lccsato@cc.kogakuin.ac.jp

Abstract

Hydrogen is garnering more and more attention as a clean energy source because of its water-only emissions when used as a fuel. In recent years, it has become even more prominent due to its use in residential fuel cells and fuel-cell vehicles. The use of hydrogen as an energy source is also being actively considered in policy matters. In 2014, the Japanese Ministry of Economy, Trade and Industry formulated a strategic road map for hydrogen and fuel cells, setting 2020 targets for the nationwide installation of 1.4 million residential fuel cells, 40,000 fuel-cell vehicles, and 160 hydrogen fuel stations. By 2040, the ministry aims for Japan to have established a completely CO_2-free hydrogen supply system. The shift in policy focus to a hydrogen society is not confined to Japan. Hydrogen initiatives are occurring worldwide, with the US and the EU establishing the Hydrogen Fuel Initiative and the Fuel Cell and Hydrogen Initiative, respectively [1].

We recently reported a photovoltaic lithium-ion-battery (PV-LIB), which can be charged by the solar-light irradiation. The PV-LIB uses two active materials, TiO_2 (Titania) and $LiCoO_2$ (LCO) thin films, on conductive transparent glass electrode for the anode and cathode respectively, and an organic electrolytic solution involving Li ion [2, 3]. However, the use of flammable organic liquid induces several problems based on the risk of liquid leakage *etc*. In order to assemble the device, which has large capacity, long cycle-life, low self-discharge, and high operating voltage, we fabricated the PV-LIB using a gel-type electrolyte.

The pastes of each active material were prepared by mixing carbon powders, polyvinylidene difluoride, and N-methylpyrrolidone and stirring for 48 h at ambient temperature. The titania paste (2.0 g) was placed on the FTO pre-coated glass substrate (40 × 66 mm^2) with titania thin film and coated on a 36 × 53 mm^2 area of the film by a doctor-blade with 0.6 mm space. The LCO (1.5 g) paste was dropped on another FTO pre-coated glass substrate (40 × 66 mm^2) and coated on a 36 × 53 mm^2 area of the film by a doctor-blade with 0.4 mm space. The gel-type electrolyte was prepared by mixing the poly(pyridinium-1,4-diyliminocarbonyl-1,4-phenylene-methylene hexafluorophosphate) with $LiPF_6$. The electrodes with the active materials, titania and LCO, were assembled into a sealed sandwich-type device. A charge/discharge test applying a current of 10 mA of the assemble device was performed with a DC voltage source/monitor. Averaged potentials of 2.6 and 1.5 V were observed by charging for 10 min and discharging for ca. 9 min, respectively. It was thus clarified that the device works as an LIB. In addition, during the irradiation of 1-sun light from a solar simulator to the device for 10 min, the averaged voltage of 1.1 V was observed. After the charging operation, it took ca. 10 min to be discharged with 0.1 mA. These voltage changes were measured with a DC voltage monitor. Therefore, it was indicated that the device can be charged by light irradiation. The charged and discharged devices were connected to platinized titanium electrodes immersed in a 30 % NaOH aqueous solution. In both cases, hydrogen and oxygen gases generated on each electrode linked to the anode and cathode respectively of the device, occurred with no electric power supply, during irradiation with light from the anode side of the device. Thus, it was revealed that the assembled device has triple functions as a metal-oxide solar cell which can generate electricity by light irradiation and an electric storage device which can be charged by both electric power supply and light irradiation.

References:

[1] Katsuya Honda, VALUENEX Japan Inc. 1-7 (2016).
[2] Hiroki Nagai, Mitsunobu Sato, InTech 111-124 (2016).
[3] Hirki Nagai, Tatsuya Suzuki, YoshihisaTakahashi, Mitsunobu Sato, Funct. Mater. Lett., 9, 1650046 (2016).

OPPORTUNITIES AND PROSPECTS OF MACROALGAE-BASED BIOREFINERY IN THE PHILIPPINES

Myra G. Borines[1]
[1]*Associate Professor, Chemical Engineering Department*
College of Engineering and Agro-industrial Technology
University of the Philippines Los Baños

Abstract - Marine algae or macroalgae have enormous potential to fully and partly displace terrestrial biomass and produce sustainable bioenergy and biomaterials. This paper aims to present the biorefinery concept and its application to macroalgae systems that will integrate the biofuel and biomaterial production. Possible products, both biofuels and biomaterials that can be derived from macroalgae, are presented. Macroalgae-based biorefinery scenarios are presented which include agar and bioethanol and coproduction of alginate and bioethanol. The most promising macroalgae species for biorefinery feedstock in the Philippines were also identified. Key factors and challenges that should be addressed during the biofuel and biomaterials production are presented that can help in the development of an efficient macroalgae-based biorefinery process in the future. The environmental and economic benefits of macroalgae-based biorefinery provide significant opportunities for the Philippines to develop a low-carbon economy. Although some of the technologies behind commercialization of the macroalgal-based biorefineries are still in its infancy, several studies demonstrated the feasibility of the concept.

Keywords: *biorefinery; macroalgae; biofuel; Sargassum ; ethanol*

Sensorless Speed Control of Induction Motor Using Artificial Neural Network

Ming-Shyan Wang[1), *] and Narongrit Pimkumwong [2)]

[1)]Department of Electrical Engineering, Southern Taiwan University of Science and Technology, Tainan, Taiwan
E-mail: mswang@stust.edu.tw
[2)]Department of Electrical Engineering, Southern Taiwan University of Science and Technology, Tainan, Taiwan
E-mail: p.narongrit@gmail.com

Abstract

Electric motors are the single biggest consumer of electricity in modern society. The consumption of Industrial and domestic electric motors per year occupies 46.2% of the global electrical demand. Induction motor (IM) is widely used in industrial applications because it provides many advantages, such as low cost, simple structure, high reliability, high efficiency, robustness, and low maintenance. Field-oriented control (FOC) and direct torque control (DTC) are the two most popular high performance control methods of linearization and decoupling for IM drives. These two control algorithms can decouple control between torque and flux and offer good dynamic and steady-state torque responses. DTC is more attractive than FOC in simplicity, less parameter sensitivity, quick torque response, and effortless implementation complexity.

This paper presents the sensorless speed control of an induction motor based on constant voltage per frequency (V/F) control technique, using artificial neural network (ANN) [1]. The magnitude of stator flux and torque errors are used to generate the stator voltage and phase angle references for controlling the induction motor by using constant voltage per frequency control method. The estimated stator current equation is derived and rearranged consistent with the control algorithm and ANN structure. For the speed control, a weight in ANN, which relates to the speed, is adjusted by using Widrow–Hoff learning rule to minimize the sum of squared errors between the measured stator current and the estimated stator current from ANN output, as shown in Fig. 1. The simulation and experimental results in high- and low-speed regions have confirmed the effectiveness of the proposed speed estimation method.

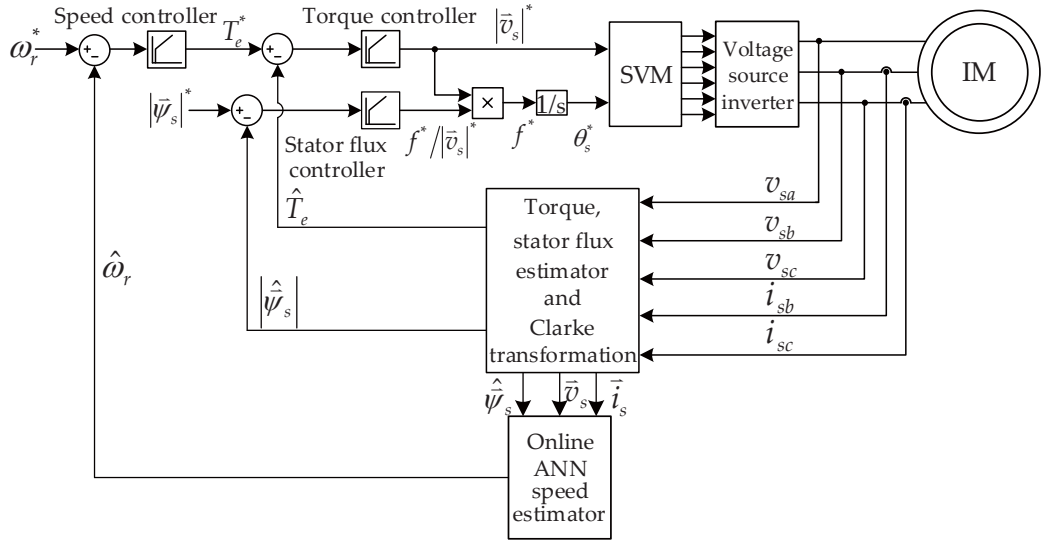

Fig. 1 The block diagram of the proposed sensorless speed control system.

References:

[1] Narongrit Pimkumwong and Ming-Shyan Wang, Online Speed Estimation Using Artificial Neural Network for Speed Sensorless Direct Torque Control of Induction Motor based on Constant V/F Control Technique, *Energies*, **11**, 2176 (2018).

A solution for the combination of solar power and electricity for normal usage

Thi Minh Tu Bui[1], Thanh Vu Van[2]

Faculty of Electronic and Telecommunication Engineering, The University of Danang, University of Science and Technology

E-mail: [1)]btmtu@dut.udn.vn

[2)]vvthanh@dut.udn.vn

Abstract

The world is moving far away from using renewable energy, especially solar power. Renewable energy technologies and government policies that encourage the use of these sources of energy to ensure sustainable development are key factors driving adoption of renewable energy. In the small-scale, renewable energy sources are often independent, meaning that energy sources are used in isolation [1, 2]. This leads to the difficulty for users when the each of the energy sources alone cannot meet the demand of the user.

This paper proposes a solution that can joint solar power with electricity. The proposed system measures the solar power supply and the power usage on real-time to determine if additional power is required and can fulfills that requirement by using power from electricity grid. In case of solar energy exceeds the requirement, the exceeded energy can be stored in separated energy storage system.

The proposed system is fully automatic and can provide reliable power for the normal usage. In addition, a monitoring system is used to keep track of the variation of solar power supply so that system modification be made if needed.

The center of this combination system is the designed control system, which receives measurement and decides to activate energy splitter or energy combinator so that no energy will be wasted and ensures the satisfaction of users. In our project, we use PIC18F4550 microcontroller to do all the processing.
Monitoring information will be sent to the server via 3G/GPRS system.

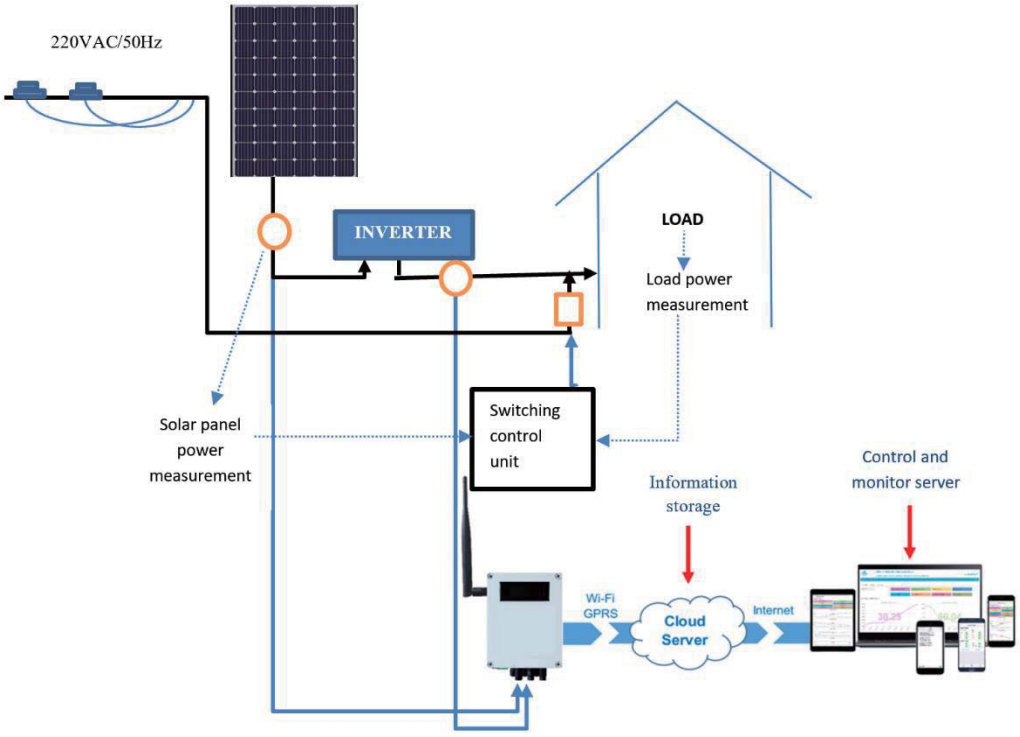

Fig. 1. Proposed solar-electricity system.

References:

[1] S. Upadhyay, M.P. Sharma, A review on configurations, control and sizing methodologies of hybrid energy systems, Renew. Sustain. Energy Rev. 38 (2014) 47-63.

[2] M. Rahman, M. Mahmodul, J.V. Paatero, Hybrid application of biogas and solar resources to fulfil household energy needs: a potentially viable option in rural areas of developing countries, Renew. Energy 68 (2014) 35-45.

Oral Presentation

Epitaxial Growth of Cu_3N Films on (0001)Al_2O_3 Substrates by Mist Chemical Vapor Deposition

T. Yamaguchi, H. Itoh, M. Takahashi, H. Nagai, T. Onuma, T. Honda and M. Sato

Department of Applied Physics, Kogakuin University, Tokyo, Japan
E-mail: t-yamaguchi@cc.kogakuin.ac.jp

Abstract

Anti-RO_3-type cubic-structured Cu_3N has been reported to be an indirect bandgap energy of approximately 1.3 eV, and its absorption coefficient reaches up to 10^5 cm^{-1} in an energy range higher than 2.2 eV.[1] In addition, bipolar doping is possible with maintaining reasonable carrier densities. The Cu_3N is thus one of candidates as a novel solar cell material.

Mist chemical vapor deposition (mist CVD) is a unique growth technique. After ingredient is dissolved in water, the solution is atomized using an ultrasonic transducer. These mist particles are transformed to a reactor using carrier gas. This unique growth method has so far entirely applied to grow oxide semiconductors.[2] Recently, we have successfully grown a nitride semiconductor of Cu_3N. In this paper, epitaxial growth of Cu_3N films on corundum-structured (0001)Al_2O_3 substrates by mist CVD is reported.

Copper(II) acetylacetonate, $Cu(C_5H_7O_2)_2$, was used as an ingredient. This ingredient was dissolved in 28% NH_3 *aq.* solution. (0001)Al_2O_3 was used as a substrate. Growth temperatures were varied between 250°C and 500°C.

Figure 1 shows X-ray diffraction (XRD) 2θ-θ patterns of all the samples. In the samples grown at 250°C and 300°C, the diffraction peaks of Al_2O_3(0006) and Cu_3N(002) were observed. This indicates that the films have an orientation relationship of [001]Cu_3N//[0001]Al_2O_3. In the samples grown at 350°C and 400°C, an additional diffraction peak of Cu_3N(111) was observed. In the sample grown at 500°C, the diffraction peaks of Cu_3N(002) and Cu_3N(111) almost disappeared and a clear diffraction peak of Cu(100) were observed instead. Thermal dissociation of Cu_3N induces an appearance of Cu diffraction peak at the highest growth temperature of 500°C. No clear diffraction peaks of CuO and Cu_2O were observed in all samples.

Figure 2 shows XRD ϕ-scan patterns of the sample grown at 300°C. Here, the reflection conditions of asymmetric Cu_3N {111} and Al_2O_3 {11-23} diffractions were used. As can be seen in Fig. 2, equivalent twelve Cu_3N {111} diffraction peaks were observed. In addition, the peaks from Cu_3N and those from Al_2O_3 were shifted by 45°. Figure 3 shows the schematic images of in-plane orientation relationship between Cu_3N and Al_2O_3, represented from the results of Fig. 2. In this sample, three different Cu_3N domains exist with in-plane rotation of 30° with respect to each other. These domains have an in-plane orientation relationship of [100]Cu_3N// [11-20]Al_2O_3.

Thus, these results show that Cu_3N was epitaxially grown on (0001)Al_2O_3.

References:

[1] K. Matsuzaki, T. Okazaki, Y.-S. Lee, H. Hosono, and T. Susaki, Appl. Phys. Lett. **105**, 222102 (2014).
[2] S. Fujita, K. Kaneko, and T. Hitora, Jpn. J. Appl. Phys. **55**, 12 (2016).

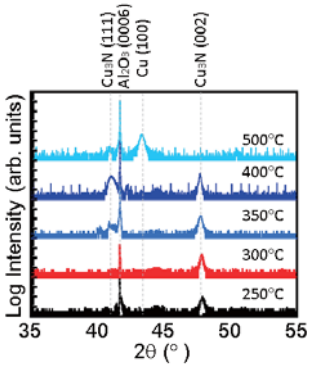

Fig. 1 XRD 2θ-θ patterns for the samples grown at 250-500°C.

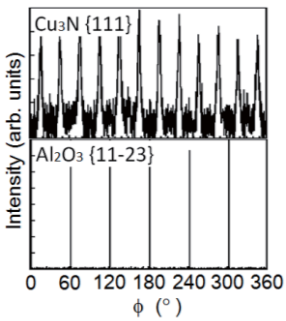

Fig. 2 XRD ϕ-scan patterns for the sample grown at 300°C.

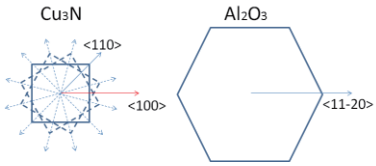

Fig. 3 Schematic image of in-plane orientation relationship between Cu_3N and Al_2O_3.

Development of Supporting System for Safety and Efficient Orthodontic Treatment

Kazuhiro SUGA[1)],

[1)]Department of Mechanical Engineering, Faculty of Engineering, Kogakuin University, Tokyo, Japan
Center for Bio Medical Engineering
E-mail: ksuga@cc.kogakuin.ac.jp

Abstract

It is an essential need for both patients and medical doctors to realize safe and effective treatments on orthodontics. Numerical prediction through computational mechanics has the potential to achieve it. However, a few trials have been carried out and there is no trial in clinical practice. We are developing a supporting system on orthodontics with the orthodontists in TMDU (Tokyo Medical and Dental University) in Japan. This report gives the goal of our support system and its current status in (1) a tooth-PDL modeling in order to predict the initial tooth movement for patient-specific clinical use, and (2) evaluation of orthodontic force and moment by a super elastic wire during tooth movement for designing treatment plan, (3) 3D model of tooth alignment from a dental CBCT through the deep learning.

A part of this research is supported by JSPS KAKENHI Grant Number JP 18K11339.

Smart Hydrogel for Biomedical Applications Through Injection

Hong-Ru Lin [*1)], Yan-Ting Chen[1)], Yu-Chun Wu[2)], Yiu-Jiuan Lin[3)]

[1)]Department of Chemical and Materials Engineering, Southern Taiwan University of Science and Technology, Tainan 710, Taiwan
[2)]National Laboratory Animal Center, National Applied Research Laboratories, Tainan 741, Taiwan
[3)]Department of Nursing, Chung Hwa University of Medical Technology, Tainan 717, Taiwan
E-mail: hrlin@stust.edu.tw

Abstract

Two topics will be presented in the conference. In order to avoid anti-cancer drugs undergoing a first-pass effect and reduce their toxicity, and to solve conventional suppositories defects, we developed an in-situ-gelling and injectable Pluronic–poly(acrylic acid) (Pluronic–PAA) liquid suppository, which could gel fast in the physiological state and had suitable gel strength and bioadhesive force. The liquid suppositories were inserted into the rectum of rabbits without difficulty and leakage, and retained in the rectum for at least 6 h and while releasing the drug. The toxicity and cytotoxic tests indicated that Pluronic and PAA were non-toxic materials and could inhibit colon cancer cells when oxaliplatin was incorporated. Cmax and AUC0→12 h values of oxaliplatin after rectal administration of an oxaliplatin suppository were higher than those for an oxaliplatin solution administered orally. These results suggest that an in-situ-gelling and injectable liquid suppository for humans can be further developed as a more convenient and effective rectal dosage form.

The other topic is a novel anti-hepatoma drug release hybrid system which is prepared by using poly(acrylic acid) (PAA) and glycol chitin as substrate in combination with Paclitaxel (PTX)-loaded bio-biofunctionalized poly(lactic-co-glycolic acid) (PLGA) micro-particles, which is intended for cancer therapy through intratumoral injection. The rheological behavior of glycol chitin (7 wt%)/PAA illustrates that it has low gelling temperature (i.e. 17℃ at pH 7.56) which ensures that the formulation turns to gel at physiological condition. The gelling time of glycol chitin/PAA is 16 minutes at 25℃ and 3 minutes at 37℃, which is convenient for doctors to inject the in-situ gel formulations into the tumor location of patient. The drug release behavior reveals that the system can dramatically postpone the drug release. The cell viability test indicates that the micro-particles with drug still have 62% inhibitory effect on hepatoma cells in the fourteenth day after combing with hydrogel. This system is a promising approach for cancer therapy through intratumoral injection of in-situ gel formulations to extend retention time at tumor sites.

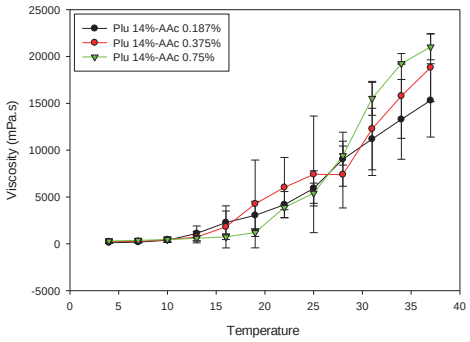

Effect of temperature on viscosity of Pluronic–PAA liquid suppository (pH 7.4). The liquid suppository was sol at 4°C and gel at 37°C.

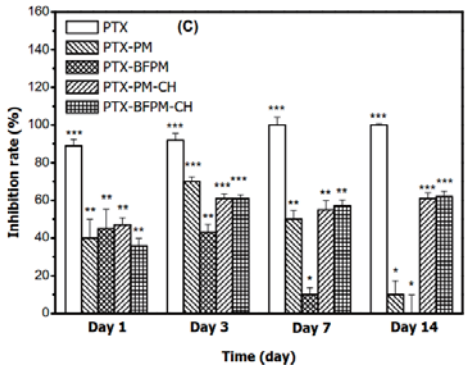

Cell inhibition rate of PTX, PTX-PM, PTX-BFPM, PTX-PM-CH, and PTX-BFPM-CH and compared to control (human hepatocellular carcinoma cell HepG2/C3A) at different time; * $p<0.05$, ** $p<0.01$, *** $p<0.001$.

References:

[1] Nanaki S, Siafaka PI, Zachariadou D, et al. *Eur J Pharm Sci.*, **99**, 32–44 (2017).
[2] Cho IS, Cho MO, Li Z, et al. *Carbohyd Polym.*, **144**, 59–67 (2016).

Dynamics of a droplet at trap-squeeze transition in contraction microchannel

Van Thanh Hoang[1,2], Quang Bang Tao[2], Duc Binh Luu[2], Jang Min Park[1,*]

[1)]School of Mechanical Engineering, Yeungnam University, Daehak-ro 280, Gyeongsan 38541, Republic of Korea
[2)]Department of Mechanical Engineering, The University of Danang - University of Science and Technology, 54, Nguyen Luong Bang Street, Danang, Vietnam
E-mail: hvthanh@dut.udn.vn

Abstract

The manipulation of a droplet in microchannel has an important role in droplet-based microfluidic systems. The dynamics of the droplet suspended in a medium fluid is controlled by the ratio between hydrodynamic forces and surface tension force. This paper aims to present droplet dynamics at trap-squeeze transition in contraction microchannel via three-dimensional simulation. Particularly, the regimes including trap and squeeze are described dependent on Capillary number (Ca), contraction ratio (C) and viscosity ratio (λ). The results of trap-squeeze behavior would be useful guideline for contraction microchannel design.

In the droplet-based on microfluidics, there have been several applications in contraction microchannel, such as breakup of single drop into smaller droplets[1], DNA molecules stretching, measurement of polymeric materials properties. Previous studies reported that the numerical studies are limited to two-dimensional contraction or axisymmetric contraction microchannel[2]. However, it can be seen that geometry of real microfluidic system has rectangular cross-section. Thus, three-dimensional model should be used for analyzing droplet dynamics rigorously.

In this study, a geometry of the contraction microchannel is used as shown in Fig. 1. Materials properties of droplet and medium phases are assumed to be Newtonian fluids, and effect of inertia is negligible in the simulation. To describe droplet dynamics in the contraction microchannel, dimensionless numbers are introduced as Capillary number, viscosity ratio and contraction ratio which ranges from 1.11 to 2. A commercial software of ANSYS fluent is employed for the simulation. Mesh modelling and computational models are used after verifying with previous experiments available in the literature[3].

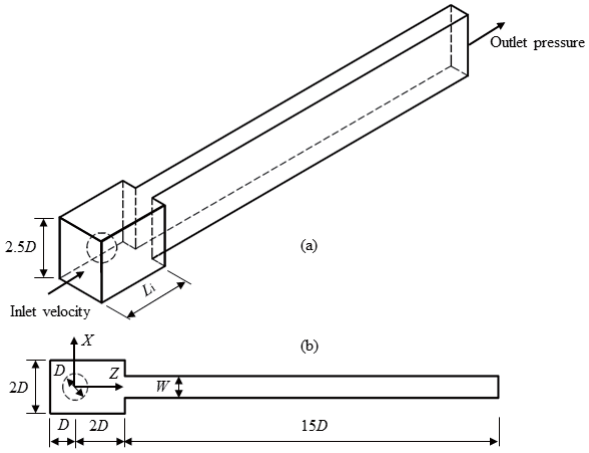

Fig. 1 Geometry of contraction microchannel: (a) a full model and (b) top view of the geometry

References:

[1] Anna, S.L., Bontoux, N., Stone, H.A. Formation of dispersions using ‘‘flow focusing” in microchannels. Appl. Phys. Lett. ***82***, 364–366 (2003).
[2] Harvie, D.J.E., Cooper-White, J.J., Davidson, M.R. Deformation of a viscoelastic droplet passing through a microfluidic contraction. Journal of non-Newtonian Fluid Mechanics. ***155***, 67-79 (2008).
[3] Van Thanh Hoang, Jiseok Lim, Chan Byon, Jang Min Park. Three-dimensional simulation of droplet dynamics in planar contraction microchannel, Chemical Engineering Science. ***176***, 59-65 (2018)

Research and Development of Next-Generation Battery Systems: Lithium-Sulfur Batteries and All-Solid-State Batteries

Shiro Seki*

Department of Applied Chemistry and Chemical Engineering, Graduate School of Engineering, Kogakuin University, Tokyo, Japan
E-mail: shiro-seki@cc.kogakuin.ac.jp

Research and development of lithium-ion batteries (LIBs) have focused on the efficient use of energy. Application fields of LIBs are spreading from portable commercial use (mobile phone and laptop PC) to large-scale energy systems (electric vehicle and accumulator for household-use). Recently, the usages (utilities, needs, requirements and demands) of industrial-scaled electricity storage systems using LIBs are increasing for applications alongside renewable energy systems (photovoltaics and/or wind energy) and frequency regulation demands. At the same time, solutions such as safety and capacity (energy density) are beginning to be strongly anticipated. In recent years, we are conducting research on 'lithium-sulfur battery' which is a high-capacity type battery and 'all-solid-state battery' which is a high-safety type battery. In this presentation, two next-generation battery systems will be introduced including developed innovative analysis techniques.

1. Lithium-sulfur (Li-S) batteries

Li-S batteries have been investigated. Because S forms compounds with Li, and is abundant, inexpensive, and non-toxic, S is suitable as a positive active material for the Li secondary battery. The total reaction between S and Li^+ is,

$$S_8 + 16Li^+ + 16e^- \rightarrow 8Li_2S \quad (1)$$

The theoretical capacity of S is estimated to be 1,672mAhg^{-1}, which is almost 10-fold greater than that of other transition metal compounds, such as conventional Li_xCoO_2 ($0.5 < x < 1$; 137mAhg^{-1}), $Li_xMn_2O_4$ ($0 < x < 1$; 148mAhg^{-1}). However, the S positive electrode (S-PE) has the following intrinsic drawbacks: volumetric expansion during Li insertion, low conductivities of S and Li_2S_x ($2 < x < 8$, intermediate), slow electrode kinetics between S and Li_2S_x, and dissolution of Li_2S_x from the S-PE into an electrolyte. The dissolved Li_2S_x diffuses to the negative electrode side and is oxidized by the redox shuttle mechanism, which leads to rapid capacity degradation and low Coulombic efficiency of the cell (Fig. 1). Mixtures of Li salts and glyme behave like ionic liquids (ILs) and are classed as 'solvate ionic liquids' (SILs). SILs show higher thermal and electrochemical stabilities in comparison with pure glyme, because the glyme molecule is strongly coordinated to Li^+ and forms the stable $[Li(glyme)]^+$ complex cation. Long-cycle-life charge-discharge of 800 cycles have been achieved in triglyme (CH_3-O-(C_2H_4O)$_3$-CH_3)-based SIL systems [1].

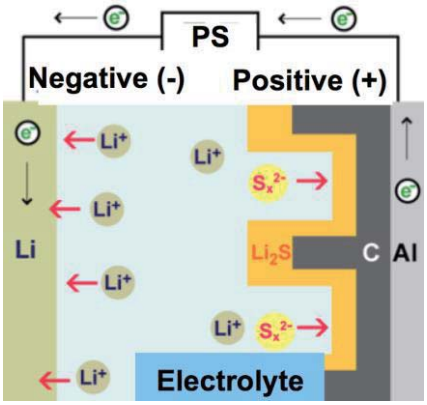

Fig. 1 Reaction mechanism of lithium-sulfur batteries..

2. All-solid-state batteries

Various electrolytes (solid polymers and inorganic electrolytes) have been considered as possible safe materials for safe battery systems. The solid inorganic and polymer electrolytes mainly used in all-solid-state lithium batteries are oxide- or sulfide-based inorganic materials and poly(ethylene)oxide (PEO). In particular, the practical application of batteries under development is of top priority, and not only improved battery performance (cycle life and rate capability) but also reduced cost and a simplified fabrication process are important. Therefore, we developed 'solvent-free' 4V-class lithium-ion polymer secondary batteries with $LiNi_{1/3}Mn_{1/3}Co_{1/3}O_2$ positive electrodes (i.e. using a reduced amount of scarce Co) and graphite negative electrodes (whose handling is very easy in the manufacturing process), as shown in Figure 2 [2]. And, recently, good compatibility between inorganic / polymer hybrid electrolytes were found. In this presentation, our attempts for sufficient solid electrolyte systems will be discussed.

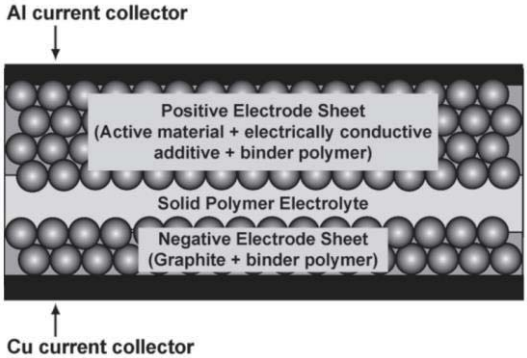

Fig. 2 Cross-sectional image of solvent-free all solid-state lithium-ion polymer secondary battery.

[1] *J. Am. Chem. Soc.*, **133**, 13121 (2011). *J. Electrochem. Soc.*, **160**, A1304 (2013). *Electrochemistry*, **85**, 680 (2017). [2] *Chem. Select*, **2**, 3848 (2017).

The apoptotic effects of pomegranate juice on prostate cancer DU145 cells

Song-Tay Lee[1)], Szu-Ting Chen[1)], and Ting-Feng Wu [1), *]

[1)]Department of Biotechnology, Southern Taiwan University of Science and Technology, Tainan, Taiwan,
E-mail: wutingfe@stust.edu.tw

Abstract

Prostate cancer has been known to be the second highest cause of death in cancer among men. Pomegranate is rich in polyphenols with the potential anticancer activities. This study demonstrated that pomegranate fruit juice could effectively hinder the proliferation of human prostate cancer DU145 cell through triggering the apoptosis.

There are about 15–30% cases of mortality among those diagnosed with prostate cancer[1]. Many reports imply that plant-derived phytochemicals may inhibit prostate cancer cell [2]. Many well-documented evidences have showed that pomegranate fruit possesses anti-cancer potential. In this study, hundred percent PFJ (Royal Chef Brand) imported from Republic of Georgia by Sky Chefs International, Inc. was bought for research purpose. MTT results demonstrated that the inhibitory influences of PFJ could be observed after treatment for 24 h of prostate cancer DU145 cells with 10 mg/ml. The suppressive effects of PFJ were more obvious after treatment for 72 h with more than 7.5 mg/ml (Fig. 1A). However, PFJ treatment had much less toxicity to human hepatic stellate cells (HSC) (Fig. 1B). The results of annexin V/PI staining showed that after incubation for 72 h of DU145 cells with 10 mg/ml of PFJ could evoke the phosphatidylserine translocation in the cell membrane, which is an initial sign of apoptosis and result in the subsequent membrane leakage (late apoptotic cell) and thus increase early and late apoptotic cell numbers (Fig. 2)

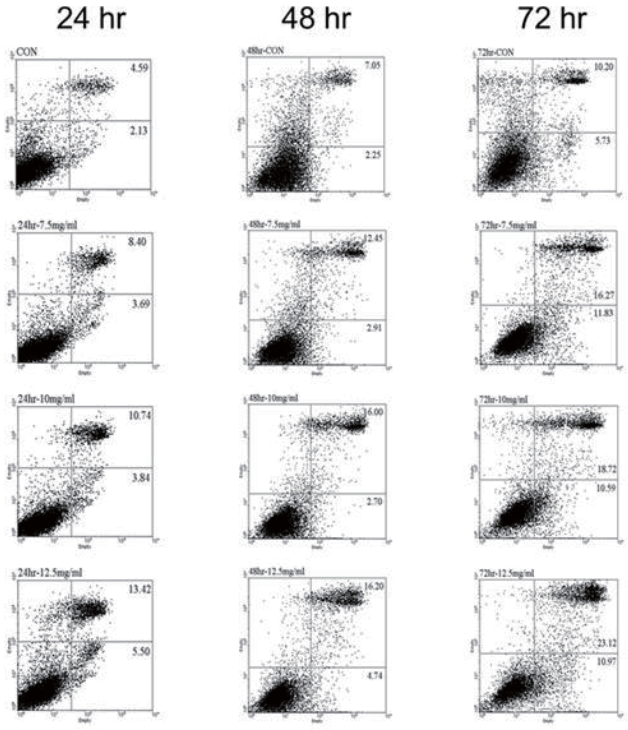

Fig. 2 The Annexin V/PI staining of PFJ-treated DU145 cells.

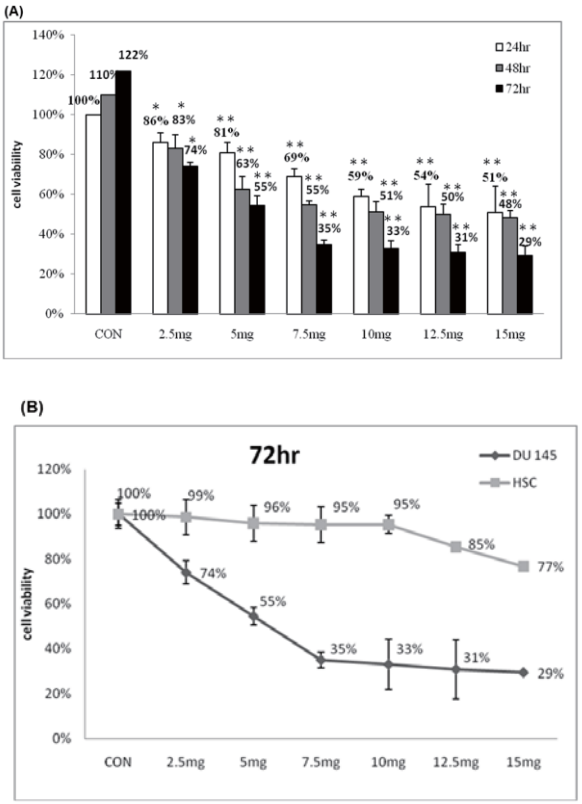

Fig. 1 The inhibitory impacts of PFJ on DU145 cells. (A) Dose-dependent effects; (B) Time-dependent effects.

References:

[1] Cancer facts and figures, American Cancer Society, Atlanta 2017.
[2] Mohammad Saleem,Vaqar Mustafa Adhami, Imtiaz Ahmad Siddiqui, Hasan Mukhtar, *Nutrition and Cancer*, **47**, 13–23 (2003).

Adsorption and rejection of hydrophobic trace organic contaminants by nanofiltration and reverse osmosis membranes

Hai Quang Dang

Department of Environmental Management, Faculty of Environment, Danang University of Science and Technology, Danang, Vietnam
E-mail: dqhai@dut.udn.vn

Abstract

This study aimed to elucidate adsorption and rejection efficiency of hydrophobic trace organic contaminants (TrOCs) by a nanofiltration membrane NF270 and a reverse osmosis membrane ESPA2 using a cross flow NF/RO filtration system. It was found that the adsorption of hydrophobic trace organic contaminants onto the membranes could be predicted based on their hydrophobicity, expressed as log D. For trace organic contaminants with higher hydrophobicity as reflected by quite high log D values, their adsorption onto membranes after 24 hours of filtration was quite significant. Hydrophobicity of the trace organic contaminants was confirmed to strongly influence the rejection mechanisms and therefore the rejection rate of the compounds. Hydrophobic trace organic contaminants with high log D value showed the lower rejections compared to the compounds with low log D value. The results also demonstrated that the rejection efficiency by the ESPA2 membrane of all trace organic contaminants studied was significantly higher than for the NF270 membrane.

Figure 1 is an illustrative example of the result, demonstrating rejection efficiency of hydrophobic TrOCs after 24 hours of filtration using the NF270 and ESPA2 membranes.

In most cases, the rejection efficiency of the TrOCs by the ESPA2 membrane was considerably higher than for the NF270 membrane. These rejection values were up to 100% for the ESPA2 membrane, while the corresponding maximum values for the NF270 membrane were approximately 87%. These could be due to the NF270 membrane having larger pore size than the ESPA2 membrane. Because of the very small pore size of the ESPA2 membrane, TrOCs do not significantly penetrate into the membrane pores, resulting in their adsorption occurring mainly at the membrane surface. Consequently, the diffusion of these compounds across the membrane was very limited, leading to the high rejection efficiencies observed.

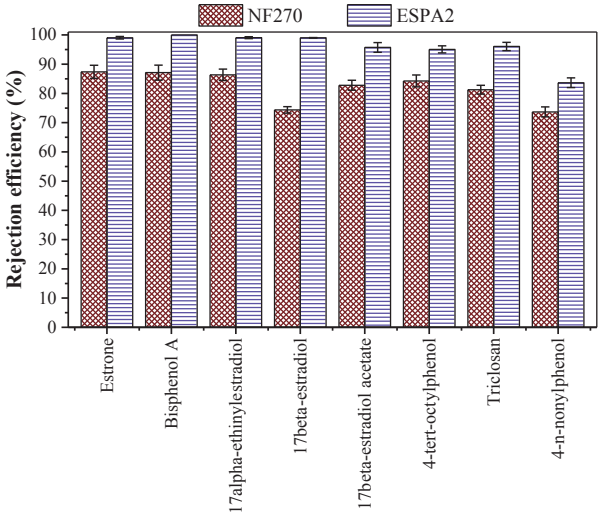

Fig. 1 Rejection efficiency of the hydrophobic TrOCs by the NF270 and ESPA2 membranes. The error bars present standard deviation of data obtained from two independent experiments

Consistent with these findings, Nghiem and Schäfer [1] observed that because of the narrow pores of RO membranes, hydraulic resistance reduced the penetration of TrOCs, and adsorption could only occur at the surface of the membranes, resulting in a higher rejection. In addition, TrOCs were rejected better by tight RO membranes compared to loose NF membranes has been also widely reported in the literature [2,3].

References:

[1] L. D. Nghiem, A. I. Schäfer, "Adsorption and Transport of Trace Contaminant Estrone in NF/RO Membranes", *Environmental Engineering Science*, **19**, 441-451 (2002).

[2] K. O. Agenson, J. I. Oh, T. Urase, "Retention of a wide variety of organic pollutants by different nanofiltration/reverse osmosis membranes: controlling parameters of process", *Journal of Membrane Science*, **225**, 91-103 (2003).

[3] P. Xu, J. E. Drewes, C. Bellona, G. Amy, T. U. Kim, M. Adam, T. Heberer, "Rejection of emerging organic micropollutants in nanofiltration-reverse osmosis membrane applications", *Water Environment Research*, **77**, 40-48 (2005).

Combining Image Processing and Tactile Sensation Actuator for Improving Athletic Training in Squat Work Out

Vo Nhu Thanh

Faculty of Mechanical Engineer, University of Science and Technology, The University of Da Nang
Email: vnthanh@dut.udn.vn

Abstract

This paper presents a research on combining image processing and tactile sensation for improving Squat motion training. Squat is a very fundamental exercises which is critical for a lower-body regimen training, and people think it is easy to do this exercise themselves. However, there are many accidents happened because people doing it the wrong way. Therefore, developing a training system combining image processing and tactile sensation would help athletics and people correctly work out with Squat motion and could prevent injuries is put into consideration. This system would consist of PC, Kinect, A/D converter, amplifier, and tactile pads. Image processing using OpenNI software together with depth sensor camera from Kinect to detect the motion of trainer, and shape memory alloy (SMA) wire tactile sensation will indicate for the trainer if the work out is done properly. The test result indicated that this system could help trainer improve their Squat motion workout.

Circuit board 30 Channel ICB-288G Sunhayato Single side glass epoxy (CEM-3) is used for distributing tactile signals. This board will distribute the signal to each tactile pad. Interface DIO Card Bus CSI-291144 – This card supports bus master DMA transfer function so the data from computer is transferred automatically to ICB-288G card. It can achieve simultaneously perform high-speed (up to 20MHz) data input / data output provides good data transfer in a multitasking operation system environment such as Windows. A/D Converter OMRON XG5 – Convert signal from analog to digital for pulse generation in order to control tactile pads. Amplifier Idec PSSN-A05A1: output 5V– 2.0A; input 100-120 VAC, 0.3-0.25A, 47-440Hz to send signal to tactile pads. The system overview is shown in figure 1.

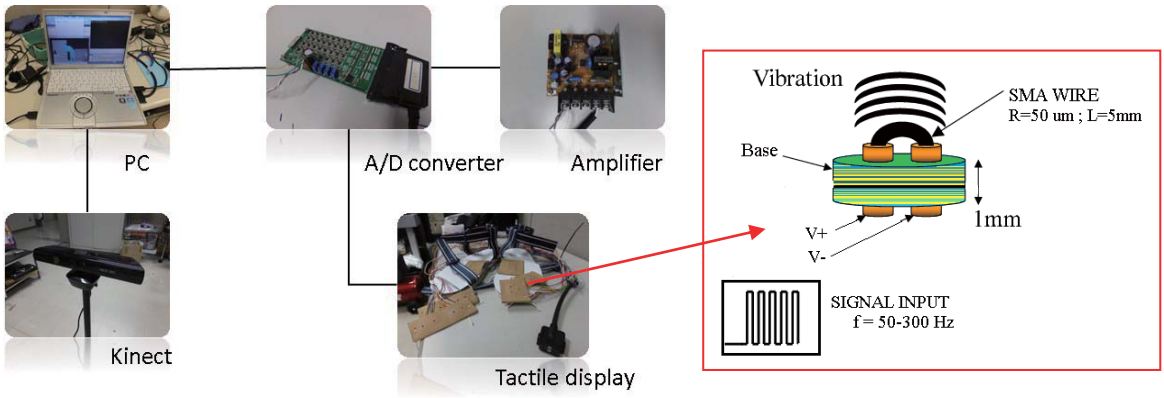

Fig.1 System overview robot

System for helping Squat motion training based on combination of image process and tactile sensation has been developed and tested. This system has been tested on 5 people whose age range from 20 to 25 with 10 repeated tests for each person. The test result indicated that after about 10 round training with this system the trainer can be able to do the Squat motion work out properly.

References:

[1] Keishi Fukuyama, Yohsuke Mizukami, and Hideyuki Sawada, A Novel Micro Vibration Actuator and the Presentation of Tactile Sensations,12th IMEKO TC1 & TC7 Joint Symposium on Man–Science & Measurement, September 3 – 5, 2008, Annecy, France

[2] Xiang LIU ,Jinhai SUN, Yaping HE, Yimin LIU,Li CAO, Overview of Virtual Reality Apply to Sports, Journal of Convergence Information Technology(JCIT), Volume6, Number12, December 2011

A Novel Approach for Evaluating the Performance Efficiency of Power Plants

Nhat-To Huynh, Thi-Kim-Oanh Le

The University of Danang, University of Science and Technology, Danang, Vietnam
Email: hnto@dut.udn.vn, ltkoanh@dut.udn.vn

Abstract

Most of performance measurements are difficult to find the strict standards for evaluation, and thus rely on relative comparisons, cross sectional or time periods. The results must identify the unit with best performance and the units with declining performance in order to make the necessary actions for improvements. In practice, multiple input factors and output factors are used to evaluate the performance efficiency. Data envelopment analysis[1] (DEA) has been employed to evaluate the relative efficiency of plants. This study aims to develop an approach based on common weights DEA and common weight global Malmquist productivity index (MPI) to evaluate relative performance of power plants.

A three-step approach to generate common-weights DEA as follows:

Step 1: Calculate the ideal efficiency for DMUs

Step 2: Derive a common set of weights

Step 3: Calculate the common-weights efficiency of DMUs

Table 1 Efficiencies based on the common-weights DEA and CCR for each period

DMU	94	95	96	97	98	99
HSIEHHO	0.9439	0.8891	0.8280	0.9430	0.7667	0.8436
LINKOU	0.5861	0.6276	0.6690	0.7660	0.4591	0.4098
SHENAO	0.5964	0.9818	0.9830	1.0000	0.8822	0.9305
TAICHUNG	0.9266	0.9208	0.7450	1.0000	1.0000	1.0000
HSINTA	1.0000	1.0000	1.0000	0.6970	0.4900	0.4270
TALIN	0.6047	0.7449	0.7670	0.7870	0.6912	0.6630
TUNGSHIAO	0.5478	0.5452	0.6000	0.7640	0.6397	0.6532
PENGCHU	0.5267	0.5438	0.5750	0.5010	0.4181	0.4456

To validate the proposed approach, a case study of Taiwan power company[2] was used. The proposed approach was compared with conventional approach. The results have shown in Table 1. In addition, the global Malmquist productivity index based on common-weights is used for evaluating the productivity changes. For calculating the annual changes, a base time period is set as year 1994. The productivity changes can be seen clearly from Figure 1.

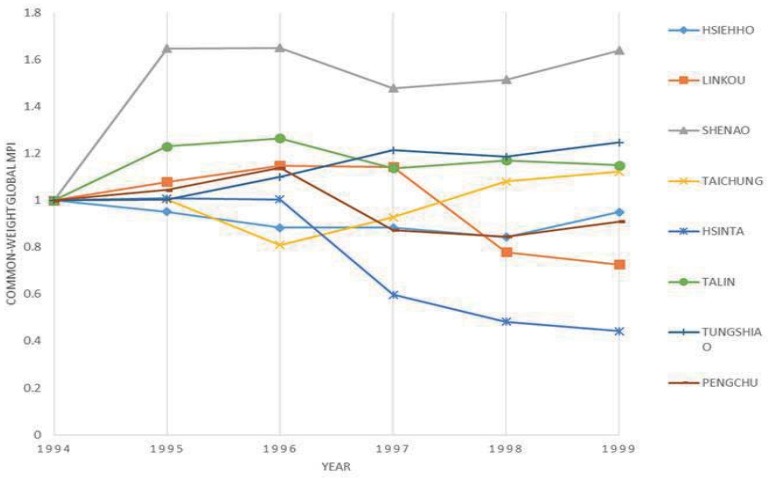

Figure 1 Productivity changes of plants over years

The proposed approach based on common-weights DEA and common weights global MPI is to evaluate and compare the performance efficiencies and the productivity changes. The common set of weights is obtained by minimizing the total squared difference between the ideal efficiency and that of each DMU obtained from the common set. Comparing to conventional DEA, this approach has provided a common basis for comparison. Furthermore, the different results between the proposed approach and conventional DEA approaches can also provide more insights to support the decision makers for evaluating the performance efficiencies and productivity changes.

References

[1] G.R. Amin & M. Toloo, *Computers & Industrial Engineering*, **52**(1), 71-77 (2007).

[2] Taiwan Power Company. Taiwan Power Company 2000 Annual Report (Taipei, Taiwan, R.O.C., 2001)

Lead-Free Piezoceramics for Low Power Vibration Energy Harvesting Applications

Da-Huei Lee and Chien-Min Cheng*

Department of Electronic Engineering, Southern Taiwan University of Science and Technology, Tainan, Taiwan
E-mail: ccmin@stust.edu.tw

Abstract

With the continuous advancement of industry, the problems of energy crisis and environment pollution have become more serious gradually. Therefore, the harvesting technique of clean energy will be a very significant research topic. In the past, lead zirconium titanate oxide ($PbZrTiO_3$) played an important role for modern electronic devices, such as transducer, ultrasonic, buzzer, speaker, actuator, sonar, pressure sensor, position sensor, earphone etc. But because of environment pollution, Pb-based ceramics must be inhibited gradually in the future. Hence, finding other lead-free ceramics to substitute Pb-based ceramics is a very imperative problem for researchers. And up to now, barium zirconium titanate oxide ($BaZrTiO_3$) has attracted considerable attention and is one of the most possible ceramic for substitution of Pb-based ceramics.

By the conventional solid state reaction method, proportional raw materials $BaCO_3$, $CaCO_3$, TiO_2, and SnO_2 powders were mixed, grounded, and calcined (1300°C / 4h) to form the $(Ba_{0.95}Ca_{0.05})(Ti_{0.93}Sn_{0.07})O_3$ (BCTS) lead-free piezoceramics. After adding 5 wt% polyvinyl alcohol (PVA) as the binder, the resulting powders were ground again, dried, pressed into bulks (diameter is 10 mm and thickness is 0.7 mm) and sheets ($30\times20\times0.4$ mm^3), respectively. These specimens were debindered and then sintered at 1300–1510 °C for 2 h. Additionally, small amount of lithium fluoride (LiF) was used as the sintering promoter to improve its sintering and piezoelectric characteristics. Finally, for vibration energy harvesting, we also used vibration system to measure the output peak-to-peak voltages of these lead-free piezoelectric sheets.

The variations of piezoelectric constants (d_{33}) and electromechanical coupling factors (k_P) of the BCTS–*y*LiF sheets are plotted in Fig. 1. It is clear from Fig. 1(a) that for all of the specimens, the d_{33} values first increase and reach a maximum value, and then decrease gradually. The maximum d_{33} value of BCTS–0.07LiF is 413 pC/N, and its sintering temperature is only 1390°C. However, for pure BCTS, the maximum d_{33} value is only 355 pC/N, and sintered at 1450°C. Hence, it obviously can be found that, owing to the addition of the LiF liquid-phase sintering promoters, the optimal sintering temperature of the BCTS sheets can be reduced significantly about 60°C, but also piezoelectric characteristics improved.

Furthermore, for the electromechanical coupling factors of the BCTS–*y*LiF sheets shown in Fig. 1(b), as the sintering temperature increased from 1300°C to 1450°C, all of the k_P values revealed the similar trend of d_{33} values. Except for the pure BCTS specimens (which happened at 1450°C), all of the maximum k_P values happened at 1390°C. For the pure BCTS specimens, the maximum k_P value is 0.40, and sintered at 1450°C; however, for the BCTS–0.07LiF specimens, the maximum k_P value is 0.48, and sintered at only 1390°C. However, with use of a vibration system, when the tip mass is 1.5 g and vibration frequency is 20 Hz, the proposed BCTS–0.07LiF sheets revealed good energy harvesting performance. The maximum output peak voltage was 4.6 V, which is large enough to be applied in modern low-power electronic products, and act in concert with backend circuits.

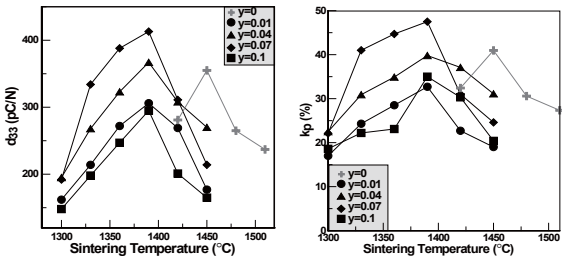

(a) d_{33} (b) k_P

Fig. 1 Piezoelectric characteristics of BCTS–*y*LiF

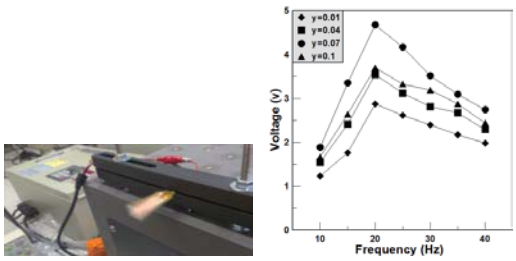

Fig. 2 Vibration system measurement

Waterproofing underground construction

Tich Do (1), Tin Do (2)

(1) Chairman & CEO, INTOC Waterproofing, Ho Chi Minh City, Vietnam.
(2) Executive Advisor & Foreign relation department, INTOC Waterproofing, Ho Chi Minh City, Vietnam.

This research provide the audience with the following information:

1. The current state of waterproofing in general civil construction and underground construction: High percentage of water damage, and the lack of solution to the problem.
   - 60% of household in America has moisture problem (Survey by the American Home Inspector Association, published on The New York Times)
   - 84.35% constructions in Vietnam has water permeation problem, and among those, 78.3% is basement. (Vietnam Journal of Construction - Vietnam Ministry of Construction)
   - The University of Minnesota: Most coating or membrane for basement waterproofing is not effective, most reliable way to deal with water damage: drainage system (collect the water and pump to the surface).
   - Expert in home improvement Bob Vila: "There's no such thing as a waterproof basement. The key is to minimize the water that gets in and get it back out again before it affects your home".

2. Identifying the 4 popular but wrong ways to choose a waterproofing solution, and introducing the most reliable way to choose an effective solution:
   - 4 Don'ts:
     + Don't rely on test results and theories. They don't translate into practical results.
     + Don't think that products from developed countries must be good. They are struggling with waterproofing themselves.
     + Don't think that a product that was used for many constructions must be good. Most constructions are having problem with waterproofing.
     + Don't rely on warranty promises. The law and business system don't hold waterproofing subcontractors accountable for more than 1 or 2 years, even if the warranty is 10 years of more.
   - 1 Do: Choose a waterproofing product/solution that has been proven to be effective in **real world construction projects** for **at least 10 years**. (Rely on practical results).

3. Introduce one of latest, if not the first solution to waterproof negatively (from the inside) basement walls, effective even with Diaphragm walls with Barrette. With result can be test immediately. Longevity of this solution:
   - Longest basement lifetime is 18 years (still currently effective) with no maintenance.
   - Longest basement with Diaphragm walls with Barrette lifetime is 11 years (still currently effective) with no maintenance
   - Other area, such as pools, terraces, and wet room: 26 years with almost no maintenance.
   - Life time estimate is 20-50 years with very little maintenance and incurred expenses.

AN EXPERIMENT STUDY ON ONE-DIMENSIONAL FLOW UNDER INFLUENT OF VERTICAL VELOCITY IN THE BED

Phuc-Hau Huynh[1)], The-Hung Nguyen[2),*], and Thi-Nam Nguyen[3)]

[1,3)]Department of Construction Engineering, The Central College of Transport No V
E-mail: hauhp@caodanggtvt2.edu.vn
[2)]Department of Water Resources Engineering, Danang University of Technology, The University of Danang
E-mail: profhungthenguyen@gmail.com

Abstract

This paper presents a laboratory experiment of one-dimensional open channel flow which has the vertical velocity at the bed orifice. The lab experiment was conducted at the National Laboratory for Coastal and River Dynamics in Vietnam. The experimental model is the flow in a glass flume having rectangular cross-section. For creating the vertical velocity at the bottom of flume, the flume was divided into two parts, the upper flow was the main stream and the lower flow was sprayed up for generating the vertical velocity W^*.

The experiment was conducted with 6 levels of discharge. The inlet discharge is controlled by a shard crested spillway. The depth along the channel is measured by the steel plate meter; the water level and the velocity are measured by a digital technology, connected to the computer. The experimental results show that the vertical velocity at the bottom of the flume creates a rise of water level in the upstream of the channel; the bed orifice act as a weir; the surface water in downstream of the orifice likes the free over fall.

Fig. 1 Water surface in flume, case study with discharge Q=0.045(m^3/s).

References:

[1] Angela Dean and Daniel Voss, 1999, Design and Analysis of Experiments, Springer - Verlag Newyork, Inc.
[2] Cameron Tropea et al., 2007, Handbook Experimental of Fluid Mechnics, Springer-Verlag Berlin Heidelberg.
[3] Nguyen Canh Cam, 2006, Hydraulics, Tome 2, Agricultural Pub.
[4] Nguyen Thi Nga, Tran Thuc, 2001, River Dynamics, Hanoi National University.
[5] Nguyen Doan Y, 2003, Planning Experiments, Science & Technology Pub.
[6] Ven-te-chow, David R. Maidment, Larry W.Mays, 1998, Applied Hydrology, McGraw-Hill, Inc.

Flow Observation of Synthetic Jets Produced by Asymmetric Slot

Hiroaki Terakado[1)], Ryota Kobayashi[2)], Koichi Nishibe[3)], and Kotaro Sato[4)]

[1)] Graduate School of Engineering, Kogakuin University, Tokyo, Japan
E-mail: am17043@ns.kogakuin.ac.jp
[2)] Mechanical Engineering Program in the Graduate School of Engineering, Kogakuin University, Tokyo, Japan
E-mail: ad18001@ns.kogakuin.ac.jp
[3)] Department of Mechanical Engineering, Tokyo City University, Tokyo, Japan
E-mail: knishibe@tcu.ac.jp
[4)] Department of Mechanical System Engineering, Kogakuin University, Tokyo, Japan
E-mail: at12164@ns.kogakuin.ac.jp

Abstract

Over the past several decades, research has been conducted on flow control using continuous jets. In recent years, research on active control of the flow field using synthetic jets as an alternative to continuous jets is actively conducted. Flow control using synthetic jet, it has been reported that the slot exit shape is made asymmetric beak shape and jet vectoring is possible only by frequency adjustment. However, findings on detailed deflection mechanisms are still insufficient. Moreover, there have been few discussions on the optimal geometric shape for controlling the jet direction of synthetic jets.

In this study, we attempt to elucidate the flow characteristics of the synthetic jet generated by an asymmetric stepped slot by experiment and numerical simulation as a fundamental study on the direction control of synthetic jets on a two-dimensional surface. Fig. 1 shows the experimental results obtained under the conditions of step length S = 5 and Re = 990. Fig. 1(a) shows the behavior observed by flow visualization in the case where the dimensionless stroke (equivalent to the reciprocal of the Strouhal number) is large. In this condition, the jet flows straight without being affected by the asymmetry of the slot. On the other hand, Fig. 1(b) shows an example of flow visualization observed when the dimensionless stroke is small. The jet can be observed to be deflected downward in this figure under the influence of slot asymmetry. If the slot shape is symmetric, vortex pairs are generated at the same position; hence, the vortex pairs translate almost linearly at mutual induction velocities. On the other hand, in the case of a stepped slot, a clockwise vortex forms near the lower corner of the slot in the jetting process. Since counterclockwise vortices are formed at the corner of the slot upper side, deviation occurs in the vortex pair generation position in the x-direction. Accordingly, the y-direction component is generated as the induced velocity. In the suction process, the clockwise vortex located near the slot is influenced by the suction flow and is attracted to the slot side, which hinders the progression of the clockwise vortex in the x-direction. As a result, the vortex pair progresses downward. From this, the traveling direction of the synthetic jet depends on the dimensionless frequency. Therefore, it was clarified that jet vectoring is possible by adjusting the frequency of the synthetic jet using an asymmetric stepped slot.

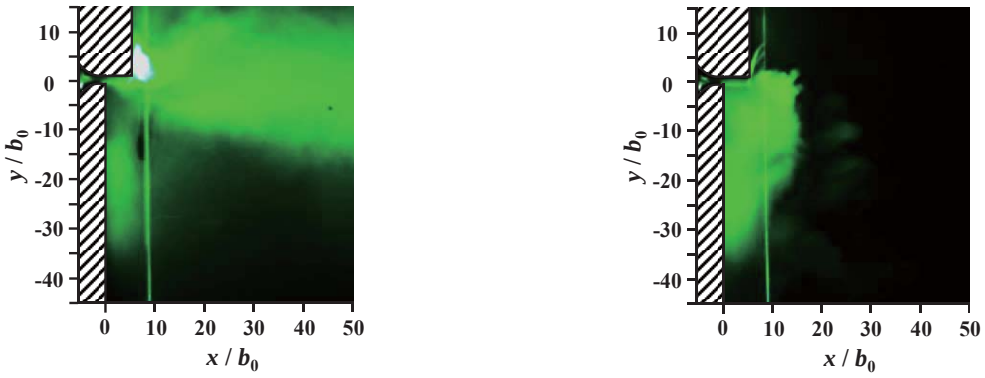

(a) L_0 = 60 **(b) L_0 = 10**

Fig. 1 Flow pattern of the synthetic jet generated by an asymmetric stepped slot ($H_2 = \infty$, U_0 = 3.0 m/s, and Re = 990).

References:

[1] Watabe, Y., Sato, K., Nishibe, K., and Yokota, K., Influence of an Asymmetric Slot on the Flow Characteristics of Synthetic Jets, Springer Proceedings in Physics, 185, pp. 101-107 (2015).
[2] Kobayashi, R., Nishibe, K., Watabe, Y., Sato, K., and Yokoya, K., Vector Control of Synthetic Jets Using an Asymmetric Slot, Proceedings of the ASME, FEDSM2016-7648(2016).

A DUAL APPROACH FOR MODELING TWO-DIMENSIONAL HORIZONTAL FLOW

Tinh Ton That[1)], The-Hung Nguyen[1),*], Dong-Anh Nguyen[2)]

[1)]Department of Water Resources Engineering, Danang University of Technology, The University of Danang
E-mail: profhungthenguyen@gmail.com
[2)]Institue of Mechanics, VAST
E-mail: ndanh@vast.ac.vn

Abstract

The two-dimensional horizontal flow model in the classic mechanics is integrated from the three-dimensional Reynolds averaged Navier-Stokes equations. With the classic mechanics approach: the integral approach is taken one time from the bed to the water surface, so in the process of integration that effects between the channel bed and the surface dissappear. According to dual approach, the setup model will more complex and more general than classic approach; the integral can be performed locally several times, in this paper, the authors performed twice integrals: the first time integral is from the bed to the intermediate surface lays between bed to water surface, the second time integral is from the bed to the water surface; the received equations allow to contain many physical phenomenas which may be losted in the classic integral process. The improved two-dimensional horizontal flow model was received from dual approach allows the calculation of flow parameters when having the unusual phenomena in the channel as solid objects, liquids containing other added ingredients, external forces f_x, f_y, f_z, reversals,…

References:

[1] Nguyen Dong Anh (2012), Dual approach to averaged values of functions, Vietnam Journal of Mechanics, VAST, Vol. 34, No. 3, pp. 211 – 214.

[2] Nguyen Dong Anh (2012), Dual approach to averaged values of functions: Advanced formulas,Vietnam Journal of Mechanics, Vast, Vol. 34, No. 4, pp. 321 – 325.

[3] Environmental Modeling Research Laboratory of Brigham Young University (2002), *Surface water modeling system, Brigham young university.*

[4] Eleuterio F. Toro (2001), *Shock-Capturing Methods for Free-Surface Shallow Flow*, John Wiley Sons LTD.

[5] J.A.Cunge, F.M.Holly, Jr, A.Verwey (1980), *Pratical aspects of computational river hydraulics*, Pitman Publising Inc.

[6] Jonh H.Mathews, Kurtis D.Fink.1999. *Numerical Methods using Matlab.* Prentice- hall, Inc.

[7] M. Hanif Chaudhry (1993), *Open Chanel Flow*, Prentice Hall, Englewood Cliffs, New Jersey.

[8] Rainer Ansorge (2003), Mathematical models of fluid dynamics, Wiley-VCH GmbH &Co. KgaA.

[9] S.Vedula, P.P. and Mujumdar (2005), *Water Resources Systems : Modelling Techniques and Analysis*, Tata-McGraw Hill.

[10] Ven Te Chow (1983), *Open Chanel Hydraulic*, McGraw-Hill Book Company, Japan, Tokyo.

[11] Ven-Te-Chow, David R. Maidment, Larry W.Mays (1998), *Applied Hydrology*, McGraw-Hill, Inc.

[12] Weiming Wu (2007), *Computation river dynamics*, Taylor and francis/Balkema.

Development of the Next-Generation Internet of Vehicles Communication System for Driving Safety (II)

Chao-Tang Yu*, Liang-Bi Chen, Wei-Wen Hu, Wan-Jung Chang, Jing-Jou Tang, and Da-Huei Lee

Department of Electronic Engineering, Southern Taiwan University of Science and Technology, Tainan, Taiwan
*E-mail: ctyu@stust.edu.tw

Abstract

In recent years, the telematics technology is gradually in the way toward the next-generation Internet of vehicles (IoV), which integrates in-vehicle, vehicle-to-vehicle (V2V), and 3G/4G mobile networks to provide flexible services and driving safety. The advanced active safety is one of the most important applications of next-generation IoV in such situation. Since July 2016, a three-year term project supported by the ministry of science and technology (MOST, Grant No. 106-2632-E-218-002), Taiwan, was started up to design and implement the next-generation communication system which integrates vehicular heterogeneous networks including low-power WANs, visible light communication (VLC) and power line communication (PLC) technologies. The proposed system can provide a high speed data transmission and faults tolerant system required by the advanced active safety applications. The proposed system architecture is shown in Fig. 1. The IoV prototype system has been implemented in the first year and presented in [1]-[2]. In the second year, we focus on applying our IoV project result to the design and implementation of a driving safety aided mechanism as shown in Fig. 2. The proposed driving safety aided function will be introduced and summarized in this paper.

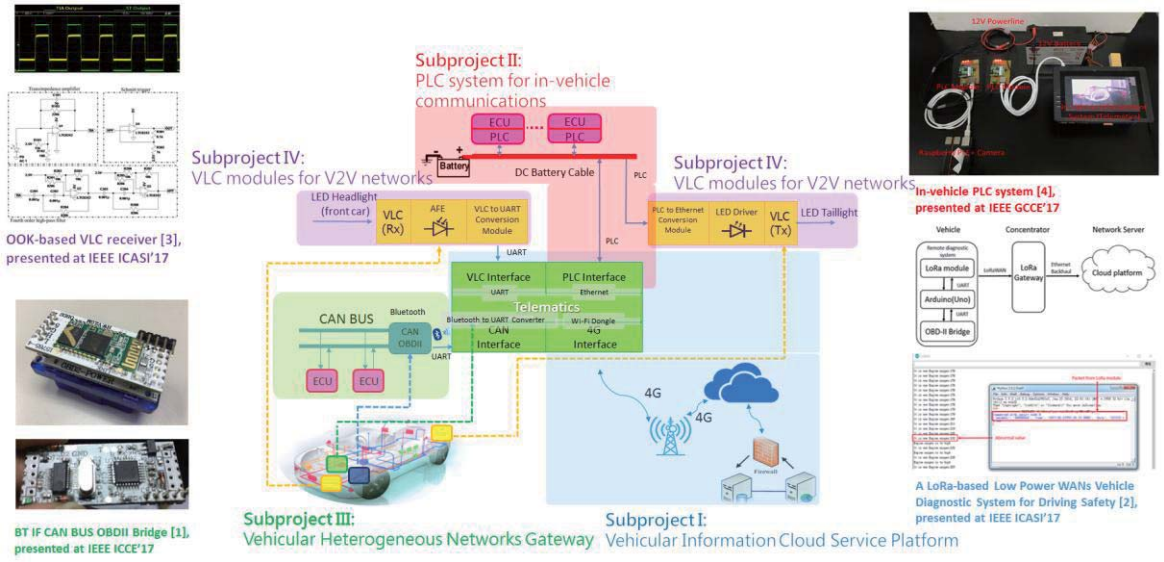

Fig. 1 The proposed IoV communication system architecture.

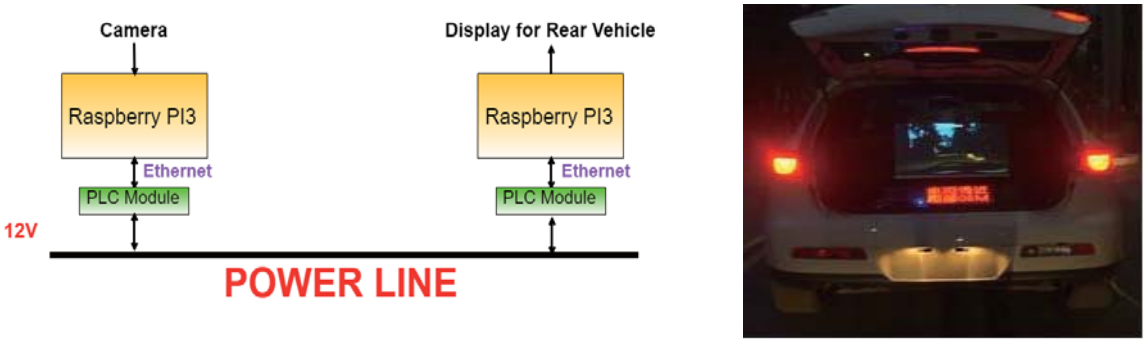

Fig. 2. A prototype of driving safety aided system with DC-based PLC.

References:

[1] F.-L. Chang, W.-W. Hu, D.-H. Lee, and C.-T. Yu, "Design and implementation of anti low-frequency noise in visible light communications," in *Proc. IEEE ICASI'17*, 1536−1538 (2017).

[2] K.-Y. Su, Y.-C. Mo, L.-B. Chen, W.-J. Chang, W.-W. Hu, C.-T. Yu, and J.-J. Tang, "An In-Vehicle Infotainment Platform for Integrating Heterogeneous Networks Interconnection," in *Proc.* IEEE 2018 ICCE-TW, May 19-21, 2018, Taichung Taiwan.

A Wind Forecasting Approach for Power System Operations

Dinh Duong Le

Faculty of Electrical Engineering, The University of Danang - University of Science and Technology, Danang, Vietnam
E-mail: lddduong@dut.udn.vn

Abstract

Nowadays, wind energy, as a clean and renewable resource, is increasingly attracting many researchers all around the world. However, together with benefits from this resource, integrating wind energy into the power system faces many challenges due to its characteristics such as high uncertainty and variability, limited predictability and dispatchability, and so on. In order to effectively exploit wind energy, accurate wind forecast is required. It is essential to accurately forecast wind speed and power output of wind farms because the information provided by the forecast not only serves the calculating and generating power of the plant itself, but also serves the operator of the grid where the wind power plant is connected. Accurate forecast can improve system operation by reducing operating costs (i.e., keep balancing the electricity supply and demand at a minimum cost), reducing wind curtailment, while maintaining appropriate level of reliability for the system. To integrate wind power into power systems, wind generation forecasting models have emerged rapidly to improve the accuracy of forecasts.

Based on time-scales, wind forecasting methods can be generally divided into 4 categories: ultra-short-term forecasting (from few minutes to 1 hour ahead), short-term forecasting (from 1 hour to several hours ahead), medium-term forecasting (from several hours to 1 week ahead), and long-term forecasting (from 1 week to 1 year or more ahead) [1]. Among them, this paper focuses on short-term wind forecasting (i.e., 24 hours ahead) for power system operation. In the paper, a methodology for modeling and forecasting day-ahead wind speed is developed by making use of multivariate time series model [2-4] combined with data processing techniques [2,5]. The model can explicitly capture the salient wind characteristics from multiple sites such as distinct diurnal and seasonal patterns, spatial and temporal correlations [6]. Once the wind speed is forecasted at sites (wind farms), the output power of each farm is calculated based on its power curve builded for each farm.

Figure 1 shows, for example, wind speed forecast at a wind farm. It can be seen from the figure that the forecasting method developed can give relatively accurate results.

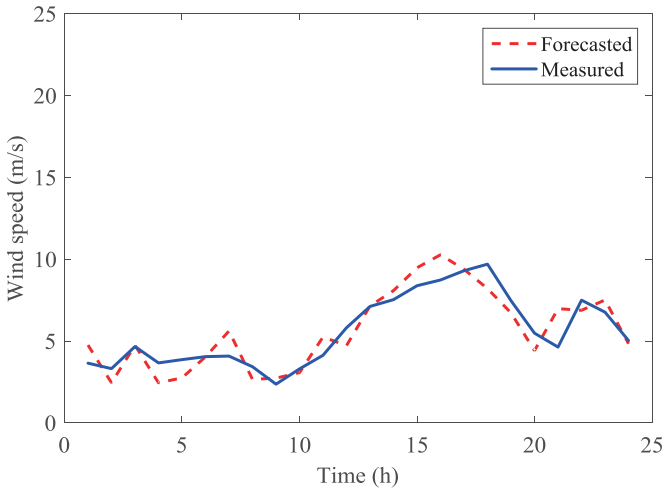

Fig. 1 Wind speed forecast at a wind farm.

References:

[1] Wen-Yeau Chang, "A Literature Review of Wind Forecasting Methods", *Journal of Power and Energy Engineering*, 2, 161–168, 2014.
[2] G. E. P. Box and G. M. Jenkins, *Time Series Analysis: Forecasting and Control, San Francisco*, CA: Holden Day, 1976.
[3] Runkle, D. E., "Vector Autoregressions and Reality", *Journal of Business and Economic Statistics*, 5 (4), 437–442, 1987.
[4] Stock, J.H. and M.W. Watson, "Vector Autoregressions", *Journal of Economic Perspectives*, 15, 101–115, 2001.
[5] F. E. Grubbs, "Procedures for Detecting Outlying Observations in Samples", *Technometrics*, Feb. 1969.
[6] D. D. Le, G. Gross, and A. Berizzi, "Probabilistic Modeling of Multisite Wind Farm Production for Scenario-based Applications", *IEEE Transactions on Sustainable Energy*, vol. 6, no. 3, pp. 748–758, 2015.

Fabrication of μ-LED arrays toward future realization of μ-LED display

Ryosuke Nawa ,[1),*] Shouma Takeda,[2)] Yoshifumi Kamei,[3)]
Takeyoshi Onuma ,[1,3)] Tomohiro Yamaguchi ,[1-3)] and Tohru Honda[1-3)]

[1)] Department of Electrical Engineering and Electronics, Kogakuin University, Tokyo, Japan
[2)] Department of Information and Communications Engneering, Faculty of Engineering, Kogakuin University, Japan
[3)] Department of Applied Physics, School of Advanced Engineering, Kogakuin University, Japan
*E-mail: cm17038@ns.kogakuin.ac.jp (R. Nawa)

Abstract

Since the triggering demonstration of the micro-LED (μ-LED) display '55" CrystalLED Display' by Sony Co. in 2012,[1] reports on the μ-LED display are explosively increasing all over the world. Several methods have been demonstrated to fabricate μ-LED display, e.g., etching down the LED wafer,[2,3] growth of nanocolumn LEDs,[4] and an arrangement of μ-LED chips on the printed substrate.[1] In this study, we fabricate μ-LED array structures by independently employing the etching down method and the LED chip mounting method to realize future hybridized application for small-sized μ-LED display panel.

Experiments

In the etching down procedure, p-GaN (100 nm) / InGaN MQW / n-GaN (1 μm) / i-GaN (2 μm) on sapphire LED structure was etched by the ICP-RIE method. First, a 200 nm Ni metal is deposited on the LED substrate by electron-beam (EB) evaporation technique. Then, the Ni metal was patterned by the photolithography, in which the mask pattern has a 32 × 32 array of 150 μm square-shape openings with a 100 μm pitch. ICP-RIE was conducted using chlorine and argon gases mixture with ICP power of 200 W, RF bias power of 80 W, and etching time of 6 min. On the other hand, a 16 × 16 array of Si micro-cups were fabricated to integrate 300 μm × 200 μm square 90 μm-thick LED chips by etching (100) Si substrate. The Si DRIE system was used to employ the BOSCH process, where SF_6 and C_4F_8 gases were alternatively introduced to the chamber for etching and forming a passivation layer, respectively. The cycle was repeated one hundred times. Resultant Si μ-cups have 320 μm × 220 μm square shape with a depth of 100 μm. Note that surface passivation layer was removed by hydrofluoric acid (HF).

Results and discussion

Figure 1(a) shows a surface SEM image of patterned LED structure by etching down the LED wafer. Magnified bird's eye view SEM image is shown in Fig. 1(b). Etching depth was measured by the stylus profiler to be 1 μm. Although the etching depth is insufficient to isolate the whole LED structure, observation of LED array having well-defined square shape mesa structure demonstrates the potential to further decrease in the size of the LEDs. As shown in Fig. 2, hexagonal shaped pillars are ocassionally found though their formation mechanism has not been understood yet. [5] We will report details in the LED chip mounting method at the conference.

Conclusion

We demonstrated two methods, i.e., etching down method and the LED chip mounting method, for future hybridized application in the μ-LED display. Especially, observation of LED array having well-defined square shape mesa structure demonstrates the potential to further decrease in the size of the μ-LEDs.

Acknowledgement

The authors would like to thank Toyoda Gosei Corporation for the LED chip furnishing, Mitsubishi Materials Corporation for technical support on the LED mounting processes and AIST for LED wafer furnishing.

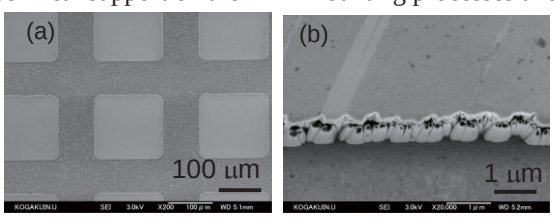

Fig. 1. (a) Surface and (b) magnified bird's eye view SEM images of patterned LED wafer.

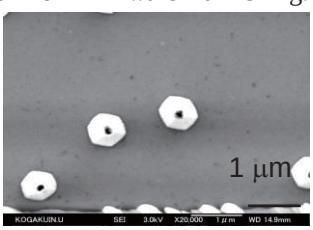

Fig. 2. Magnified surface SEM image of patterned LED wafer.

References:

[1] https://www.sony.jp/crystal-led/about/
[2] H.-V. Han *et al.*, Optics Express **23**, 25 (2015).
[3] H.-Y. Lin *et al.*, Photonic Reserch **5**, 411 (2017).
[4] K.Kishino GaN nanocolumn Photonic device.
[5] R. Qui *et al.*, Appl. Surf. Sci. **257,** 2700 (2011).

Characteristics of Flow Generated by Annular Inlet Guide Vanes with Outlet Pipe

Kazuya Takeda[1)], Kotaro Yamanaka[2)], Kotaro Sato[3)], Koichi Nishibe[4)]
[1)]Graduate School of Engineering, Kogakuin University, Tokyo, Japan
E-mail: am17039@ns.kogakuin.ac.jp
[2)] Department of Mechanical System Engineering, Kogakuin University, Tokyo, Japan
E-mail: a215103@ns.kogakuin.ac.jp
[3)]Department of Mechanical System Engineering, Kogakuin University, Tokyo, Japan
E-mail: at12164@ns.kogakuin.ac.jp
[4)]Department of Mechanical Engineering, Tokyo City University, Tokyo, Japan
E-mail: knishibe@tcu.ac.jp

Abstract

Inlet guide vanes (IGVs) to produce the rotational flow are sometimes installed at the impeller inlet in the turbomachines such as centrifugal compressors, turbo pumps, and pump turbine and are used for flow rate control, reduction of collision pressure loss at blades, and expansion of operation range [1,2]. It is known that the two dimensional flow instabilities with the cell structure and the specific frequency occur downstream of the IGVs, if the vane angle of IGVs is set to be small. The oscillation characteristics and onset conditions of flow instabilities have been reported to avoid the performance or the machine lifespan of the compressor deteriorates in such situation. On the other hand, it is known that periodic velocity-/-pressure oscillation caused by the whirling motion of vortex core occurs in the suction pipe with swirling flow. This phenomenon has also been confirmed by many researchers [3,4]. However, to the best of our knowledge, there are no reports on the interaction between the flow instabilities induced downstream of the annular inlet guide vanes and the oscillation produced by the whirling vortex core in the pipe.

In this study, we attempted to clarify the relationship between the flow instabilities occurring downstream from the IGVs and the oscillation produced by the whirling vortex core of the swirling flow in the circular pipe (the suction pipe of a centrifugal compressor) ; an outlet circular pipe was attached downstream from the annular inlet guide vanes. The pressure fluctuation and the velocity distribution were measured and the flow visualization was performed.

The typical experimental results are shown in figure 1. This figure shows the power spectrums of the pressure fluctuation for variable measurement points on the pipe surface. The vane angle is β_2 = 10°, the inside and outside radius ratio of the IGVs is r_3/r_2 = 0.6 and pipe length L = 300 mm (L/r_3 = 6). The dominant frequency of f / f_0 =1.3 appears on the upper disk. It is caused by the flow instabilities downstream of the IGVs and it propagate into the outlet circular pipe; however, the amplitude of fluctuation decays further downstream. It is observed another clear peak at f / f_0 = 0.64. It can be seen that the disturbance by the whirling of the vortex center generated at the outlet of the pipe propagates upstream the upper disk without attenuation, in comparison with the result for the upper disk. When the pipe is relatively long, the oscillation caused by the whirling vortex core in the circular pipe occurs with frequency different from that of the flow instabilities caused by the IGVs except the lock-in phenomena.

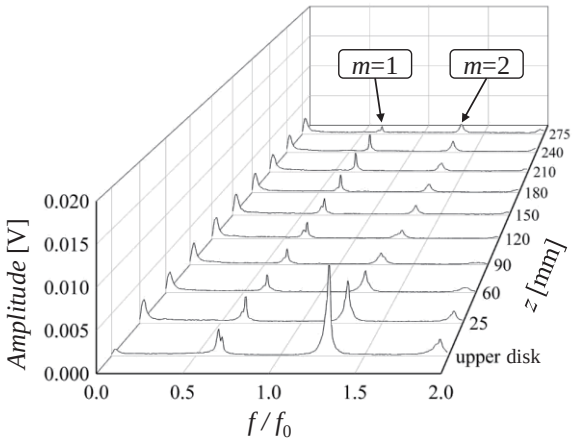

Figure 1 . *Power spectrums on the pipe surface*
(r_3 / r_2 = 0.6 , β_2 = 10° , L/r_3 = 6 , L = 300mm)

References:

[1] Takama, N., and Yoshiki, H., 1996, "Unstable Air Stream Arising Near the Rear of Inlet Guide Vane, Effects of Guide Vane Width," Proc. 11th Autumn Conference of Gas Turbine Society of Japan, **11**, pp. 19-22.
[2] Takama, N., and Yoshiki, H., 1997, "Unstable Flow Around Rear Part of Inlet Guide Vanes. Effect of Guide Vane Chord Length," Proc. 12th Autumn Conference of Gas Turbine Society of Japan, **10**, pp. 33-38.
[3] Baba, T., Nishikawa, T., Fukao, Y., Tsujimoto, Y., and Yoshida, Y., 1999, "Investigation of the Swirling Flow in a Suction Pipe with Inlet Guide Vanes. Experimental Studies of the Swirling Flow in a Suction Pipe of a Centrifugal Compressor," Tran. Japan Society of Mechanical Engineers, **65**(636), pp. 2726-2733
[4] Hatazawa, M., 2009, "Characteristics of Turbulent Swirling Flow in a Straight Pipe: Swirl Decay in Wide Range of Swirl Strength(Fluids Engineering)," Trans. Japan Society of Mechanical Engineers, **75**(754), pp. 61-72.

Toward Long Time Use of Stone-based Wall Panel in High-rise Building between Past and Future in Japan

1)Erika Futami, 2)Masaki Tamura
1)Bachelor of architecture, Kogakuin University
db15412@ns.kogakuin.ac.jp
2)Professor, Department of Architecture, Kogakuin University, Tokyo Japan
masaki-t@cc.kogakuin.ac.jp

Abstract

Regarding the geological environment in Japan, there are four continental plates along Japan island which is called Pacific Plate, Philippine Plate, Eurasian Plate and North american Plate, and those plates have been complexily raising and downwelling by repeatition for over a periods of billion years. These earth crust has been generating Igneous rocks which magma had been cooled and solidified, Sedimentary rocks which laminated materials had been weathered and fined, and Metamorphic rocks which igneous and sedimentary rocks had been heated and high-pressed under the crust. The whole three types of rocks has been using as raw materials of stone-based building panel in interior or exterior.

On the other hand, the area along these crust plates in Japan island has been occuring a lots of earthquakes in Japan, Accordingly, the earthquake resistance technologies for high-rise building has kept developing since few decades ago. Regarding the diffusing technologies for stone-based building panels in Japan, the two types of methods has been developed, the first is the stone panel attaching method with mortar applied under 10m height levels of building, the second is the stone panel fastening by stainless zipper applied under 45m height levels. These methods have ensured the safety condition for the building wall panel against usual conditions as sheltering wind and rain and unusual condition as effecting by earthquake. Such stone-based wall panels are often using the reinforced concrete in structural body, and these concrete buildings had been spreading wide district in Japan area.

In present, the supply and demand conditions of stone-based wall panel has some problems regarding the resource depletion and the price rising. According to the investigation for Japanese stone company, the number of stone-panel company in Japan are decreasing yeat after year, and the quantities of import stone materials from abroad are increasing. In this study, it is investigated the demand and supply conditions of stone-based wall panel in order to develop the sustainable construction environment toward the future.

Fig.1 stainless zipper applied under 45m height level

Table.1 Concrete accumulation volume in covered land area

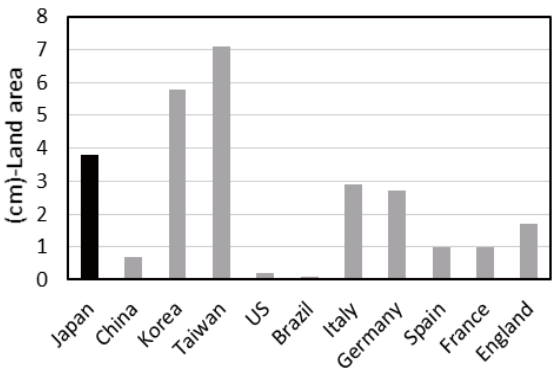

Reference
Demand and supply conditions of stone materials, The Agency for natural resources and energy, (http://www.enecho.meti.go.jp
Building Construction, Shokokusya

Identifying Blur Car License Plate Numbers Using Machine Learning

Ayaka Fujima[1)], Seiichi Gohshi[2)]

[1)]Department of Informatics, Kogakuin University, Tokyo, Japan
E-mail: j215109@ns.kogakuin.ac.jp
[2)] Department of Informatics, Kogakuin University, Tokyo, Japan
E-mail: gohshi@cc.kogakuin.ac.jp

Abstract

Due to advances of semiconductors, smartphones become common tools and security cameras are filled in downtowns. Smartphone pictures and recorded security camera images sometimes give us important information about crimes. Car license plate numbers are one of them because cars are often used by criminals. However, the recorded images/pictures are blurry and the license plate numbers cannot be readable. Although there is a machine learning system to read blur numbers, its performance changes depending on classifier. In this paper, the performances of the classifiers are compared and the best one is reported.

Proposed Methods

Machine learning is a technology to detect the nature from huge amount of data. The machine learning system finds the hidden characteristics in the data. Currently the application of machine learning is extended to the predication of the stock market and image recognition. The machine learning can be applied to the blurry numbers of the car license plates to make readable. Since the fonts of number plate is the same in Japan, it is possible to read the numbers if we extract the characteristics of the numbers. HOG is used to extract the characteristics of the numbers and five classifiers (k-NN, Support Vector Machine (SVM), Linear Discriminant Analysis (LDA), Naive Bayesian Method and Classification Tree) are used.

Experimental Results

Figure1 explains results in this study which shows 5 classifiers performances. A horizontal axis is the number of learning data. The number of data increases from left to right up to 5,000. A vertical axis is identification rate. The percentage is from75% up to 100%. The numbers are from 0 to 9 and 20 test data are used for each number. We prepared 10 test data sets and it means the total number of the test data is 200. The best performance is obviously 100% in the vertical axis. As shown in Figure 1, this rate was high in the order of Naive Bayesian Method, SVM, k-NN, LDA, Classification Tree when we identify numbers used 3500 to 5000 learning data. The order changed in the time that we used 500 to 3000 data. It appears that variance of learning data has large influence on classifiers. So we compare identification rate in the range of 3500 to 5000 so that we evaluate identification precision each classifier. Therefore, we compare identification rate in the range of 3500 to 5000 and find out that Naive Bayesian Method is the highest at all times of 5 classifiers.

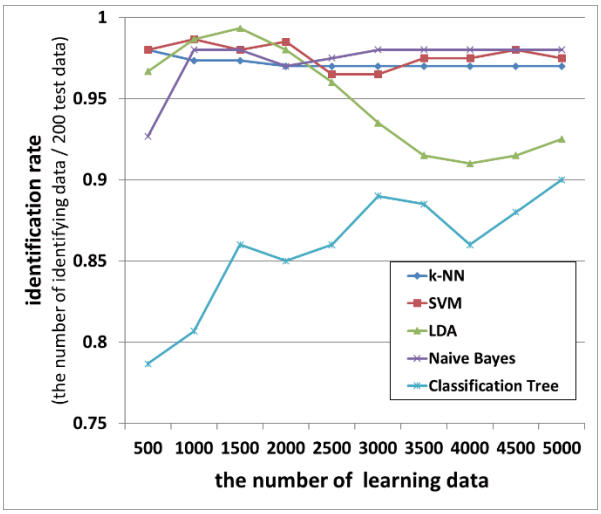

Fig. 1 Relationship between identification rate and the number of learning data

Conclusion

According to our research Simple Bayesian Method showed the best performance in the five classifiers. It is considered that other four classifiers do not use all data for analyzing. When we use a machine learning technology for the blurry car license numbers, Naive Bayesian Method is the best selection.

References:

[1] Hironobu Fujiyoshi, “Feature extraction to base gradient on-SIFT and HOG-”
Information Processing Society of Japan Information Report, **CVIM160**, pp211−224 (2007).

Poster Presentation

Inspection of Outer Wall Tiles in High-rise Building by Measuring Impact Response Value

Yuhei Oppata[1)] *, Masaki Tamura[2)]

[1)]Graduate Student, Kogakuin University, Tokyo, Japan
E-mail: dm18014@ns.kogakuin.ac.jp
[2)]Professor, Department of Architecture, Kogakuin University, Tokyo, Japan
E-mail: masaki-t@cc.kogakuin.ac.jp

Abstract

Tiles have been currently used a lot for the outer walls of high-rise buildings in Japan. As for the characteristics of wall tiles, they are materials with strong performance against deterioration such as fire resistance, durability and water resistance, and in addition to being aesthetics in designability. However, since the existing high-rise building, one of the wall tiles are attached with mortar, in case, these tiles may peel off due to aged deterioration of the mortar. Therefore, nowadays in Japan, the regular inspection for wall tiles in high-rise building is enforced to prevent the falling accident by wall tiles.

Wall tiles peeling inspection is generally enforced by a sounding test in Japan. The inspector listens to the reflected sound of the tile wall with his ears and detects the peeled parts of wall tiles. Therefore, there is a difference in judgement accuracy depending on the inspector, and it is difficult to detect small peeled parts of wall tiles.

The purpose of this research is to developed the peeling inspection method independent of inspectors by analyzing reflected sound of tiles. In this research, at first, we conducted tiles peeling surveys of the high-rise building built in 1989 (Fig. 1). As a result, it was confirmed that the peeling wall tiles ratio has been increasing by aging of building. Next, we conducted the experiments using specimens having a deteriorated peeling parts. The tile peeled area ratio of specimens is 0%, 10%, 30%, 50% in all tiles, and we measured hardness values (HLD) of specimens by non-destructive hammering test (Fig. 2) As shown in Figure 3, it was possible to evaluate the condition of the deteriorated the area by HLD value and these peeled parts became small by HLD value. With the results, we confirmed the possibility of tile peeling diagnosis by mechanical impedance method, and evaluate peeling tendency by measuring impact response value.

Fig. 1 High-rise building in Shinjuku, Japan

Fig. 2 Image of non-destructive hammering test (HLD)

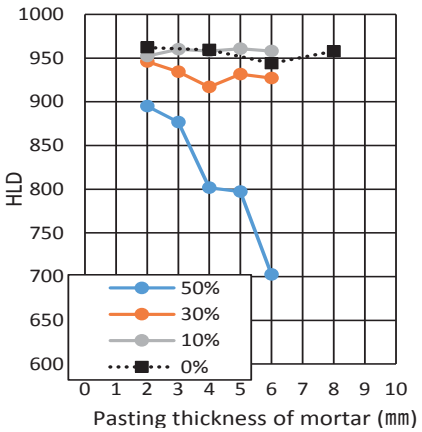

Fig. 3 Results of non-destructive hammering test

References:

[1] Oppata Yuhei, Tamura Masaki, Flaking risk assessment of wall tiles by non-destructive hammering test and sounding test for skyscraper constructed thirty-one years ago, papers of AIJ annual meeting, 2018 (in Japanese)
[2] Oppata Yuhei, Tamura Masaki, Peeling state assessment of wall tiles by non-destructive hammering test, papers of JSFT annual meeting, 2018 (in Japanese)

Deterioration Evaluation of the Stucco Lath Ceilings in the Historic Building in Japan

Misako Hanza[1],Masaki Tamura[2],Kentaro Oka[3],and Osamu Goto[2]
[1] Master Course, Dept. of Arch., Graduate School of Engineering,Kogakuin Univ.,Tokyo,Japan
E-mail: dm18045@ns.kogakuin.ac.jp
[2] Professor, School of Architecture, Kogakuin University,Tokyo,Japan
[3] Visiting Researcher, Kogakuin University,Tokyo,Japan

Abstract

The stucco ceiling have been using in Western-style buildings to be built during from last half of Edo-era to middle twenty century. Currently, almost 100 years have passed which these buildings have been built, and there deteriorations of the stucco lath ceilings might be progressing.Such a type of ceilings is composed by grid framework with small timbers, and wire mesh materials called lath are attached into the inner ceiling and the surface of lathes are covered with laminated stucco. Although the adhesion surface properties by stucco have tendency to depend on the execution condition and would have given some effects to make weak. Besides, a lot of earthquakes occurring in Japan might give an effect of peeling of the plaster ceiling.

In this research, at first we analyze the reason and mechanism of the stucco lath ceiling peeling off, and the next we develop the preventing method of the plaster ceiling from deterioration and peeling off phenomenon.

Fig.1 shows the lath base stucco ceiling which was constructed almost 100 years ago and we could observed the deteriorated conditions. In detail, the lath steel completely seems to be made corrosion regardless of the plaster was thicker than general one. In addition, the using environment of the ceiling might be touching moisture in the room, so with the result, it was the condition that was easy to peel off plaster with the lath.

Fig.2 shows the results of X-ray analyzer (EDX) and a thermal gravimetry analyzer (TG-DTA). The ingredient of $CaCO_3$ was contained in the all plaster layers, and the original ingredient of stucco on Ca $(OH)_2$ was completely carbonated. From this result, the carbonated environment of ceiling space in the room would make the lath corroded. In addition, the ingredient of zinc was not confirmed in the whole lath ingredient, so it was understood that there was no corroding prevention treatment for lath surface, and the lath was easily corroded, and causing peeling off stucco ceilings.

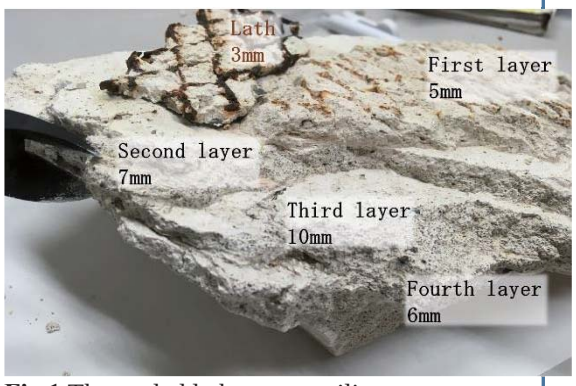

Fig.1 The peeled lath stucco ceiling

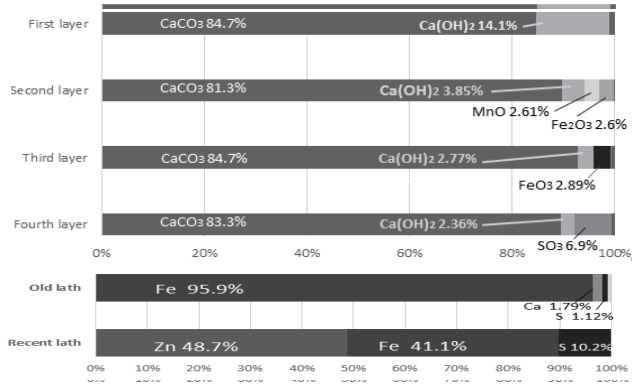

Fig.2 Analysis result of ingredient on lath and stucco

References:

[1]Misako Hanza,Masaki Tamura,Kentaro Oka,Osamu Goto, Evaluation of deterioration of peeled lath plaster ceiling material in heritage architecture,The paper of AIJ on annual meeting, 2018(in Japanese)

[2] Misako Hanza,Masaki Tamura,Kentaro Oka,Osamu Goto, Evaluation of deterioration of peeled lath plaster ceiling material in heritage architecture 100 years after construction, The paper of JSFT of annual meeting,2018(in Japanese)

Designing a program to forecast the service life of mechanically stabilized earth wall used steel reinforcement

Truong-Linh CHAU[1)], Thu Ha NGUYEN[2)]

[1)] Faculty of Bridge and Road Engineering, University of Science and Technology, Da Nang City, Viet Nam
E-mail: chau-linh@dut.udn.vn
[2)] Faculty of Bridge and Road Engineering, University of Science and Technology, Da Nang City, Viet Nam
E-mail: ntha@dut.udn.vn

Abstract

In this study, a program to forecast the service time of mechanically stabilized earth (MSE) wall used reinforcement - MSE-T was developed. To build the software, the authors used the database collected at French Research Institute of Motoways and Highways (SETRA), and National School of Bridges and Roads. The MSE program was developed based on the Visual Studio, using the C # programming language. Calculated result of the software is the corrosion of the reinforcement and service time of the wall. The software was applied to design the retaining wall of Trinh Tung Bridge belonging to the Noi Bai - Lao Cai Highway; then, these calculation results and simulate the corrosion scenarios of reinforced concrete in the wall by FLAC 2D software to calculate the stress - strain, displacement of the wall at the different time.

Keywords: Mechanically stabilized earth wall, database, MSE-T software, corrosion scenario, service life, Principal component analysis (PCA), Response surface.

References:

[1] Duong Hoc Hai, *Design and construction of mechanically stabilized earth wall*, Vietnam Constructuon Publishing edition (2012).
[2] LCPC, ed., *Guide technique - Recommandations pour l'inspection détaillée, le suivi et le diagnostic des ouvrages de soutènement en remblai renforcé par des éléments métalliques*. p.102 (2003).
[3] Truong Linh Chau, Corfdir A., Bourgeois E., *Corrosion des armatures sur le comportement des murs en terre armée - Effect of reinforcement corrosion on the behavior of earth walls reinforced by steel elements*, ISBN 978-3-8417-2710-7, Éditions Universitaires Européennes (2016).
[4] BS 8006:1995-*Code of practice for strengthened/reinforced soils and other fills*. British Standards Institution.
[5] 22TCN 272-2005: Bridge designspecifications. Ministry of transport in Vietnam.
[6] Les ouvrages en terre armée, recommendation et règles de l'art. Guides techniques. SETRA, ed. Ministère des Transports (1979).
[7] Châu Trường Linh, Phạm Văn Lim, *The behaviour and service life research of mechanically stabilized earth wall through reinforcing steel corrosion scenario*, Science Journal of Transportation, Vietnam, ISSN 2354-0818, No. 12/2014. Pages: 36-39 (2014).
[8] Lê Hồng Long, Châu Trường Linh, *Study on effect of types of natural subgrade on interact of soil and steel in Mechanically Stabilized Earth Wall*, Science Journal of Transportation, Vietnam, ISSN 2354-0818, No. 7/2016. Pages: 69-72 (2016).
[9] Jolliffe I.T. *Principal Component Analysis*, Second Edition. Springer Ed (2002).
[10] Faravelli L. *Response surface approach for reliability analysis*. J. Eng. Mech., 115(**12**), 2763- 2781 (1989).

The production of peach-flavored yogurt enriched in isoflavones from soymilk and sweetened condensed milk

Thi Minh Hanh Truong [1)]*, Thi Ngoc Thu Tran[2)], Thi Dong Phuong Nguyen[2)], Xuan Vung Bui[3)], Thi Tuyet Anh Le[3)]

[1)] Department of Chemical Engineering, University of Science and Technology, The University of Danang, Vietnam
Email: ttmhanh@dut.udn.vn
[2)] Department of Chemical Technology-Environment, University of Technology and Education, The University of Danang,Vietnam
Email: ttnthu@ute.udn.vn
[3)] Department of Chemistry, University of Education, The University of Danang, Vietnam
Email: vungxuanbui@gmail.com

Abstract

Fermentation of soybean products by lactic acid bacteria is considered be the most suitable method due to develop more digestible and palatable soy foods but there is only a disadvantage of this method that is the low water holding capacity of (WHC%) protein in soymilk. This study aimed at processing of yogurt from soy milk and condensed milk with the addition of peach aroma and isoflavones from soymilk (SYM) and sweetend condensed milk (SCM). The ratio of soybean milk / condensed milk with 20% condensed milk gave the best sensory characteristics of structure, smell and taste. The product ensured the chemical norms of common yogurt products such as crude protein content of 3.43%, pH 4.43, dry content of 20.64% and isoflavones content of 7,144 mg / 100ml product. Their obtained shelf-life were 9 days at 4°C. When comparing the preference with control sample by hedonic test on a 9-point scale, the results from 100 consumers (26 men and 74 women, from 20 to 25 years of age, unused soy yogurt sample before) showed that the research product was preferred to the control one ($p < 0.005$). This study showed that the addition of isoflavones from soybean extract and peach-flavored increased nutritive (isoflavones content of 14,046 mg/100ml sample) and sensory value, contributed a healthy product for consumers, and diversified yogurt products in the market.

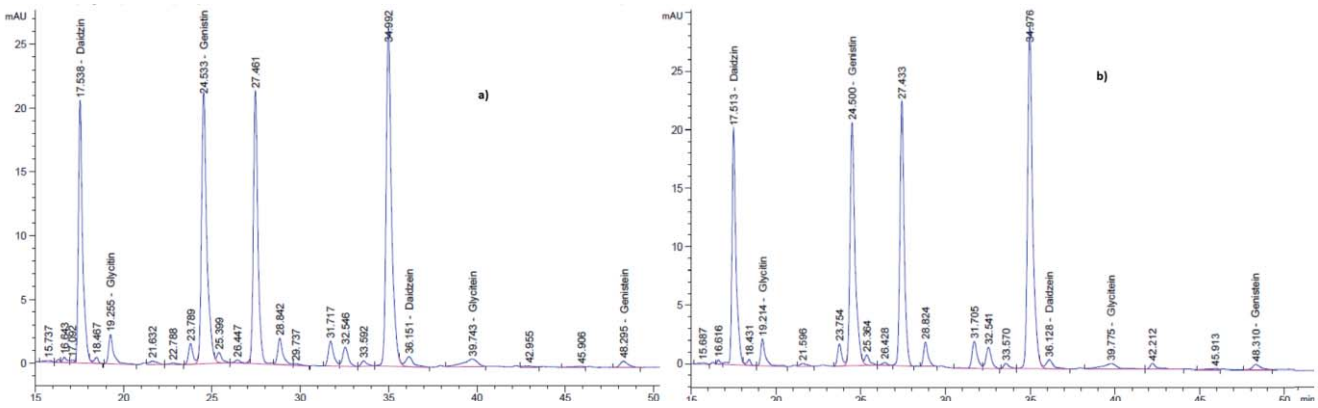

Fig. 1 HPLC chromatograms of isoflavones

a) Isoflavones of pre yogurt SSY3 b) Isoflavones of yogurt sample SSY3

References:

[1] F. Remeuf, S. Mohammed, I. Sodini, J.P. Tissier, International Dairy Journal,**13**, 773–782 (2003)
[2] F Tamjidi, A Nasirpour and M Shahedi, Food Science and Technology International, **18**(4), 381–390 (2012).
[3] Jun Mei, Fei Feng & Yunfei Li, Cyta – Journal of Food, **15**(1), 21–26 (2017).

Electrochemical Measurements for Rechargeable Batteries Single Positive Electrode Particle

Takahiro Saito[1)], Tatsuya Nakamura[2)], Shiro Seki[1)]
[1)]Graduate School of Applied Chemistry and Chemical Engineering, Kogakuin University, Tokyo, Japan
E-mail: bm18021@ns.kogakuin.ac.jp
[2)]Graduate School of Electric Engineering, University of Hyogo, Hyogo, Japan

Abstract

Rechargeable batteries including lithium-ion battery have been used as many power sources. Electrode active materials react as intercalate/de-intercalate component of metal ion, which are governing battery properties. Moreover, electrode fabrication process, porosity and thickness influence for battery performances, such as rate capabilities. So far, most of studies were carried out on composite and thin-film electrodes containing electric conductive additives and binder. Therefore, it is desirable to apply for single electrode active mateeial particle (species, quantities). Single particle electrochemical measurement is important to understand essential battery materials. Therefore, we developed a microelectrode manipulation. By applying this technique, we can obtain essential responses independently from the reaction at the active material and electrolyte interface.

In this study, electrochemical properties of active materials for lithium ($LiCoO_2$) batteries were investigated by single particle electrochemical measurements.

Experiments

The electrochemical measurements were carried out in the argon-filled glovebox (-70℃ dew point). A Pt microelectrode (20 μm diam.) was directry attached to a $LiCoO_2$ particle (10-20 μm diam., Figure 1) into the electrolyte using a micromanipulator under optical microscope observation, then the electrochemical measurements were carried out. 1M-$LiPF_6$/propylene carbonate solution was used as electrolyte. Li foil was used as negative (counter) electrode. All electrochemical measurements were carried out at room temperature. We measured electrochemical performance of two fabricated batteries; single particle (a) and pasted type cells (b) by cyclic voltammetry (CV), constant current charge and discharge (CDC), and electrochemical impedance spectroscopy at several potentials (3.8-4.4 V).

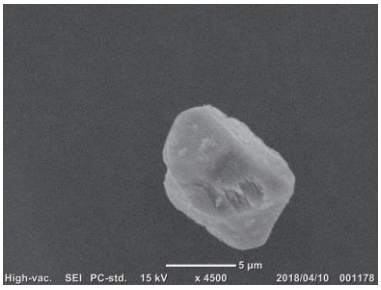

Fig.1. SEM image of $LiCoO_2$ single particle.

Results & Discussion

CV for $LiCoO_2$ particle (19.0 μm diam.) result shows quite small order current peaks (nA) and stable oxidation/reduction reactions in 30 cycles. Fig.2 (a) shows nyquist plots for $LiCoO_2$ particle (22.4 μm diam.). We detected up to MΩ order resistance in a frequency range from 20 kHz to 10 mHz. Comparing the Nyquist plots, it is shown that the response frequencies of the first semicircular arc of the single particle and the second semicircular arc of the paste cell are almost same. If the first semicircular arc of the paste cell is assumed to be the resistance component derived from the negative electrode, the resistance component with the matching response frequency is considered to be derived from the positive electrode active material / the electrolyte solution interface. Furthermore, in this presentation, we will discuss the electric capacity of single particles from the results of CDC of comparison for single particles and pasted type cells.

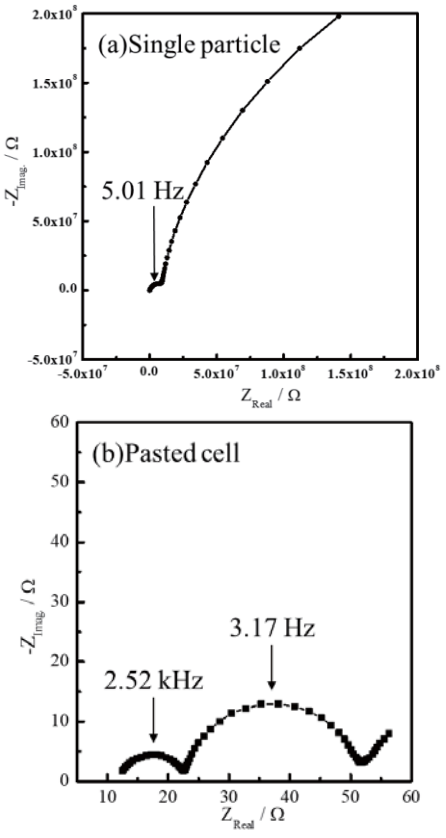

Fig.2. Nyquist plots for lithium battery (a) $LiCoO_2$ single particle, (b)pasted electrode.

References

[1] T. Saito, T. Nakamura, and S. Seki, Fall meeting of Electrochemical Society in Japan, 1F19 (2018).

Na conductive polymer/inorganic hybrid electrolyte for high performance-all-solid-state battery

Koji Hiraoka[1)], Kato Masaki[1)], Hidefumi Motobayashi[2)], Hiroshi Kaneko[2)], Yuzo Tasaki[2)], Shiro Seki[1)]

[1)] Graduate school of applied chemistry and engineering, Kogakuin University, Tokyo, Japan

E-mail: bm18040@ns.kogakuin.ac.jp

[2)] TOSHIMA Manufacturing Co., Ltd., Saitama, Japan

Li-ion batteries reveal increasing demand for expanding market of electric vehicle (EV) and energy storage for renewable energy. But recently, depletion of elemental Li are concerned due to the low presence in the earth crust. Na have not constraint resource because of a large quantity in the crust more than 100 times compared to Li. Moreover, Na is expected as low cost elemental resource. There, Na batteries has been attracted attention as an environmental friendly application. However, like conventional Li-ion batteries, Na batteries are used flammable electrolyte including organic solvent. In recent years, the accidents of EV are increasing by firing of batteries. Therefore, all-solid-state batteries using solid electrolyte has been desired. There are mainly two types of solid electrolytes, inorganic electrolyte and polymer electrolyte. Inorganic electrolytes are known to exhibit relatively high ionic conductivity (~10^{-3} Scm^{-1} at room temperature). But stability at interface between electrode and electrolyte are shown the low value for many inorganic electrolytes. On the other hand, polymer electrolytes has high interfacial stability and flexibility, however, these electrolytes exhibits relatively low ionic conductivity (~10^{-5} Scm^{-1} at room temperature). In this study, we prepared polymer/inorganic hybrid electrolyte for utilize both advantages and apply these electrolytes to all-solid-state Na battery.

In the globe box ([H_2O] <0.5ppm, [O_2] <5ppm), polymer/inorganic hybrid electrolytes were prepared by mixing of polyether based polymer, NaN $(SO_2CF_3)_2$ as an alkaline salt, 2, 2-dimethoxy-2-phenylacetophenone as a photoinitiator, acetnitrile as a solvent, $Na_3Zr_2Si_2PO_{12}$ (NZSP) as an inorganic electrolyte. NZSP has structure of Na super ionic conductor (NASICON) and high ionic conductivity. In this study, composition percentage of NZSP were 0~ 300wt% compounded. After stirring, the solution vacuum dried were casted to glass substrate and polymerized by UV irradiation to form hybrid electrolyte membrane. Hybrid electrolytes were evaluated characterization, interaction of molecular bound, thermal properties and ionic conductivity by scanning electron microscopy (SEM), energy dispersed X-ray spectroscopy (EDX), fourier transform infrared (FT-IR), differential scanning calorimetry (DSC) and AC impedance method, respectively. Moreover, Na ion transference number were evaluated by AC impedance up to low frequency.

Fig. 1 shows SEM image of cross-section of polymer/inorganic hybrid electrolyte containing 30wt% NZSP. The dark and bright point were detected as polymer phases and NZSP particles by EDX mapping, respectively. It is confirmed that the NZSP particles were uniformly dispersed to polymer phase in this composition. Furthermore, flexibility of hybrid electrolyte membranes improved compared to NZSP free sample. However, mechanical strength was decreased in the system containing high composition NZSP. In this study, glass transition temperature (T_g) were defined as the points that the baseline of DSC curve changed. Although T_g appeared approximately -25°C in composition 0wt%, T_gs were decreased to 3~10°C by compounding NZSP. T_g similar with 0 wt% were confirmed in the case of high composition NZSP. The temperature dependence of ionic conductivity are shown in the Fig. 2. The 30wt% NZSP sample were exhibited the highest ionic conductivity in the all temperature range, especially, this composition was improved the value about 6 times compared to 0 wt% at the low temperature. On the other hand, hybrid electrolytes beyond 100wt% NZSP were showed low ionic conductivity compared to 0 wt% in the all range. In the Nyquist plot, semicircle shows approximately symmetric shape, but beyond 100wt% exhibited asymmetric semicircle. Therefore, it is considered that the decreasing ionic conductivity were caused by formation of grain boundary of each NZSP particles. From the above, there are possibility of Na ion transport two types of path, polymer phase and NZSP particles.

From this study, the polymer/inorganic hybrid electrolyte containing 30wt% NZSP was suggested low temperature operation of all-solid-state Na batteries.

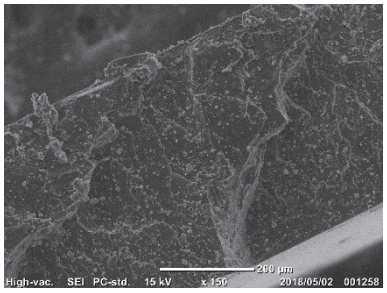

Fig. 1 SEM image of polymer/inorgnic hybrid electrolyte (30wt% NZSP).

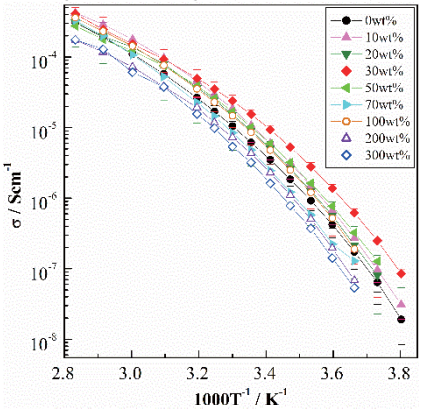

Fig. 2 Temperature dependence of ionic conductivity.

A Method Football Team Model Optimization and Application of the Optimization Control

Nguyen Hoang Mai
Department of The Electrical Engineering, Danang University of the Science and Technology, Vietnam
E-mail: nhmai@dut.udn.vn

Abstract

The development of the AI, IoT, and Big Data have to find an optimization method to reduce the number of parameters in the calculation at any time. We introduce a Football Team Optimization (FTO) method, which is a new method to do optimization problem while control with many parameters system. The application and analysis to compare any method as PSO, traditional PID, which takes out the difference of this algorithm.

We have to meet many applications in the practice to control with a selection of the parameters for one target. In the MIMO systems, as swarm optimization of robot team, choice sensors system in the machines, control planes go up and go down to runway and etc…we have one target for control variables. We call that is a Football Team Model, which is advanced control by self-organized.

There is a system MIMO as figure 5. In that, $\mathbf{x} = [x_1, x_2, \ldots, x_n]'$ is a state vector with assume continuous signal and exists high order of derivations, the **x** includes input signals $\mathbf{y_0}$, which is a subset of **x**, $\mathbf{y} = [y_1' y_2, \ldots, y_m]'$ is an output vector, $\mathbf{d} = [d_1, d_2, \ldots, d_r]'$ is a disturbance vector.

$$\mathbf{x} = \left[x_1, x_2, ..., x_n\right]'; \mathbf{x}^{(1)} = \left[\dot{x}_1, \dot{x}_2, ..., \dot{x}_n\right]; ...; \mathbf{x}^{(l)} = \left[x_1^{(l)}, x_2^{(l)}, ..., x_n^{(l)}\right]$$

We define "distance of control" is a state variable x. That is a difference of set parameter value and output value. Because output signal depends on some input signals (MISO), so we can see that's crossing of the input signals with output signals as figure 6 to calibrate parameters of controller [8],[9].

In figure 6, the block **f**(**e**) decides **e**vector and choices parameter area for calibration. After reduces area of searching, **f**(**e**) does any parameter to directly calibrate.

We go back to our football team as figure 1. A system controls one target at a time with the choice main parameter. Start at $\mathbf{x} \in R^{nx1}$, we choose the main parameter as follow with absolute values:

$$\tilde{x}_k = Min\left(x_1, x_2, ..., x_n\right) \quad \dot{\tilde{x}}_i = Max\left(\dot{x}_1, \dot{x}_2, ..., \dot{x}_n\right) \quad \ddot{\tilde{x}}_j = Max\left(\ddot{x}_1, \ddot{x}_2, ..., \ddot{x}_n\right) \quad \ldots$$

We could choice higher order so it isn't well because have to difficultly calculate. After defining the main parameter, we have tree variables with sequence *k, i, j*. In general, $k \neq i \neq j$, so we continue to filter for one time to decide tree couples of variables $\left(\dot{x}_k, \ddot{x}_k\right), \left(x_i, \ddot{x}_i\right), \left(\dot{x}_j, x_j\right)$. If we choose a higher order then we will have set as follow:

$$\left\{\tilde{x}_k = Min\left(\mathbf{x}\right) with\, k \in 1..n ... with\, j \in 1..n ... \tilde{x}_q^{(p)} = Max\left(\mathbf{x}^{(p)}\right) with\, q \in 1..n;\right.$$

And set filter:

$$\left\{\left(\dot{x}_k, \ddot{x}_k, ..., x_k^{(p)}\right); \left(x_i, \ddot{x}_i, ..., x_i^{(p)}\right); \left(x_j, \dot{x}_j, ..., x_j^{(p)}\right) ...; \left(x_q, \dot{x}_q, ..., x_q^{(p-1)}\right)\right.$$

We define a set of the time variable:

$$t_k = \frac{x_k}{\dot{x}_k}, t_k^{(1)} = \frac{\dot{x}_k}{\ddot{x}_k}, ..., t_k^{(p)} = \frac{x_k^{(p-1)}}{x_k^{(p)}} \quad \ldots \quad t_q = \frac{x_q}{\dot{x}_q}, t_q^{(1)} = \frac{\dot{x}_q}{\ddot{x}_q}, ..., t_q^{(p)} = \frac{x_q^{(p-1)}}{x_q^{(p)}}$$

We choice x_l with $t_l^{(1)}$. If we have any time variables as same then we continue select to the end of the set variable. After we calculate:

$$t_l = Min\left[\left(\prod_{d=0}^{p-1} t_k^{(d)}\right), \left(\prod_{d=0}^{p-1} t_i^{(d)}\right), ..., \left(\prod_{d=0}^{p-1} t_q^{(d)}\right)\right]$$

And the main parameter is an x_l. So we have to choose the correct parameter to do priority control.

From that, we have a theory:

Theory: If there is a MIMO as (2), we can choice control variable with the law from (6) to (14) to ensure the control time is a minimum.

Simulation

We start action with estimation of PID parameters [10],[11]. Although robot manipulator is a nonlinear system, so we could use PID controller to control with strain domain. After design controller and do it, we receive an error of the trajectories of joint 1st is 15% and joint 2nd is 10% (average value). This is a big error in practice if use big trajectory more.

Reference

[1]. Natika W. Newton, *Understanding and Self-Organization*, Front Syst Neurosci. 2017, Mar 2. doi: 10.3389

Application of PGM absorbent for plating wastewater treatment

Le Thi Xuan Thuy[1)], Nguyen Ngoc Huy[2)], Le Thi Suong[2)] and Nguyen Thi Sao Mai[2)]

[1)] Faculty of Environment, University of Science and Technology, The University of Da Nang, Da Nang, Viet Nam
E-mail: letxthuy@gmail.com
[2)] SUSTECH Green Environmental Company Limited, Da Nang, Viet Nam

Abstract

Plating wastewater is known as both high concentration of heavy metals and low pH. Because of these two characteristics, there are many issues related to the neutralization method to raise the pH and remove completely heavy metals in wastewater for requirement of QCVN 40:2011/BTNMT - National Technical Regulation on Industrial wastewater. In this study, we experiment on wastewater that include a lot of heavy metals with high concentration from Da Nang Mechanical - Plating Factory. Athough the current method use limes to raise pH from 2-3 to 6, lots of heavy metals remained in treated water. Therefore we proposed hybrid method for combining oxidation-reduction, neutralization, coagulation and adsorption methods by γ-Poly Glutamic Acid Coated Magnetite Nanoparticles (PGM) for treatment of heavy metals in wastewater.

The 500 Liters/batch model for treating wastewater was installed at Danang Mechanical - Plating Factory. The wastewater from Hot-Dip Galvanizing process included acid picking tanks, rinsing tanks, flux tank and passivation tanks led to the containers forming the wastewater mixture. This process also produced redox reaction where Cr (VI) in passive waste water was mostly degraded into Cr (III) by acidic wastewater (acid picking tanks, rinsing tanks). The results showed that the mixed effluent had low pH and high concentration of heavy metals including Fe, Zn, Pb, Cd and Cr (Table 1).

The wastewater then was pumped into the Caustic soda Mixing tank to raise pH to 9. Next, the anionic polymer was added to promote the flocculation of the cotton as well as shorten the settling time of heavy metal hydroxides. Post-settling water was passed through the PGM Mixing tank to thoroughly treat the heavy metal ions left. The separation of PGM in water was facilitated by the magnetic field of the permanent magnets placed in the water pipe after adsorption. The treated water then kept in clean water containers. The sludge produced in the Caustic soda Mixing tank was passed through a Vertical Basket Top Discharge Centrifuge to reduce moisture content before contained to drying areas. PGM was retained by a magnet that was easily separated thanks to the design of nylon sheathed magnets and was desorbed to reuse for subsequent batches.

The results of heavy metals concentrations after treatment in 3 batches showed very high treatment efficiency (Table 1, Fig. 1). Heavy metals concentrations reached QCVN 40: 2011/BTNMT, column B.

Table 1 Waste water treatment performance of the experimental batches

Batches		Heavy metals				
		Fe	Zn	Pb	Cd	Cr total
No. 1	Before treatment (mg/L)	1961	3720	0,99	0,13	1,22
	After treatment (mg/L)	0,25	0,16	0,46	0,07	0,23
	Remove efficiency (%)	**99,99**	**99,99**	**53,36**	**45,74**	**81,17**
No. 2	Before treatment (mg/L)	1867	1194	1,30	12,6	15,6
	After treatment (mg/L)	0,02	0,18	0,17	0,06	0,06
	Remove efficiency (%)	**99,99**	**99,99**	**87,09**	**99,52**	**99,59**
No. 3	Before treatment (mg/L)	3582	1933	0,34	0,011	9,75
	After treatment (mg/L)	0,20	0,20	ND	ND	0,15
	Remove efficiency (%)	**99,99**	**98,82**	**100**	**100**	**98,51**
QCVN 40: 2011/BTNMT, column B		**5**	**3**	**0,5**	**0,1**	**-**

(ND: Not detected)

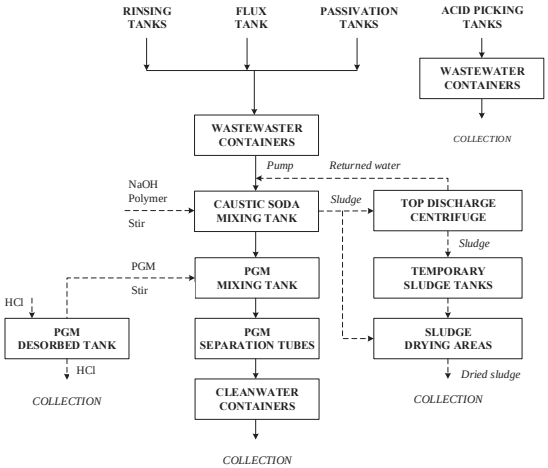

Figure 1 *Technological process diagram*

References:

[1] Baskaran Stephen Inbaraj, Bing-Huei Chen, *Interantional Journal of Nanomedicine*, 7, 4419 - 4432 (2012).

[2] Chang Jing, Zhong Zhaoxiang, Xu Hong, Yao Zhong and Chen Rizhi, *Chinese Journal of Chemical Engineering*, 21(11), 1244 - 1250 (2013).

[3] Le Thi Xuan Thuy, Mikito Yasuzawa, Tomoki Yabutani, *Lambert Academic Publishing* (2015).

[4] Zhang Juan, *Dissertation*, Tokushima University (2011).

Can reaction-transport diagenetic modelling support management efforts? A case study in the Bay of Quinte (Lake Ontario), Canada

Phuong T.K. Doan[1]

[1)] Department of Water Resources Engineering, The University of Danang, University of Science and Technology, Vietnam
E-mail: dtkphuong@dut.udn.vn; kimphuongdhbk@gmail.com

Abstract

In this study, we investigated phosphorus (P) cycling in the Bay of Quinte, an embayment of Lake Ontario, Canada. Despite a decline of external P loading to the Bay of Quinte during last decades, it still experiences harmful cyanobacterial algal blooms, which were hypothesized to be connected to nutrient loading from sediments. However, dynamics of nutrient loading from sediments remain largely unknown. We applied a non-steady state reaction-transport diagenetic model to conduct specific modelling scenarios for a 20% reduction of agriculture based total loads to evaluate how further long in the future for the new sediment based equilibrium to be established and to investigate the impact of organic matter loading on seasonal dynamics of P release, and burial efficiency in three different basins (Belleville, Napanee, Hay Bay) of the Bay. Our modelling framework integrated physical and biogeochemical processes at the sediment water interface (SWI) and incorporated dynamic boundary conditions, such as oxygen, soluble reactive phosphorus concentrations and organic matter sedimentation at the SWI. In the model, P was divided into adsorbed, redox-sensitive, organic, aluminum-bound, and apatite forms.

Our scenarios suggested that P release and burial efficiency can profoundly respond to shifts in sedimentation conditions. At all three studied stations, P release and burial efficiency did not change significantly after the scenario year 2034 when we reduced 20% flux of organic matter. Especially, it had a large reduction of P release at the station B in 2034 after reducing 20% P flux comparing to the present condition. However, for the station HB, the reduction of 20% flux of organic matter may not large enough to be able to reduce P release remarkably.

Keywords:
Great Lakes,
Phosphorus release,
Phosphorus burial efficiency,
Sediments,
Diagenetic modelling.

Multi-class classification model for urban land cover

Trang Thi Phuong Pham

Department of Civil Engineering, Danang University of Technology and Education, Vietmam
E-mail: trangpham3112@gmail.com

Abstract

Land cover in urban areas plays an important role in modern urban planning and management. Information about land cover is important in every city because it is used for many purposes, including tax assessment, setting land use policy, city planning, zoning regulation, analysis of environmental problems, and management of natural resources. Therefore, accurate and readily produced land cover classification maps are of great importance in studies of global change. This study proposed a classification model that integrates the decomposition approach and the support vector machine (SVM). Based on the provided engineering data - Urban land cover, the analytical results confirm the proposed model has 85.778% predictive accuracy.

Decomposition strategies [2] are commonly used to solve multiple class problems. Some studies [3, 4] demonstrated one-against-one (OAO) [5] is one of the most effective decomposition strategies. Support vector machines (SVM) [6] has been a powerful technique in solving pattern recognition problems. It is time-saving in computation when solving high-dimension problems, which cannot be achieved by artificial neural networks, logistic regression, decision tree, etc [7]. Hence, this study could be addressed by the OAO strategy which modifies the binary SVM to handle multiclass tasks-urban land cover. The proposed model is called OAO-SVM.

The dataset of urban land cover comes from the UCI Machine Learning Repository. The land cover dataset includes a total of 147 features, which include the spectral, magnitude, formal and textural properties of image of land. The data specify nine forms of land cover - trees (Class 1), concrete (Class 2), shadows (Class 3), asphalt (Class 4), buildings (Class 5), grass (Class 6), pools (Class 7), cars (Class 8) and soil (Class 9), which are treated as the predictive classes.

The performance of the proposed model was evaluated in terms of accuracy which is the most common and important used index, precision, sensitivity, specificity and the area under the curve (AUC). To verify the effectively of the proposed model, this study compare the result of proposed model with other multiple models - Multiclass Classifier, Logistic and the Library Support vector machine (LibSVM) - and experimental results. Durduran (2013) used three classification algorithms - k-NN, SVM and extreme learning machine (ELM), each combined with the OAR scheme - to predict urban land cover [1]. Table 1 showed the comparison results of several multi-class models, empirical models and OAO-SVM model. As shown in Table 1, the OAO-SVM model had an accuracy of 85.778%, a precision of 85.800%, a sensitivity of 86.000%, a specificity of 89.000% and an AUC of 0.875. Clearly, the OAO-SVM model outperformed the other models in almost these respects.

Table 1 Comparison results

Empirical models reported in primary works and single multi-class models	Performance measure				
	Accuracy (%)	Precision (%)	Sensitivity (%)	Specificity (%)	AUC
Multiclass Classifier	64.900	64.900	64.800	99.400	0.821
Logistic	65.926	65.900	65.900	95.300	0.806
LibSVM	18.370	18.400	19.000	81.400	0.502
k-NN classifier [1]	80.140	-	-	-	-
ELM classifier [1]	84.700	-	-	-	-
SVM classifier [1]	84.890	-	-	-	-
OAO-SVM	85.778	85.800	86.000	89.000	0.875

References:

[1] S.S. Durduran, Automatic classification of high resolution land cover using a new data weighting procedure: The combination of k-means clustering algorithm and central tendency measures (KMC–CTM), Applied Soft Computing 35 (2015) 136-150.

[2] A.C. Lorena, A.C.P.L.F. de Carvalho, J.M.P. Gama, A review on the combination of binary classifiers in multiclass problems, Artificial Intelligence Review 30(1) (2009) 19.

[3] M. Galar, A. Fernández, E. Barrenechea, F. Herrera, DRCW-OVO: Distance-based relative competence weighting combination for One-vs-One strategy in multi-class problems, Pattern Recognition 48(1) (2015) 28-42.

[4] S. Kang, S. Cho, P. Kang, Constructing a multi-class classifier using one-against-one approach with different binary classifiers, Neurocomput. 149(PB) (2015) 677-682.

[5] M. Hall, E. Frank, G. Holmes, B. Pfahringer, P. Reutemann, I.H. Witten, The WEKA data mining software: an update, SIGKDD Explor. Newsl. 11(1) (2009) 10-18.

[6] V.N. Vapnik, The nature of statistical learning theory, Springer-Verlag, New York, 1995.

[7] Y. Tian, M. Fu, F. Wu, Steel plates fault diagnosis on the basis of support vector machines, Neurocomputing 151, Part 1 (2015) 296-303.

Optimization of mangiferin extraction from mango (*mangifera indica l.*) leaves using ultrasound-assisted methodology

Truc Loan Nguyen, Trinh Pham

Department of Chemical Engineering, The University of Danang-University of Science and Technology, Da Nang, Viet Nam
E-mail: nttloan@dut.udn.vn, trinh.pham@dut.udn.vn

Abstract

In the present study, an ultrasonic- assisted extraction method was developed for the effective extraction of mangiferin from mango leaves with ethanol solvents. Mangiferin extraction from mango leaves was investigated by single experiments with optimal conditions: solvent concentration 70º, w /v, solid-to-liquid ratio 1:20, 80% amplitude, cycle 0.8 seconds, ultrasonic time 20 minutes and optimized using the Box Behnken model and DOE software. The regression equation expressing the relationship between optical absorption and independent variables is as follows: $Y = 0.66223 - 0.03525X_1 + 0.05X_2 - 0.021X_3 - 0.05482X_{12} - 0.09132X_{32} + 0.02750X_1X_3$ where Y is optical absorption, X_1 is the solvent concentration, X_2 is the w/ v (g/ ml) ratio and X_3 is the ultrasonic time (minutes). The optimal conditions for the highest extraction efficiency were calculated: 66.3º ethanol, the solid-to-liquid ratio was 1:30, and extraction time for 17.1 min under ultrasound irradiation (200 W) with a 0.8 seconds cycle, 80 % amplitude. Under the optimal conditions the optical absorption of the extract is 0.7204 Abs. The presence of the mangiferin in the extract was confirmed using high performance liquid chromatography. Under optimal conditions of ultrasonic-assisted extraction, the yield of mangiferin was 59.427 mg/g, significantly higher than that of Shoxlet extraction and microwave – assisted extraction.

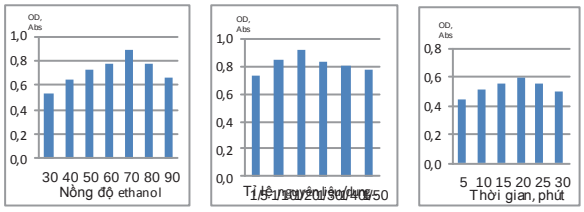

Fig 1: The effect of ethanol concentration, solid-to-liquid ratio, ultrasonic time to optical absorption of extract from mango leave.

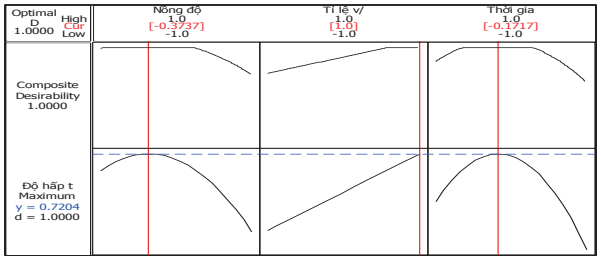

Fig 2: Optimal condition for highest yield extraction.

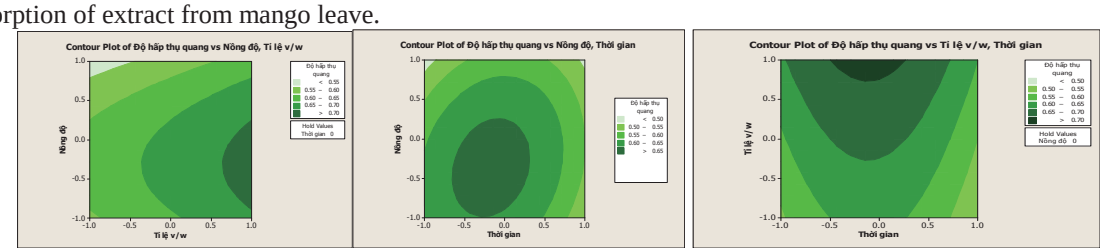

Fig. 3: The chart of the 2D value value for each condition extraction

References:

[1] S. Muruganandan, K. Srinivasan, S. Gupta, P.K. Gupta, J. Lal, Effect of mangiferin on hyperglycemia and atherogenicity in streptozotocin diabetic rats, *Journal of Ethnopharmacology*, **97**, 497 – 50, (2005).

[2] Tang-Bin Zou, En-Qin Xia, Tai-Ping He, Ming-Yuan Huang, Qing Jia and Hua-Wen Li, Ultrasound-Assisted Extraction of Mangiferin from Mango (Mangiferin indica L.) Leaves Using Response Surface Methodology, *Molecules*, **19(2),** 1411 – 1421 (2014).

[3] XIE Yu+qi, LIN Cui-wul,LAI Qing-hua, HUANG Cui-you, Determination of chlorophyll and mangiferin content in mango leaves by using UV-VIS Spectrum, *Journal of Southern Agriculture*, **03**, 463-468 (2014).

[4] Zhang, X.; Su, B.; Li, J.; Li, Y.; Lu, D.; Zhu, K.; Pei, H.; Zhao, M. Analysis by RP-HPLC of mangiferin component correlation between medicinal loranthus and their mango host trees. *Chromatography Science*. **52**, 1–4 (2014).

[6] http://naturalchemistry.utu.fi/research/qualitative-analysis/uv-spectra-of-polyphenols/.

[7] Zou, T.B.; Wu, H.F.; Li, H.W.; Jia, Q.; Song, G. Comparison of microwave-assisted and conventional extraction of mangiferin from mango (Mangifera indica L.) leaves. *Journal of Separation Science*, **36**, 3457–346 (2013).

A Study on Development of a Tangible Interface for an Introduction to Computer Programming Education Using QR codes

Ryota Tominaga[1)], and Hidetoshi Saito[2)]

[1)] Graduate School of Engineering, Kogakuin University, Tokyo, Japan
E-mail: cm18054@ns.kogakuin.ac.jp
[2)] Department of Applied Physics, School of Advanced Engineering, Kogakuin University, Tokyo, Japan
E-mail: h-saito@cc.kogakuin.ac.jp

Abstract

Recently, there is increasing interest in informatics and programming education at the elementary and secondary level around the world. In this report, we introduce a programming support tool to learn about basics of computer programming for an elementary school student. Using this tool, it provides a simple programming environment with a *tangible user interface* (TUI). That is to say, students can write programs using a QR reader (QR scanner) which scan a specific previously determined codeword one by one in our system. This input method provides a relatively easy programming processes compared to the conventional method using an input interface such as a keyboard or mouse.

Introduction

Nowadays informatics or computer science is important subject in school education. Informatics requires a consistent discipline for understanding modern *information and communications technology* (ICT) systems using computer programs. So far informatics has been developing its own fundamental concepts of communication, knowledge, data, interaction and information, and relating them to such phenomena as computation, language, and implementation [1], [2]. Bringing Informatics to schools means preparing young people to be creators of future ICT services not only to be users of technological devices. Therefore, not only professionals but also everyone use programming and we will need more easy-to-use programming environments. It points out that a TUI gives some benefits of collaborative learning and interaction[3], [4]. In this study, we develop a programming environment with a prototype of the TUI.

Proposed Programming Support Tool for Education

Fig. 1 shows the block diagram of our proposed system. In this system, the TUI for physical manipulation is a QR reader. Typically, a TUI can integrate two representations by mixing the input and the output of the software. The input is often a manipulation of physical objects related to familiar objects and the output can be displayed on a screen or augment the objects with the help of a projector. The input is a specific codeword in the used QR code and the output is lighting at each LED lamp in our system. In our proposed programming method, the QR reader scans the codeword for the starting process at first. To control LED lighting, the reader scans the codewords for the identifying number of each LED lamp and for the timer to set a lighting period of lighting each light source, respectively. Finally, the reader scans the codeword for the ending process. When a user ends all of the programming processes, the reader scans the codeword to compile and execute an application programming language in a managed QR code environment.

Conclusions

Implications of the proposed programming support tool based on the TUI are discussed in terms of the benefits of tangibility for education. In our future works, it needs to find the other application using such a proposed tool.

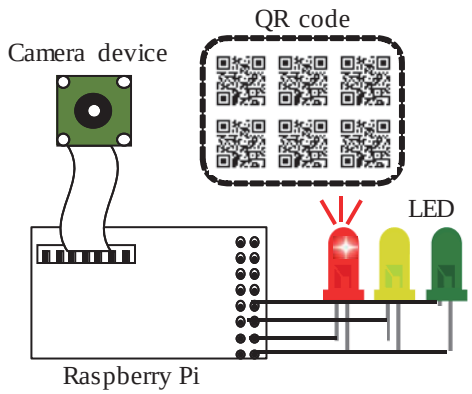

Fig. 1 Block diagram of the proposed system.

References:

[1] V. Dagiene *et al.*, *Journal of Information Processing*, **24**, 4, 732–739, July 2016.
[2] S. Kanemune *et al.*, *Olympiads in Informatics*, **11**, 143–150, 2017.
[3] M. S. Horn *et al.*, *in Proc. of the 27th international conf. on Human factors in computing system (CHI'09)*, 975-984, Boston, MA, USA, April 4-9, 2009.
[4] B. Schneider *et al.*, *IEEE Trans. Learn. Technol.*, **4**, 3, 222-232, July-Sept. 2011.

Analysis of Deep Ultraviolet Emission Properties in Rocksalt-structured $Mg_xZn_{1-x}O$ Films

Mizuki Ono[1)], Kyohei Ishii[2)], Kentaro Kaneko[2,3)], Tomohiro Yamaguchi[1)], Tohru Honda[1)], Shizuo Fujita[2,3)] and Takeyoshi Onuma[1)]

[1)] Department of Electrical Engineering and Electronics, Kogakuin University, Tokyo, Japan
E-mail: cm17013@ns.kogakuin.ac.jp
[2)] Department of Electric Science and Engineering, Kyoto University, Kyoto, Japan
[3)] Photonics and Electronics Science and Engineering Center, Kyoto University, Kyoto, Japan

Abstract

Deep ultraviolet (DUV) and vacuum ultraviolet (VUV) lights are drawing attention in the field of medical care, material science, and so on. Bandgap energies E_g of $Mg_xZn_{1-x}O$ alloys can be tuned from 3.3 eV (x = 0; ZnO) to 7.8 eV (x = 1; MgO) with the MgO molar fraction x [1,2]. Especially, E_g values higher than 6 eV cannot be realized by (Al, Ga, In)N alloy system. Recently, successful growths of atomically-flat rocksalt-structured (RS) $Mg_xZn_{1-x}O$ ($x > 0.5$) epitaxial films on (001) MgO substrates have been demonstrated by the mist chemical vapor deposition (mist CVD) method [3,4]. In this paper, excitation density and temperature dependent cathodoluminescence (CL) spectra are comprehensively shown to clarify the detailed emission mechanism.

250-550-nm-thick RS-$Mg_xZn_{1-x}O$ films were grown on (001) MgO substrates by the mist CVD method [3,4]. The x values were evaluated by energy dispersion X-ray measurements to be x = 0.92, 0.81, 0.74 and 0.61. The CL measurements were carried out as functions of temperature from 6 to 300 K and excitation current density from 1.1×10^{-5} to 3.4×10^{-2} A/cm^2.

As shown in Fig. 1(a), excitation current density dependent CL spectra at 6 K for $Mg_{0.92}Zn_{0.08}O$ film exhibit UV and DUV luminescence bands around 5.4-6.1 and 4.4-5.1 eV, respectively. The peaks energies are lower than E_g of 6.5 eV [5]. In order to investigate the origin of the luminescence bands, normalized spectrally integrated CL intensities and fitting curves by the rate equation for the luminescence bands are plotted as a function of generation rate in Fig. 1(b). Calculated results indicate that DUV and UV luminescence are originated from near band edge (NBE) transition and transition involving the deep level states, respectively. Temperature dependent CL spectra for x = 0.92, 0.81, 0.74, and 0.64 are shown in Fig. 2(a)-(d). DUV luminescence band was predominantly observed in all samples. Large full width at half maximum values and large Stokes-like shift for the NBE emissions imply the E_g fluctuation in the RS- $Mg_xZn_{1-x}O$ alloys [5].

This work was supported in part by Grants-in-Aid for Scientific Research No. 17H01263 from MEXT, Japan.

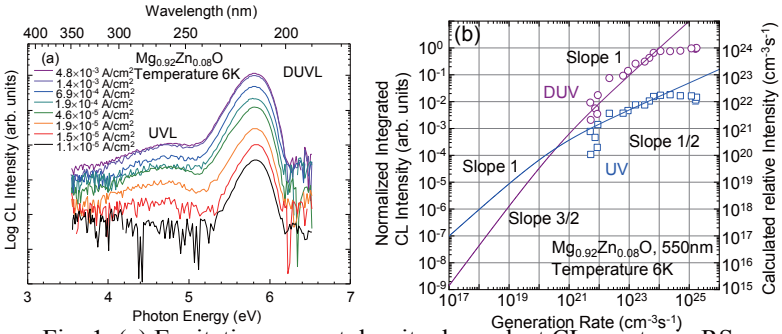

Fig. 1. (a) Excitation current density dependent CL spectra in RS-$Mg_{0.92}Zn_{0.08}O$ film and (b) normalized integrated CL intensity and fitting curves.

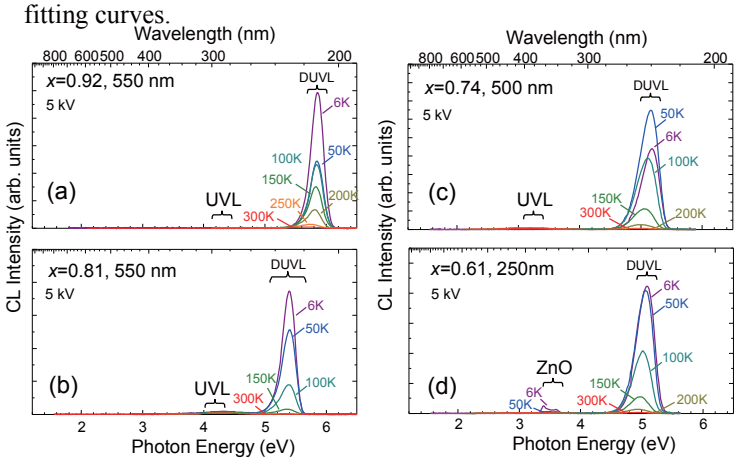

Fig. 2. Temperature dependent CL spectra of RS-$Mg_xZn_{1-x}O$ films for (a) x=0.92, (b) x=0.81, (c) x=0.74, and (d) x=0.61.

References

[1] A. Ohtomo *et al*., Appl. Phys. Lett. **72**, 2466 (1998).
[2] R. C. Whited and W. C. Walker, PRL **22**, 1428 (1969).
[3] K. Kaneko *et al*., APEX **9**, 111102 (2016).
[4] K. Ishii *et al.*, *JSMS Committee on Semiconductor Electronics*, Kyoto, July 15 (2017), No. 9.
[5] T. Onuma *et al*., Appl. Phys. Lett. **113**, 061903 (2018).

Growth and Characterization of Single Crystalline α-Ga_2O_3 Film on *c*-plane Sapphire Substrates by Mist CVD

Kenichiro Rikitake*, Tomohiro Yamaguchi, Takeyoshi Onuma and Tohru Honda

Department of Electrical Engineering and Electronics, Graduate School of Engineering,
Kogakuin University, Tokyo, Japan
E-mail: cm17055@ns.kogakuin.ac.jp

Abstract

Gallium oxide (Ga_2O_3) has six polymorphs including α-, β-, γ-, δ-, ε-, [1] and κ-phase [2]. Among them, β-phase Ga_2O_3 is the most thermally stable crystal structure, and other phases are in metastable structures. Nevertheless, the growth of corundum-structured gallium oxide (α-Ga_2O_3) films with this metastable structure has been realized by mist Chemical Vapor Deposition (mist CVD) [3]. α-Ga_2O_3 has a wide bandgap of 5.3 eV, and the bandgap engineering is possible in whole composition range of α-(Al, Ga, In)$_2O_3$ alloys [3, 4]. Moreover, they can be heteroepitaxially grown on a variety of corundum-structured oxide materials, e.g., α-Cr_2O_3, α-Fe_2O_3, etc. In addition, Schottky barrier diodes (SBDs) have reported using α-Ga_2O_3 [5]. Therefore, α-Ga_2O_3 has been attracted increasing interest due to the above reasons.

In this study, single crystalline α-Ga_2O_3 film on *c*-plane sapphire substrates was grown by mist CVD and investigated its characteristics.

Unintentionally-doped α-Ga_2O_3 film was grown on *c*-plane sapphire substrates by mist CVD. Gallium acetylacetonate was used as a source material for this mist CVD growth, and this was solved in deionized water with a small amount of hydrochloric acid. The concentration of Ga was 0.05 mol/L.

Figure 1 shows XRD 2θ-ω scan profile. (0006) α-Al_2O_3 and (0006) α-Ga_2O_3 diffraction peaks were observed. This indicates that the film has an orientation relationship of [0001]α-Ga_2O_3//[0001]α-Al_2O_3. Figure 2 shows ϕ-scan profiles. The reflection condition of asymmetric Ga_2O_3 {10-14} and Al_2O_3 {10-14} diffractions were observed. The in-plane orientation relationships between the epitaxial Ga_2O_3 film and α-Al_2O_3 substrates are investigated using Fig. 2. This result indicates that the in-plane orientation relationship was [10-10] Ga_2O_3//[10-10] Al_2O_3 and this film was a single crystalline film. Figure 3 shows XRD X-ray rocking curve (XRC) scan profile. The full-width at half maximum of the XRC in (0006) α-Ga_2O_3 diffraction peak is 40 arcsec. Thus, these results show that high-quality single crystalline α-Ga_2O_3 film was epitaxially grown on (0001) α-Al_2O_3. The result of asymmetric XRC in this film will be discussed.

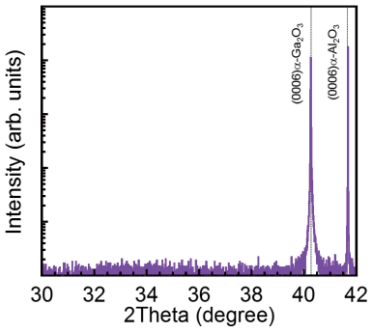

Fig. 1 XRD 2θ-ω scan profile of Ga_2O_3.

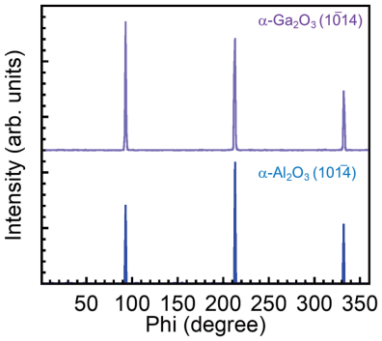

Fig. 2 XRD ϕ-scan profile of Ga_2O_3.

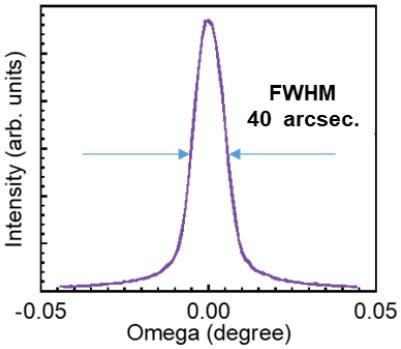

Fig. 3 XRD XRC profile of (0006)α-Ga_2O_3.

References:

[1] R. Roy, V. G. Hill, and E. F. Osborn, J. Am. Chem. Soc. **74**, 719 (1952).
[2] Helen Y. Playford, Alex C. Hannon, Emma R. Barney and Richard I. Walton, Chem. Eur. J. **19**, 2803 (2013).
[3] N. Suzuki, K. Kaneko and S. Fujita, J. Cryst. Growth **401**, 670 (2014).
[4] H. Ito, K. Kaneko and S. Fujita, Jpn. J. Appl. Phys. **51**, 100207 (2012).
[5] M. Oda, R. Tokuda, H. Kambara, T. Tanikawa, T. Sasaki and T. Hitora, Appl. Phys. Express **9**, 021101 (2016).

GEO-CHEMICAL ENVIRONMENT STATUS IN SUOI RAM HAMLET, LONG GIAO COMMUNE, CAM MY DISTRICT, DONG NAI, VIETNAM

Le Phuoc Cuong[1)*], Luong Van Tho[2)], Tatjana Juzsakova[3)] and Ákos Rédey[3)]

[1]*The University of Danang, University of Science and Technology, 54 Nguyen Luong Bang st., Lien Chieu, Danang, Vietnam, Email: lpcuong@dut.udn.vn*
[2]*The University of Danang, University of Education, Danang, Vietnam, 459 Ton Duc Thang st., Lien Chieu, Danang, Vietnam, Email: tho.luong@gmail.com*
[3]*Institute of Environmental Engineering, University of Pannonia, Veszprem, 10 Egyetem st., Veszprém, 8200, Hungary, Email: yuzhakova@almos.uni-pannon.hu (TJ); redey.akos@gmail.com (ÁR)*

Abstract

This paper presents the results of the geo-chemical distribution study in Suoi Ram hamlet, Cam My district, Long Giao, Dong Nai Province via 2D electrical resistivity tomography (ERT). From this, the correlation between tectonic formation, geological distribution, geological composition and groundwater distribution, environmental health status and level of groundwater pollution in the geological environment was assessed.

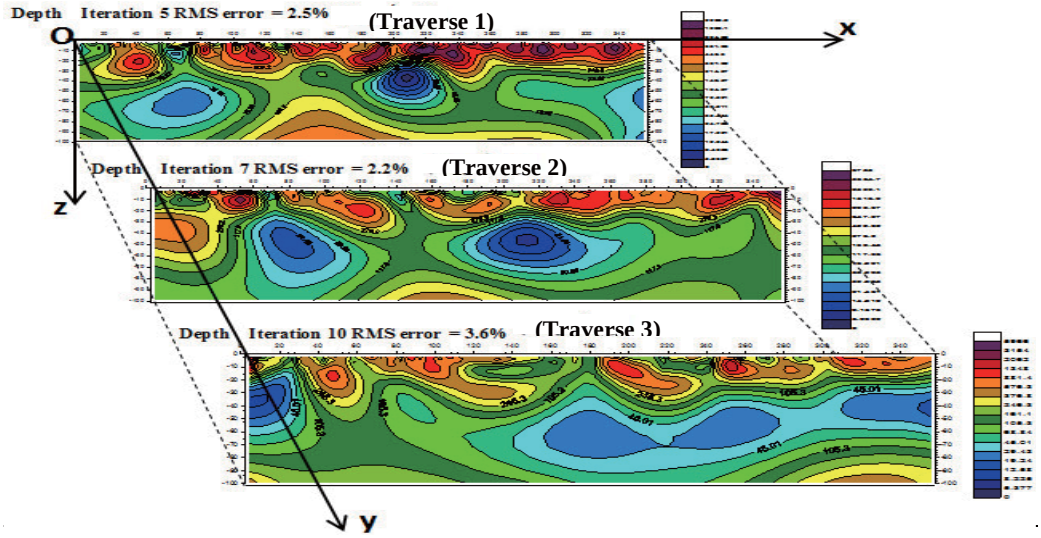

Fig. 1 2D image of the three traverses at Suoi Ram Hamlet, Long Giao Commune, Cam My District, Dong Nai Province

Observing the image results in Fig.1, we can basically see this area divided into 3 geological layers based on the difference in characteristics of resistivity.-The top layer is distributed from the ground to a depth of about 20 meters, thinning toward the East with high electric resistivity values (above 750Ω.m), they reflect clay of reddish brown basalt weathered product which contains no water. If linking all three traverses, it can be seen in this layer from 40 meters - 140 meters position (along the traverse) there were signs associated with the tectonic breakage zone with deep sloping slope and a longitudinal fault along the measuring traverse (only the 3rd traverse can be seen from 180 meters to the end of the traverse).

The second layer is distributed in the range of 20 meters to 80 meters in depth with resistivity ranging from 5 to 250Ω.m, which contains a layer of clay and weathered basaltic rocks. They are quite humid and flexible, some of which are composed of layers of basalt laterite crushed with strong shear. Extremely strong cracking levels in the basaltic areas at this area have shown a very low resistivity picture, which has a capacity of high water holding. The third layer is assumed to be the origin in the surveyed area (the resistivity value varies from 140.6 to 647.6 Ωm), which includes foam basalt which is less cracking and firm. At the center of the 1st traverse, we can meet this layer at a depth of about 82 meters or less and it can be deeper on both sides because the bottom of the section is quite narrow so it is not specifically defined.

References:

[1] Caterina, D., Flores-Orozco, A., and Nguyen, F. Long-term ERT monitoring of biogeochemical changes of an aged hydrocarbon contamination, *J. Contam. Hydrol*., **201**, 19–29 (2017).

Aquaculture Water Quality Monitoring Based on Wireless Sensor Networks Using LoRA Technology

Quoc-Huy Le[1), *], Van-Tien Huynh[2)], Thanh-Hieu Tran[3)], Ngoc-Tan Huynh[4)], Ngoc-Quoc Duong[5)]

[1)]Faculty of Advanced Science and Technology (FAST), The University of Danang - University of Science and Technology (UD-DUT), Vietnam
E-mail: lqhuy@dut.udn.vn
[2)]Faculty of Electrical Engineering, UD-DUT, Vietnam
E-mail: tienhuynh14tdhclc@gmail.com
[3)]Faculty of Electrical Engineering, UD-DUT, Vietnam
E-mail: tranthanhhieu95@gmail.com
[4)]Faculty of Electrical Engineering, UD-DUT, Vietnam
E-mail: huynhngoctan14tdhclc@gmail.com
[5)]Faculty of Electrical Engineering, UD-DUT, Vietnam
E-mail: ngocquoc2407@gmail.com

Abstract

Aquaculture is one of the most important economic sectors of Vietnam, bringing annual value of exportation reaching billions of US dollar and creating many jobs, particularly in rural and coastal areas. Despite many advantages of aquaculture, there are a lot of difficulties that farmers are still struggling such as: lack of training on basic knowledge and scientific standards, lack of financial resources to equip monitoring systems. Most shrimp farms are of medium or small sizes and are located far from residential areas, making the management and monitoring difficult, especially in the rainy season. Due to these difficulties, farmers do not check any environmental parameters, or if they do, the process is only performed by hand based on their own experience, one or two times per day but not continuously. Consequently, when the aquaculture environment is unstable, or any diseases occurs, it is very difficult to detect the problems in time and thus shrimps or fishes can be died easily, or products quality doesn't match with the standard and only a small portion of production can be exported. A system for real-time monitoring of the aquaculture water quality could help to cut down the production lost between 40% and 50%, because lost are usually due to preventable diseases that can be avoided if water quality is controlled [1], [2].

In this work we aim to design, build and test a system for aquaculture water quality monitoring based on wireless sensor networks using LoRA technology [2]. The system is targeted for medium and small size aquaculture farms, thus must be low cost, simple and easily to use, convenient for even not well-trained farmers.

Experimental results show that the system can measure critical aquaculture water parameters, namely dissolved oxygen (DO), pH and temperature, with accuracy within ±5%. The measured data is transmitted from the farm to a gateway through the low-power, wide-area LoRA communication network. The transmitting distance is tested up to 7 km. The LoRA gateway is then responsible for pushing all the data to the cloud server where an application is built to analyze the obtained data, display information on a web and a mobile phone app to help the farmers easily monitor the situation. The system can also remotely control equipment in aquaculture farm such as oxygen generators, lighting systems, automatic feeding systems, etc. via a simple web and mobile app HMI. The system automatically alerts farmers in case of any environmental problems or situations, thus helping the farmers to react timely, e.g. by remotely controlling equipment in the farm to create a suitable aqua environment for shrimps or fishes.

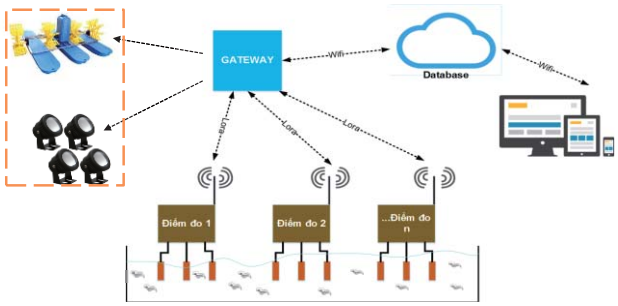

Fig. 1 Components and working principle of the system.

References:

[1] http://www.libelium.com/fish-farm-monitoring-in-vietnam-by-controlling-water-quality-in-ponds-and-tanks
[2] R.S. Sinha, Y. Wei, S.H. Hwang, *ICT Express*, Volume 3, Issue 1, March 2017, Pages 14-21
[3] W. Ding, Y. Ma, In: Li D., Chen Y. (eds) Computer and Computing Technologies in Agriculture V. CCTA 2011. IFIP Advances in Information and Communication Technology, vol 370. Springer, Berlin, Heidelberg

Development on tire performance prediction tool based on tire mechanics

Shunya Hidano[1)], Yukio Nakajima[2)]

[1)]Department of Mechanical Engineering, Graduate School of Engineering, Kogakuin University, Tokyo, Japan
E-mail: am18056@ns.kogakuin.ac.jp
[2)]Department of Mechanical Engineering, Graduate School of Engineering, Kogakuin University, Tokyo, Japan
E-mail: y-nakaji@cc.kogakuin.ac.jp

Abstract

1. Introduction

In recent years, the finite element method (FEM) is used for tire design, and various tire performances can be quantitatively predicted, so FEM is the most important tool of tire design. However, although FEM can quantitative predict tire performance, it is difficult to understand the mechanism related to tire performance improvement. Therefore, this research developed a simplified performance prediction tool called 1D-CAE based on tire mechanism, and made it possible to overlook overall tire performances at the conceptual design stage. Furthermore, this tool enables us to consider tire performances and expects to support tire designers.

2. Overview of the developed tool

As shown in Fig.1, the tool has a hierarchical structure made of tire performance prediction modules. It has a function to calculate for each performance, a function to calculate all the performance at once, and it is possible to quickly know which parameter influences which characteristic and how much. Therefore, it is useful when engineer discuss what the tire should be at the conceptual design stage. Furthermore it can be used for education of designers.

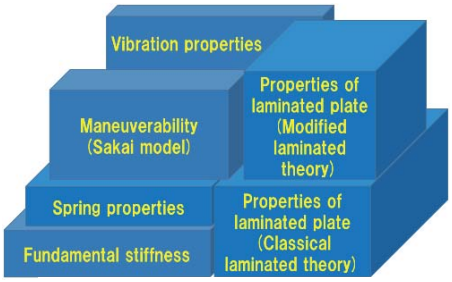

Figure 1 Overview of tire performance prediction tool with hierarchical structure

3. Verification of the developed tool

The tool was verified by comparing the prediction to the measurement of the material, spring properties of the tire, maneuverability, vibration properties (natural frequency, transfer characteristic). The prediction in good agreement with the measurement in every property.

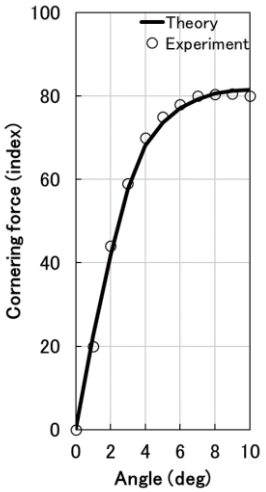

Figure 2 Comparison example between measure and prediction

4. Design tires using tools Tire development examples

We proposed a new tire structure using the developed tool. The rigidity of the tire is expressed by three elements of fundamental stiffnesses in the lateral direction (ks), fundamental stiffness in the tangential direction (kt), fundamental stiffness in the radial direction (kr). Target values of kt decreased by 5%, kt and kr increased by 20% as target values for improvement. The various parameters were changed using the tool and the rigidity of the tire was calculated. It was found that by changing the length of the bead filler and the thickness of the rubber, it becomes closer to the target value. In the subjective evaluation at the proving ground proposed tire had a better performance than the control tire.

5. Conclusion

We developed a simple design tool that can predict the properties of laminated plate, spring properties, maneuverability, vibration properties (natural frequency, transfer characteristic). The prediction tool relatively agreed with the measurement. We proposed the new tire structure using the developed tool.

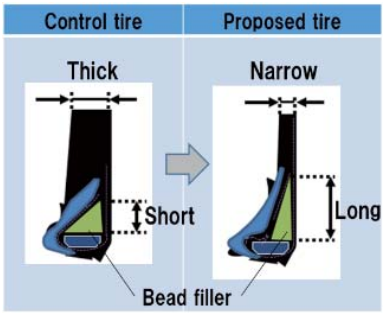

Figure 3 Change of tire structure

Reference:

Ed. Bridgestone, Fundamentals and application of vehicle tires (in Japanese), Sankaido, 2006
Yukio Nakajima, Advanced Tire Mechanics, Springer (planned to be published in 2019)

Performance Control by Guide Vanes for Axial-Flow Fan with a Blockage Disk

Sho Yamagiwa[1)], Kotaro Sato [2)], Koichi Nishibe [3)], Donghyuk Kang[4)]

[1)]Graduate School of Engineering, Kogakuin University, Tokyo, Japan
E-mail: am18064@ns.kogakuin.ac.jp
[2)] Department of Mechanical System Engineering, Kogakuin University, Tokyo, Japan
E-mail: at12164@ns.kogakuin.ac.jp
[3)] Department of Mechanical Engineering, Tokyo City University, Tokyo, Japan
E-mail: knishibe@tcu.ac.jp
[4)] Department of Mechanical Engineering, Aoyama Gakuin University, Kanagawa, Japan
E-mail: kang@me.aoyama.ac.jp

Abstract

Because the mechanism of the axial-flow fan is simple, it offers high versatility. Furthermore, it is suitable for high air flow rates and it effectively reduces noise. Axial-flow fans are one of the most widely used of the available blower designs, and environments in which they are implemented are extremely diverse, including thermal control (cooling / heating), drying, and ventilation. In some cases, they are used in adverse conditions, thus, axial-flow fans can be arranged under circumstances that subject them to spatial restrictions such as the presence of obstacles. Various researche studies have been fundertaken focusing on the relationship between the performance of axial-flow fans and obstacles[1]-[2]. In addition, it has been reported that the flow instabilities with the cell structure propagating to the circumferential direction occur in the gap between the fan and the blockage disk. However, the depth and diversity of studies on how to reduce performance degradation due to flow instability caused by obstacles are still insufficient.

In this research, an inlet guide vane is installed between an axial-flow fan and a disk type obstacle to reduce the performance degradation caused by the obstacle, and the influence of the inlet guide vane on the performance of the axial-flow fan is discussed. The focus of the investigation is on the relationship between the fan performance (performance curve, efficiency), blade angle, and number of blades.

Figure 1 is an illustrative example of the result, demonstrating a pressure performance curve when the relative distance *G / Df* between the fan and the obstacle is 0.15 and the number of blades is 12. Symbols ●, ▲, and ◆ are experimental results of blade angle β = 10 ° , 30 ° and 90° , respectively. For reference, the results in the case of *G / Df* = ∞ (no obstacle) and of no guide vane (*G / Df* = 0.15) are indicated by symbols ✳ and ■, respectively.

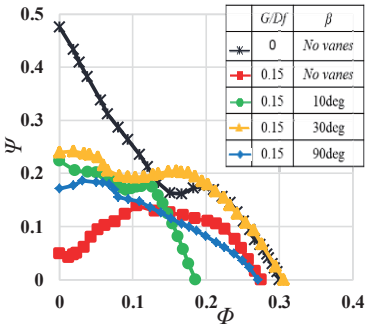

Fig. 1 Performance curves of the axial-flow fan (*Dd/Df* = 2.46, *Dc/Dd* = 0.41 *Dd* = 320 mm, β = 10 – 90°, *n* = 12)

From the comparison between ✳ and ■, the performance drops markedly when the entrance obstacle is introduced. Conversely, it is confirmed that the pressure performance increases in the low flow-rate range under any conditions in which the inlet guide vanes are present, in comparison with the case without the inlet guide vanes (■), and the various of β indicated by ●, ▲, and ◆. Especially when β = 30 ° (▲), pressure performance is improved across a wide ranges of flow-rates. The research, results indicate that the performance characteristics of axial-flow fans in the presence of obstacles on the upstream side depend on the installation and characteristics of the inlet guide vanes, which can be expected to reduce the performance deterioration in conjunction with appropriate blades.

References:

[1] Hideo Taniguchi, Ken-ichi Funazaki, Tomoe Takahashi and Kouta Chiba, 2011, "Unsteady Flow Field and Noise Characteristics of a Small Axial Flow Fan Used in Narrow Space", Journal of Turbomachinery Society of Japan, Vol. 40, No. 2, pp.50-58

[2] Sinsaku Nakamura, Kotaro Sato, Masayuki Takahashi, Kazuhiko Yokota "Influence of an Upstream Obstacle on the Flow Characteristics of Axial-flow Fans", Transactions of the ASME, FEDSM2014-21251

Development of the Residual Ammonia Removal System for Installation on Vehicles

Ryutaro HANAZAKI[1)], Masahiro INAMOTO[1)], and Takashi SAIKA[1)]

[1)]Mechanical Engineering, Graduate School of Engineering, Kogakuin University, Tokyo, Japan
E-mail: am17058@ns.kogakuin.ac.jp

Abstract

In recent years, global warming caused by greenhouse gas has become a problem. Fuel cell vehicles are expected as countermeasures to reduce emissions of carbon dioxide. However, hydrogen, which is a power source of a fuel cell, has problems when it comes to transportability and storability. Therefore, we constructed the ammonia-hydrogen generation system to use ammonia as the hydrogen carrier. Using a suitable catalyst, ammonia can be decomposed into hydrogen and nitrogen by thermal decomposition. However, this system has problems; when ammonia is thermally decomposed, a very small amount of ammonia remains (hereinafter called "residual ammonia"). It has been observed that when the residual ammonia concentration of 0.1 ppm or more is mixed in the gas supplied to the fuel cell, the catalyst electrode poisons and causes a decrease in output. Therefore, this study treats residual ammonia by utilizing the property of ammonia which is well soluble in water.

1. Characteristics of Ammonia

Ammonia is a colorless gas, a substance with a pungent odor that can be immediately identified. It can be liquefied at about 0.84 MPa at a temperature of 20°C and is excellent in transportability and storability. Ammonia has a high hydrogen content rate of 17.8 % which is higher than 12.6 % of methanol containing carbon. Furthermore, the hydrogen production cost from ammonia is smaller than when hydrogen is liquefied. When mounting on the vehicle, a space, safety, and a cruising range must be taken into consideration. So, we considered that it is suitable not to use hydrogen, but to use ammonia as the hydrogen carrier.

2. Residual Ammonia Removal Experiment

Fig. 1 shows a graph indicating the time change in residual ammonia concentration at the outlet of the removal equipment (Fig. 2) in the presence or absence of the aeration tube. From this result, the time change of residual ammonia concentration at the outlet of the removal equipment can be confirmed. Initially, the residual ammonia was completely removed and using the removal equipment, it was measured that it takes about 120 minutes for the residual ammonia to reach 10 ppm over in a single tube whereas it takes 180 minutes in aeration tube. It is confirmed that increase of the amount of residual ammonia concentration becomes moderate or mild when the aeration tube is used.

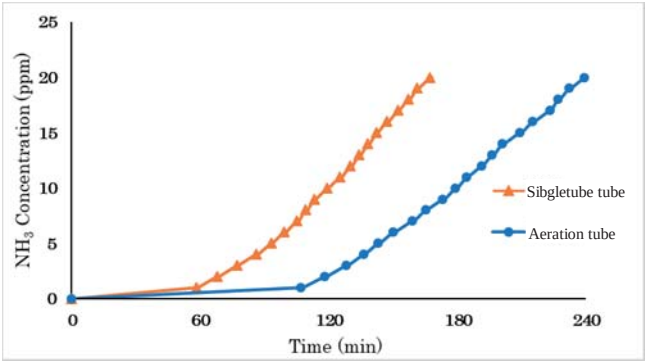

Fig. 1 The comparative result of analysis by aeration tube and single tube

Fig. 2 The removal equipment

3. Conclusion

In the current equipment, there are problems that can be observed. The time that the residual ammonia concentration can be 10 ppm or less takes 180 minutes, the weight of the remover is about 30 kg which makes the mounting on the vehicle difficult and, the fact that it is inflated by internal pressure because it is not in pressure-resistant shape. It is for this reason that we have designed and developed removal equipment to solve these problems.

Development of a Hydrogen Generation System by Ammonia Decomposition

Masahiro INAMOTO[1)], Ryutaro HANAZAKI[1)], and Takashi SAIKA[1)]

[1)] Mechanical Engineering, Graduate School of Engineering, Kogakuin University, Tokyo, Japan
E-mail: am17007@ns.kogakuin.ac.jp

Abstract

Carbon dioxide derived from fossil fuel accounts for more than half of greenhouse gases. Hydrogen energy is expected as a new energy, and there is a merit that it does not emit greenhouse gases because of no carbon atoms. However, hydrogen is usually generated from fossil fuels such as natural gas, and there is a problem of discharging carbon dioxide during refining. The previous study focused on ammonia gas consisting of nitrogen and hydrogen, and constructed a hydrogen generation system by thermal decomposition of ammonia. The merit of using ammonia is the large hydrogen content of 17.8 wt%. However, the first problem is the high temperature condition required for gas decomposition. Therefore, this research developed a resolvable ammonia decomposition system with highly efficiency.

1. Characteristics of ammonia

Ammonia is a gas composed of nitrogen and hydrogen. It is colorless and have an irritating smell at an ordinary temperature and normal pressure. It can be liquefied at 20°C and under approximately 0.85 MPa. So it excels at portability and storage quality. It can be thermal decomposed into nitrogen and hydrogen with catalysts as below.

$$NH_3 \rightarrow \frac{1}{2}N_2 + \frac{3}{2}H_2 \qquad (1)$$

At the time, no greenhouse gases are discharged, therefore it can contribute to solve global warming. Its hydrogen content rate is 17.8 wt% and comparative high. It is higher than methanol of 12.6 wt%.

2. Differences between each catalyst shape of ammonia decomposer

Experiments of ammonia decomposition which catalysts shapes are metal honeycomb, pellet and microchannel were conducted (Fig. 1). Ruthenium-catalysts which have high decomposition efficiency at low temperature were used. Characteristics of each decomposer are shown in Table 1. The electric heating type (Fig.2) heat ammonia from the inside. The cylindrical type (Fig.3) heat ammonia with the external heater. The heat exchange type (Fig.4) transfer the heat from the heated air to ammonia.

Table 1 Characteristics of ammonia decomposer

	Ammonia decomposer		
	Electric heating type	Cylindrical type	Heat exchange type
Catalyst shape	Honeycomb	Pellet	Microchannel
Catalyst	Ru/Al2O3 : 5g/L	Ru/Al2O3 : 5g/L	Ru/Al2O3 : 5g/L
Quantity	300mL	300mL	44mL
Efficiency	App. 100% (650℃)	App. 100% (700℃)	App. 32% (500℃)
Maximum flow rate	12L/min	8L/min	0.5L/min
Heat source	Inside	Outside	Outside

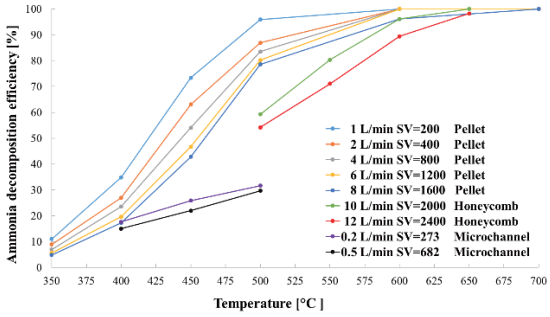

Fig. 1 Experimental results

Fig.2 Electric heating type

Fig.3 Cylindrical type

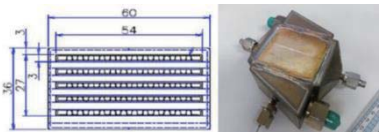

Fig.4 Heat exchange type

3. Conclusions

12.05 L/min flow of hydrogen is required to operate 1 kW declared power fuel cell produced by FC-R&D, viz. 8.033 L/min flow of ammonia is required for it. The electric heating and the cylindrical types can provide ammonia at the flow rate. The decomposition efficiency of the cylindrical type is higher than the electric heating type, and the type can replace the catalyst easily. Hereafter, we will produce the new cylindrical ammonia decomposer with pellet catalyst to advance the research of the cylindrical type and the hydrogen generation system for fuel cell vehicles.

Study on the effect of road roughness on tire wear

KEI OMURA [1], YUKIO NAKAJIMA [2]

[1]Department of Mechanical Engineering, Graduate School of Engineering, Kogakuin University, Tokyo, Japan
E-mail: am17013@ns.kogakuin.ac.jp
[2]Department of Mechanical Engineering, Graduate School of Engineering, Kogakuin University, Tokyo, Japan
E-mail: y-nakaji@cc.kogakuin.ac.jp

Abstract

1. Research background and purpose

The reduction of greenhouse gas is the urgent issue in the automotive industry and the compatibility between fuel saving performance and wear resistance is therefore required for tires. Because tire wear is also related to not only environmental performance but also safety, and economic aspect, the improvement of tire wear is an important subject.

2. Factors of tire wear

Tire wear involves various factors as shown in **Fig. 1**. Since tire design, driving condition and vehicle factors have been studied, we focused on the study on the effect of road roughness on tire wear.

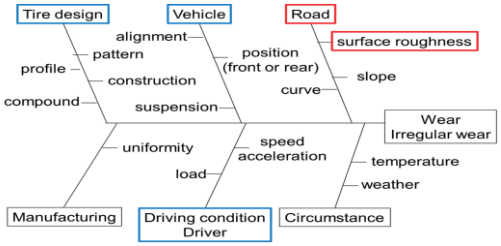

Fig. 1 Factors of tire wear

3. Creation of artificial road surface

There are both macro and micro roughnesses in the road. Since it is important to express the surface roughness in a wide scale, the measured waveform of the road surface is analyzed by space frequency and its amplitude using FFT. Compared the power spectrums of the artificial road and the actual road, we made an artificial road surface closer to the actual road (**Fig. 2**). This new arificial road will be used for the surface of the wear drum tester and it is expected to improve the accuracy of the drum tester (**Fig. 3**).

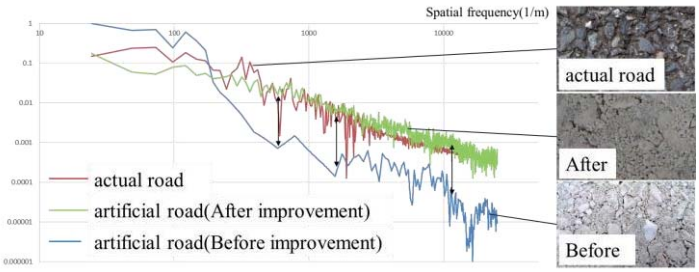

Fig. 2 Power spectrum of surface

Fig. 2 Drum type tire wear tester

4. Finite element analysis

In order to investigate the interfacial phenomena between rubber and road surface,we modeled the road using laser measurement. The rubber block is loaded on the road and is slid (**Fig. 4**). The friction coefficient of various road roughness are calculated by dividing the shear force by the normal force.

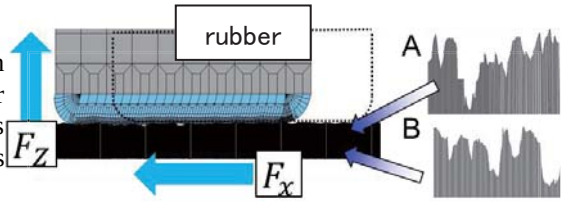

Fig. 4 Slide analysis of the rubber block

6. Conclusion

A device to mesure road roughness is developed and the artificial road which spectrum is close to that of the actual road is also developed. The finite element analysis is performed for the sliding rubber block on the various road roughness and the effective friction coefficient are obtained for these roads. We plan to conduct FEA using the friction coefficient and investigate the influence of road surface roughness on wear energy.

References:-[1]Yukio Nakajima Journal of the Society of Rubber Science and Technology, Japan / 75(2002)

Aerodynamic Characteristics of Multicopter Hovering near a Boundary

Kazuki Konno[1)], Kotoro Sato[2)], Koichi Nishibe[3), *]

[1)] Graduate School of Engineering, Kogakuin University, Tokyo, Japan
E-mail: am18031@ns.kogakuin.ac.jp
[2)]Department of Mechanical System Engineering, Kogakuin University, Tokyo, Japan
E-mail: at12164@ns.kogakuin.ac.jp
[3)]Department of Graduate School of Engineering, Tokyo City University, Tokyo, Japan
E-mail: knishibe@tcu.ac.jp

Abstract

The quadcopter is a type of multi-copter and it has popularized as a mainstream type of unmanned-aerial-vehicle (drone) rapidly. Nowadays, it is active in various fields. Various researches have been made due to popularize of drone. Furthermore, it is expected to gather accurate information by using drone in situations where rubble is scattered due to disasters and it is difficult to move on ground or in a closed space of complicated three-dimensional shape filled with harmful substances due to a plant accident. In other words, drones will not only fly in the sky, but will also be required to fly in narrow spaces in the future. However, there are many questions about the aerodynamic characteristics of drones in narrow spaces.

This research is regarded as a fundamental research on stable flight of multicopter in a narrow space, and elucidation of the influence of the rigid wall on the upper side of the drone on aerodynamic characteristics from aerodynamic point of view was attempted. Fig. 1 shows the experimental apparatus. We created a prototype drone with a single motor drive system and a controller so that the rotation speed N and phase φ of the rotor blade can be arbitrarily set. There are four rotors (two pairs with different rotational directions), and the number of blades per rotor is $N = 2$. In addition, the drone was installed between two acrylic plates and a hole to measure the pressure acting on the upper wall. The distance between the flat plates is h, the distance from the rotor to the upper wall is h_1, and the distance from the rotor to the lower wall is h_2. The dimensionless lengths based on the representative length (rotor diameter D) for h, h_1, and h_2 are H, H_1, and H_2, respectively. We conducted an experiment with $H = 4.72$, and the ceiling effect on the lift characteristics of the drone was discussed according to weight measurements made by the electronic balance. In addition, we investigated nonstationary characteristics such as blade passing of the drone based on pressure fluctuation measurements of the rigid wall surface above the drone. Fig. 2 shows the relationship between H_1 and the lift coefficient C_L. The parameter in this figure is the phase φ. It can be seen that the lift coefficient C_L increases as the drone approaches the upper wall (H_1 decreases). On the other hand, it is confirmed that C_L does not depend on φ under this condition.

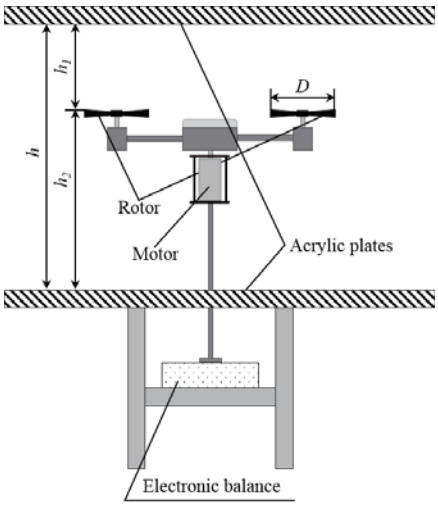

Fig.1 Experimental apparatus

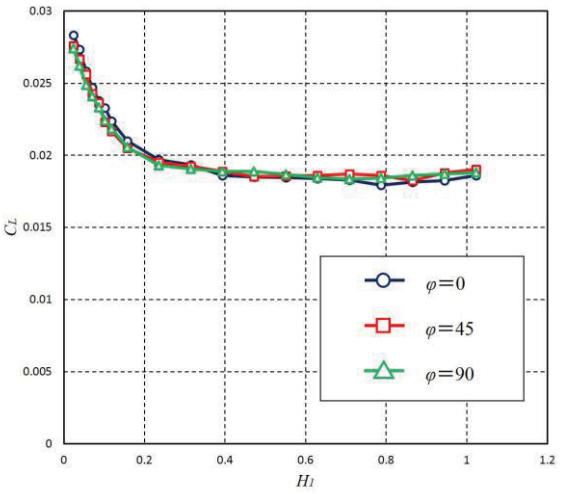

Fig.2 The relationship between H_1 and the lift coefficient C_L

References:

[1] Wataru Tobo, Satoshi Kataoka, Daiki Tsuji, Mizue Munekata, and Hiroyuki Yoshikawa,2015, "Effects of Side-Walls on the Aerodynamic Characteristics of a Micro Quad-Rotor in Hovering",The 13th Asian International Conference on Fluid Machinery, pp.1-7

Behavior of Pulsating Jets near a Rigid Boundary

Daiki Yamaguchi [1], and Kotaro Sato [2]

[1] Graduate School of Engineering, Kogakuin University, Tokyo, Japan;
E-mail: am18065@ns.kogakuin.ac.jp
[2] Department of Mechanical System Engineering, Kogakuin University, Tokyo, Japan;
E-mail: at12164@ns.kogakuin.ac.jp

Abstract

Research is actively conducted to control flow fields using jet flow. The number of studies on excited jets such as pulsating jets [1] and synthetic jets [2] is increasing compared with those on conventional continuous jet. A pulsating jet is a flow in which the jet flow rate periodically changes by applying pulsation to the steady jet. It is known that the jet flow structure changes with the amplitude of velocity fluctuation and frequency in a pulsating jet. In the case of a pulsating jet, control the flow field (space) is expected using the vibration characteristic (time), which does not exist in the steady jet. However, there are many unclear points regarding the relationship between the Coanda effect and vibration characteristic, which is one of the major features of the jet. There are also few reports on the interference between the pulsating jet and rigid boundary, which are important in practical use.

In this study, we focus on the Coanda effect and discuss the flow characteristics of pulsating jets in the vicinity of the rigid boundary by experiments and numerical simulation. We investigate the pulsating jet with a sinusoidal unsteady component added to the steady jet. In particular, we attempt to elucidate the influence of the frequency of the velocity fluctuation on the flow pattern, and clarify the relationship between the frequency and time-average flow reattachment point.

Fig.1 shows an example of a typical flow pattern of a pulsating jet in the vicinity of the rigid boundary calculated under the condition of Re=1980. The jet offset ratio $H_2 = 10$, dimensionless frequency f^*=0.033, and dimensionless velocity amplitude U_{pa}/U_{c0}=0.92. Vortex pairs are formed periodically owing to velocity pulsation, and it is observed that the vortex staggered owing to the asymmetry of the flow field. In this condition, the Coanda effect forms a time-averaged jet reattachment point near x/b_0 = 20.4.

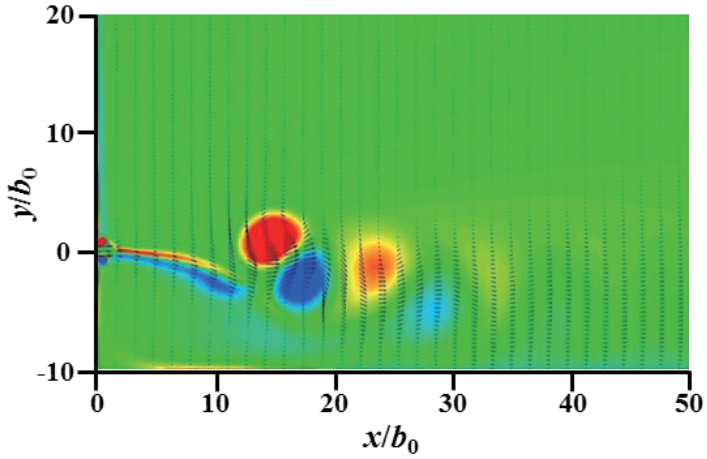

Figure 1 The flow pattern of the pulsating jet near a rigid boundary ($H_2 = 10$, f^*=0.033,U_{pa}/U_{c0}=0.92)

References:

[1] H. Kobus, P. Leister, B. Westrich, *Journal of Hydraulic Research*, **17**, 175-192.
[2] R. Holman et al., 2005, *AIAA Journal*, **43**, .2110-2116 (2005).

Development of a Receptionist Robot: Mechanical and Control System Design

Danh Ngoc Nguyen[1)], Hoang Trung Ngo[2)], Ha Linh Le[2)] and Hoai Nam Le[1)]

[1)]Faculty of Mechanical Engineering, The University of Danang – University of Science and Technology, Danang, Vietnam;
E-mail: {ndngoc; lehoainam}@dut.udn.vn
[2)]FPT Global Automation Company, Danang, Vietnam
E-mail: {hoangtrungngovan.td; halinh09cdt1}@gmail.com

Abstract

Recently, many mobile service robots have been deployed in human environments including the robot for elderly and patient care [1], security tasks [2], receptionist [3] and so on. Due to demand of the Danang FPT Complex to have a receptionist robot that can flexibly move indoors, recognize employee faces and perform some basic gestures, a cooperation project is launched with the participation of students in Mechatronic Engineering and Electronic & Telecommunication Engineering programs, university and company tutors. For 4 months, a receptionist robot with required functionalities are designed, created and tested. The receptionist robot is a complex system whose hardware configurations can be represented in Fig. 1(a). Fig. 1 (b) and (c) illustrate the CAD model and real prototype of the robot respectively.

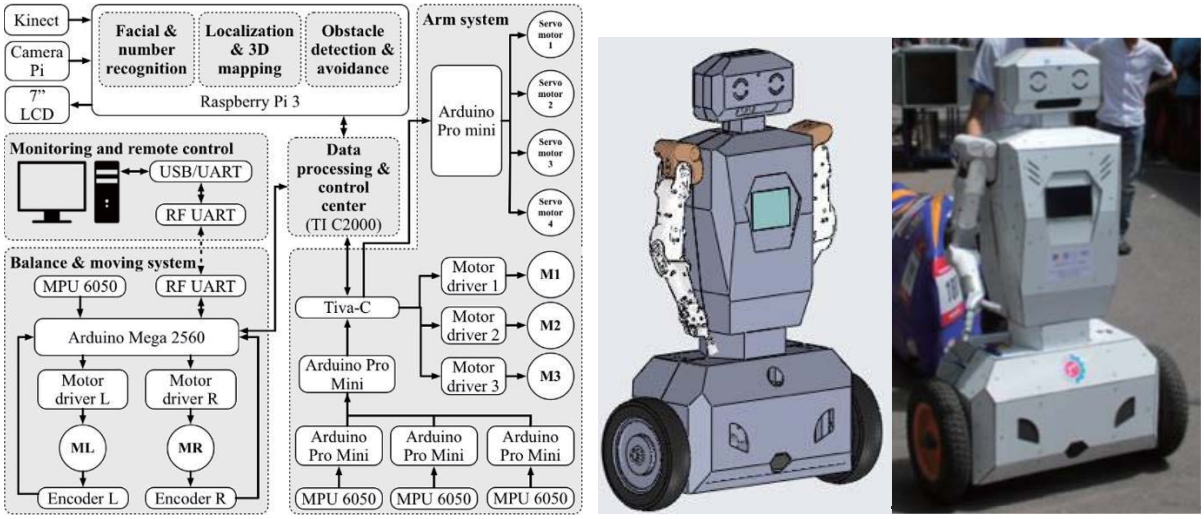

(a) (b) (c)

Fig. 1: Receptionist robot: (a) hardware configuration, (b) CAD model and (c) Real prototype

This paper focuses on the development of mechanical structure and control system of the robot. The remainder of this paper is organized as follows. Section 2 is devoted to the description of the system overall structure, interactions between the functional blocks and hardware configuration. Section 3 and 4 focus on the mechanical and control system design, respectively. The performance of the systems in real situations are illustrated by some experiments in Section 5. Finally, the conclusion drawn from this work and possible ways for further studies are given.

References:

[1] M. Hans, B. Graf, and R. Schraf, "*Robotic home assistant Care-O- bot: Past – present – future*" in Proc. of the 2002 IEEE Int. Workshop on Robot and Human Interactive Communication, Berlin, Germany, 2002, pp. 380–385.

[2] A. Treptow, G. Cielniak, and T. Duckett, "*Active people recognition using thermal and grey images on a mobile security robot*" in Proc. of IEEE/RSJ Int. Conf. on Intelligent Robots and Systems (IROS), Canada, 2005, pp. 2103–2108.

[3] Bellotto, N., Rowland, S., & Hu, H. (2008, July). *Lux-An interactive receptionist robot for university open days.* In Advanced Intelligent Mechatronics, 2008. AIM 2008. IEEE/ASME International Conference on (pp. 1355-1360), IEEE.

Characterization of Plain Journal Bearings Using an Original Test-Rig

Phuoc Vinh Dang[1*], Thanh Nghi Ngo[2]

[1,2] Department of Mechanical Engineering, The University of Danang – Danang University of Science and Technology. Nguyen Luong Bang 54, Danang, Viet Nam
E-mail:[1] dpvinh@dut.udn.vn ,[2] ntnghi@dut.udn.vn

Abstract

The installation of oil-film plain journal bearings in industrial machines remains a good choice for their simplicity and low cost, if compared to oil-film tilting-pad journal bearings or rolling element bearings. Typical applications include reciprocating machines with small diameter shafts, operating at high speeds, where the high dynamic behaviors offered by other bearing types are not required. Critical applications are represented by machines with medium/large diameter shafts, operating at very low Sommerfeld numbers and characterized by both low tangential speeds (less than 1m/s) and high loads.

Because of the merit, a large of theoretical and experimental studies have been executed to study important characteristics of the plain journal bearings such as fluid–film thickness, static shaft position, load capacity, temperature distribution, pressure distribution, dynamic stiffness and damping coefficients and so on. However, the theoretical evaluation of these coefficients for plain journal bearings is difficult because of their complex geometry, boundary and thermal conditions and turbulent flow. Therefore, it is very essential to design and build a suitable test rig for performing experiments.

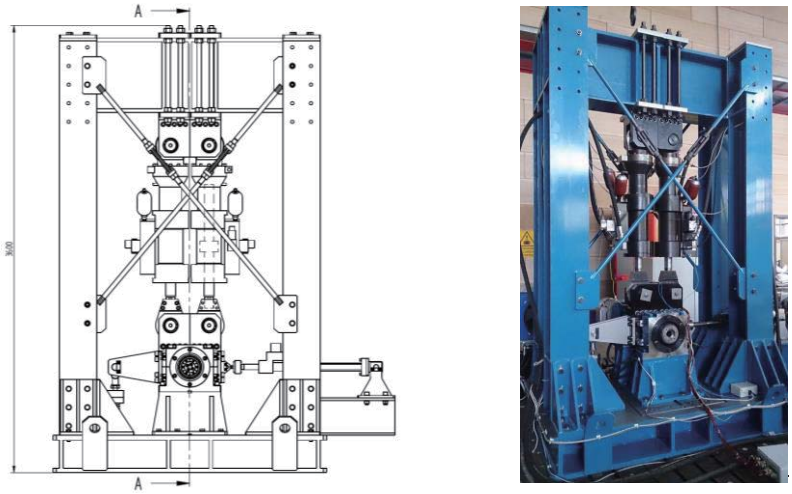

(a) **(b)**

Fig. 1 Sketch (a) and picture (b) of the test rig

This paper describes a large-scale test rig with for the experimental characterization of plain journal bearings. A bearing with the nominal diameter of 160 mm and the length of 145 mm was used. The rotational speed was fixed at 60rpm, while the applied load varied from 20 kN up to 400 kN in the vertical direction. Sommerfeld number, steady–state and transient temperatures, pad pressure, dynamic stiffness and damping coefficients in different operation conditions could be estimated.

References:

[1] Ahmad MA., Kasolang S., and Dwyer-Joyce RS. Experimental Study on the Effects of Oil Groove Location on Temperature and Pressure Profiles in Journal Bearing Lubrication. *Tribology International*, **74**,79-86 (2014)

[2] Lu X., Khonsari, M.M., and Gelinck, E.R.M. The Stribeck Curve: Experimental Results and Theoretical Prediction. Journal of Tribology, **128**, 789-794 (2006).

[3] Chatterton Steven, Pennacchi Paolo, Dang Phuoc Vinh, Vania Andrea. Identification Dynamic Force Coefficients of a Five-Pad Tilting-Pad Journal Bearing. Proceedings of 9th International Conference on Rotor Dynamics (IFToMM); Milan, Italy; **21**, 931-941 (2014).

[4] Dang Phuoc Vinh, Chatterton Steven, Pennacchi Paolo, Vania Andrea. Effect of the load direction on non-nominal five-pad tilting-pad journal bearings, *Tribology International*, **98**, 197-211 (2016).

Prediction and prevention of pressure ulcers in patients using wheelchairs

He-Thong Bui[1),*], Quang-Bang Tao[2)]

[1)] The University of Da Nang - University of Technology and Education, Danang, Vietnam
E-mail: bhthong@ute.udn.vn
[2)] The University of Da Nang - University of Science and Technology, Danang, Vietnam
E-mail: tqbang@dut.udn.vn

Abstract

Pressure ulcers (PUs) is a pathology, it usually occurs in the contact areas of skin overlying bony prominences (between the buttocks-thighs and wheelchair cushion) (**Fig. 1**). This pathology is common in patients who use a wheelchair or people with disabilities, because they have to sit for several hours in a position. There are many factors contributing to the development of pressure ulcers: pressure, shearing forces, friction, moisture, stress inside the buttocks-thighs, temperature and humidity… [1]. Pressure is now considered to be the most important cause of pressure ulcer formation. Continuous prolonged sitting, feeling deficiency, blood disorders and poor nutrition have been identified as important risk factors in the development of pressure ulcer formation. The risk of paying a very high cost of treatment, such as in the United States: the cost to treat pressure ulcers can be up to 30,000 USD [2]. Therefore, the choice of pressure ulcer prevention is considered a top priority in today's context.

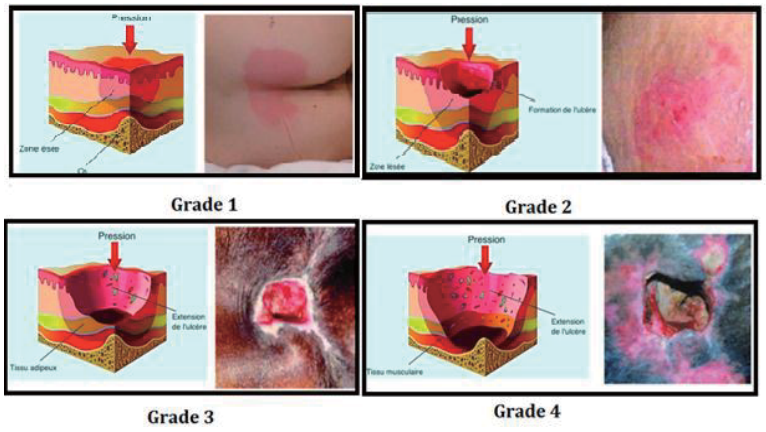

Fig. 1 Pressure ulcers depending on severity, grades 1 to 4 [3]

The purpose of this study is to focus on the factors that cause the development of pressure ulcers and identify the prevention of pressure ulcers. After introducing the context of pressure ulcers, we will propose a summary of the causes of pressure ulcer formation, which were published in the literature. Then, we will introduce diagnostic measures to prevent pressure ulcers by methods of numerical simulation and experimental.

The results of this study contribute to the prediction of factors that can cause pressure ulcers to improve on comfort seating and the quality of life for people with disabilities.

References:

[1] Kruger EA, Pires M, Ngann Y, Sterling M, Rubayi S. Comprehensive management of pressure ulcers in spinal cord injury: Current concepts and future trends. *The Journal of Spinal Cord Medicine*, **36**(6):572-585 (2013).
[2] Bennett G, Dealey C, Posnett, J. The cost of pressure ulcers in the UK. *Age and ageing*, **33**, 230–235 (2004)
[3] NPUAP, EPUAP, PPPIA. Prevention and Treatment of Pressure Ulcers: *Quick Reference Guide* (2014)

Construction of disassemble technology for lithium batteries towards material investigation

Yusuke Ushioda *, Yuki Ishino, and Shiro Seki

Department of Environmental Chemistry and Chemical Engineering, School of Engineering, Kogakuin University, Tokyo, Japan
E-mail: s315011@ac.kogakuin.ac.jp

Abstract

Lithium-ion batteries (LIBs) are excellent rechargeable energy storage device essential for dairy life and are used for tablet and other electronic devices. Recently, lithium-sulfur (Li-S) battery is attracted attentions because of having high capacity (1,645mAhg^{-1}) more than conventional LIBs. Li-S batteries have some problems for practical use. One of serious problem is dissolution of intermediate products of positive electrode Li_2S_x (lithium polysulfide) to electrolyte.

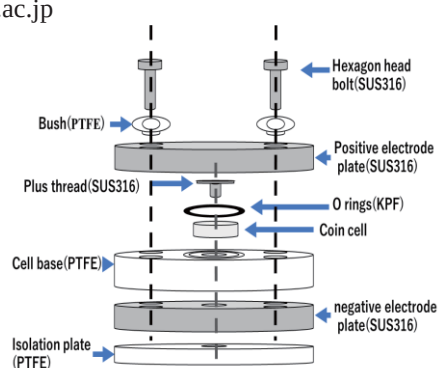

Fig. 1 Schematic image ofvdisassemble cell.

Generally, performance evaluations for batteries use a coin cell that difficult to disassemble. This method measures some electrochemical parameters that a charge-discharge experiment. The aim of study is establishment of disassemble and analyze technology by using developed cell (Fig. 1). This cell is hermetically sealed by O-rings with pressure, and can avoid contamination with moisture and reactive atmosphere. In this study, we tried analyze and observation for conventional graphite (C_6) electrodes (Fig.2 (a)) of disassemble cell after electrochemical measurement.

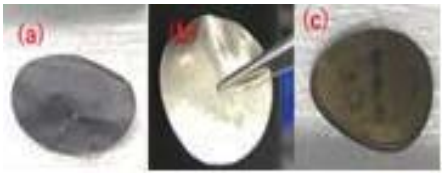

Fig. 2 (a) C_6 electrode, (b)lithium metal, (c)charged C_6Li_x electrode.

Experimental

We prepared [C_6 | EC+DEC / LiFSI | Li (Fig. 2(b))] cell by using coin cells and disassemble cells for charge-discharge experiments. Charge-discharge tests were performed with the voltage range :2.5-0 V, current density: C/12, temperature: 303 K, respectively.

Results and discussion

Fig. 2 shows appearance of electrode using this study. Color of C_6 electrode turned from black to gold because of lithium inserted in graphite C_6Li_x.

Fig. 3 shows charge-discharge profiles of [C_6 | EC+DEC / LiFSI | Li] coin cell and disassemble cell. Both cell measurement results can't see significant differences. We confirmed the easily and sufficient use of disassemble cell for electrochemical reactions.

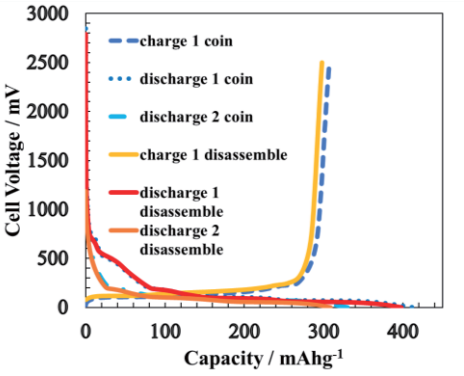

Fig. 3 Charge-discharge profiles [C_6 | EC+DEC / LiFSI | Li] about coin and disassemble cells.

In future, we'll investigate effect on cycle performances or disassembled potentials of sulfur electrodes by X-ray diffraction for [C_6Li_x | [$Li_1(G3)_y$]TFSA | S] cells. We will also report on composition dependences for Li-S cells (y=0.8,0.9,1,1.11,1.25).

Photoluminescence measurements of GaInN grown at different temperatures by RF-MBE

Ryosuke Yoshida[1)], Yusuke Nakazima[2)], Hiroki Hirukawa[1)], Takeyoshi Onuma[1,2)], Tomohiro Yamaguchi[1,2)], and Tohru Honda[1,2)]

[1)]Department of Applied Physics,School of Advanced Engineeering Kogakuin University, Tokyo, Japan
[2)] Department of Electrical Engineering and Electronics, Graduate School of Engineering, Kogakuin University, Tokyo, Japan

E-mail: s415049@ns.koguin.ac.jp

Introduction

GaInN is an alloy semiconductor of InN and GaN with band gaps of about 0.7 eV and 3.4 eV, respectively. This indicates that GaInN can emit lights over the entire visible range by controlling its composition ratio. Therefore, GaInN is a useful semiconductor material for full-color μ-LED flat panel display [1]. However, it is difficult to realize high-quality and high-efficient red LED with $Ga_{1-y}In_yN$ quantum wells (QWs) embedded in $Ga_{1-x}In_xN$ matrix ($x<y$). Typically, $Ga_{1-x}In_xN$ is grown on GaN bulk substrate or GaN/Al_2O_3 template. When the lattice relaxation of $Ga_{1-x}In_xN$ occurs on GaN due to the large lattice mismatch between GaN and GaInN, many crystal defects such as dislocations are formed in $Ga_{1-x}In_xN$ [2]. The generation of lattice relaxation and the formation of crystal defects should be strongly affected by the growth temperature. Indeed, the crystal defects affect the optical properties of $Ga_{1-x}In_xN$ as well as those of $Ga_{1-y}In_yN$ QWs on top of $Ga_{1-x}In_xN$.

In this paper, photoluminescence (PL) measurements of $Ga_{1-x}In_xN$ grown at different temperatures by radio-frequency plasma-assisted molecular beam epitaxy (RF-MBE) were carried out.

Experiment

$Ga_{1-x}In_xN$ films with a thickness of about 0.4 μm were grown by RF-MBE on the commercially available GaN/Al_2O_3 templates. The growth temperatures were varied between 520°C and 780°C, where these temperatures were monitored by the thermocouple set in the backside of substrate. Other growth conditions were fixed. The growth time was for 60 minutes. X-ray diffraction (XRD) reciprocal space mapping (RSM) measurements were used for determining In composition x of $Ga_{1-x}In_xN$. PL was used for the measurements of optical properties of $Ga_{1-x}In_xN$ films.

Table I In composition x of $Ga_{1-x}In_xN$

Growth temperature(℃)	In composition(%)
530	27
560	25
580	25
620	26
660	28
700	29
740	23
780	17

Result

Table I shows the In composition x of $Ga_{1-x}In_xN$ measured by XRD RSM measurements. The In composition was almost constant of 25±6 % at the growth temperatures of 580~700°C. The In composition is determined by the supply flux ratio of source materials during growth [3]. The In composition decreased with increasing growth temperatures in the ranges of 700~780°C. This can be explained by the incorporation phenomenon of In associated with nitrogen desorption [4].

The band gap E_{GaInN} was estimated from the calculation using the following equation; $E_{GaInN} = xE_{InN} + (1-x)E_{GaN} - bx(1-x)$ (1), where E_{InN} of 0.67 eV, E_{GaN} of 3.4 eV and b of 1.8 eV are used. In Fig. 1, the PL peak energies of grown samples are plotted as a function of growth temperature. The band gap energies estimated from the equation (1) are also plotted. The PL peak energy and the estimated band gap energy are well fitted in the samples grown at over 620°C, while the difference between these energies was observed in the samples grown at below 580°C. Details will be discussed.

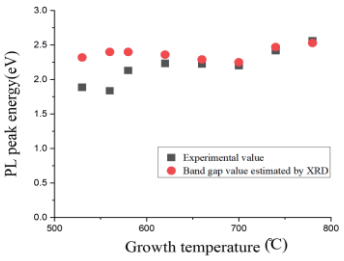

Fig.1 PL peak energy

References

[1] Jacob Day *et al*., Appl. Phys. Lett. **99**, 031116 (2011).
[2] H. Sekiguchi *et al*., Appl. Phys. Lett. **96**, 231104 (2010).
[3]T.Yamaguchi *et al*., J. Crystal Growth **377**, 123 (2013).
[4]S.Valdueza-Felip *et al*., Appl. Phys. Lett. **116**, 233504 (2014).

Polyether/$Li_{1.5}Al_{0.5}Ge_{1.5}(PO_4)_3$ hybrid electrolyte for high performance all-solid-state Li battery

Naamo Suzuki*, Masaki Kato, Tatsuya Hayano, and Shiro Seki

*Department of Environment Chemistry and Chemical Engineering, School of Advanced Engineering, Kogakuin University, Tokyo, Japan
E-mail: s315040@ns.kogakuin.ac.jp

Abstract

Recently, demands for energy storage systems, such as batteries are increasing as a counterplan toward global warming. Practical use of those batteries has started to electric vehicle and output control of renewable energy. One of the most popular high performance system is Li-ion battery(LIB). Owing to LIB having high energy density, LIBs are built in smartphone and laptop computer. However, it has a problem of safety, ignition accidents have been reported. Main cause is flammability of solution electrolyte. In order to use it for electric vehicle and output control of renewable energy, we should develop safe battery. Therefore, recently, 'solvent-free' all-solid-state batteries have attracted attention from the viewpoint of essential safety. Solid state battery has two type of solid electrolytes. One is inorganic electrolyte and the other is Polymer electrolyte. Each of them have both merit and demerit. Then, we propose inorganic/polymer hybrid electrolyte to get only advantage. We investigated hybrid electrolytes with P(Eo/Po) and $Li_{1.5}Al_{0.5}Ge_{1.5}(PO_4)_3$ (LAGP) for developing high-performance all-solid-state Li batteries.

Experimental

Macromonomer of P(Eo/Po) (TA-210, Dai-ich Kogyo Seiyaku) was used as host matrix of solid polymer electrolyte. It has a good self-standing property, formation of interface with electrode and mechanical property. However, it exhibits relatively low ionic conductivity and Li cation transpot number. On the other hand, ionic conductivity of LAGP is 7×10^{-4} S/cm, and it has high chemical stability in the atmosphere. All samples were prepared in a glove box under Ar atmosphere. $LiN(SO_2CF_3)_2$, LAGP, DMPA (photoinitiator) and acetonitrile (solvent) were dissolved into polyether macromonomer. Amount of hybridized LAGP were 0, 1, 3, 5 and 10 wt% with polymer electrolytes. After that, samples were dried in vacuum, then, cast on glass plate and radical polymerized by UV irradiation. Ionic conductivity and glass-transition temperature of this electrolyte were measured.

Results & Discussion

DSC thermograms and temperature dependences of ionic conductivity for prepared electrolytes are shown in Fig.1 and Fig.2, respectively. Glass transition temperature slightly decreased with on the amount of LAGP. This result shows possibility of changing mobility of polymer segment by dissolving LAGP. As a result of ionic conductivity measurements, ionic conductivity decreases when LAGP is hybridized into electrolyte. Ionic conductivity is thought to correlate parameter with glass transition temperature. Hybrid electrolyte were expected having only advanyages, even though ionic conductivity has not increased. Mechanically strong (non-broken) solid thin-film electrolytes were realized.

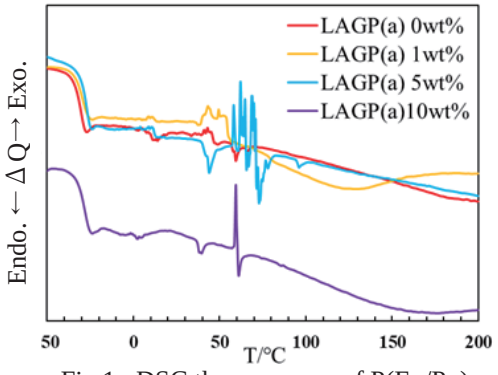

Fig.1 DSC thermograms of P(Eo/Po) and LAGP hybrid electrolytes

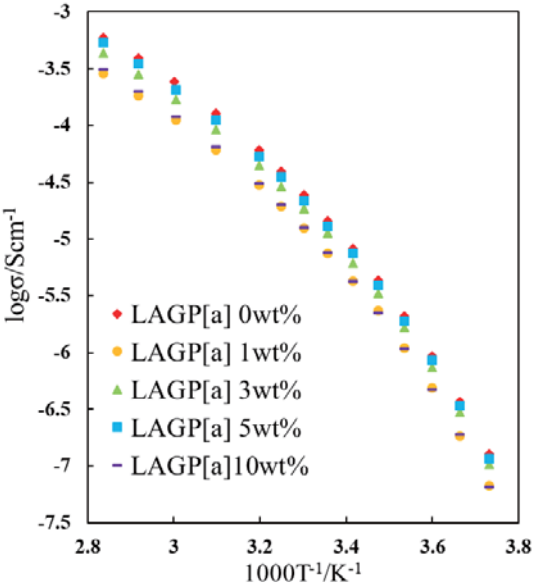

Fig.2 Ionic conductivity of P(Eo/Po) and LAGP hybrid electrolytes

Proposal of sulfolane electrolyte with high lithium salt composition for realization of new generation batteries

Kohei Inaba*, Keitaro Takahashi, Yuki Ishino, Yusuke Ushioda, Satoshi Katou, and Shiro Seki

*Department of Environmental Chemistry and chemical enginieering, Graduate School of Engineering, Kogakuin University, Tokyo, Japan
E-mail: s315007@ns.kogakuin.ac.jp

Abstract

Recently, New generation batteries with high energy density are required for environmental problem. Energy density can be increased by operating the high voltage. However, voltage is applied over 4.0V, the electrolye solution will be oxidize decomposed. Therefore, the development of electrolyte solution having wide electrochemical window is strongly desired for high voltage operated battery systems. Significant improvement for stability of electrolyte solution has been reported by high-salt concentration (ether series[1]/acetonitrile[2]) owing to strong interaction between Li salt and solvent molecule. In this stady, following two approches are proposed to prepare an electrolyte solution for high voltage operation.

1. Using sulfolane as a solvent
2. High salt concentration for stabilizing

In this study, we investigated thermal properties in electrolyte solutions of various compositions. Consideration of composition which becomes liquid.

Experiments

The samples were prepared by mixing $LiN(SO_2CF_3)_2$ (LiTFSA) to sulfolane (SL) in an argon-filled glove box . Solid samples at room temperture are heated by thermoplate. Thermal properties of prepared samples were investigated by thermogravimetry(TG) and differential scanning calorimetry (DSC).

Result & Discussion

Fig.1 shows the apparances of SL+LiTFSA electrolytes. High LiTFSA composition sample, such as higher than SL+LiTFSA=1:1, exhibited solid state. Moreover, these liquid electrolyte had high viscosity, even though it exists liquid state.

Fig.2, shows the TG curves of SL+LiTFSA electrolyte. Thermal stability was improved with high Li salt concentration. Moreover based on the thermal stability of SL solvent, volatile temperatures of SL were shifted with Li salt concentration.

Fig.3, showed the phase diagram of SL+LiTFSA mixtures. Although glass transition temperatures (Tg) were linearly changed with composition of SL, melting points (Tm) were also intricately changed. Govering factors for liquid / solid transition are considered as stability / instability parameters for liquid forming.

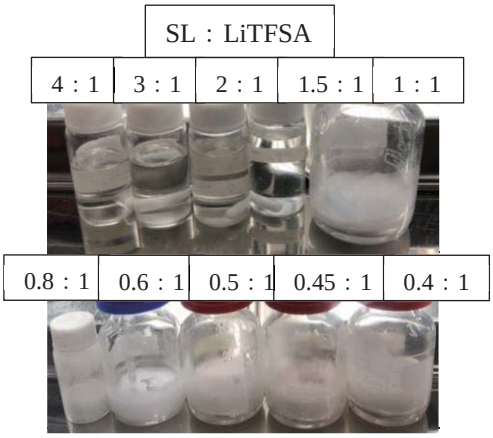

Fig. 1 State of sample at room temperature

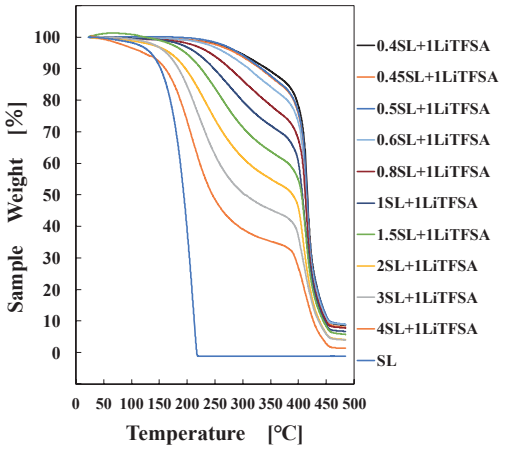

Fig. 2 Thermal gravimetric-differential thermal analyzer (TG-DTA) result.

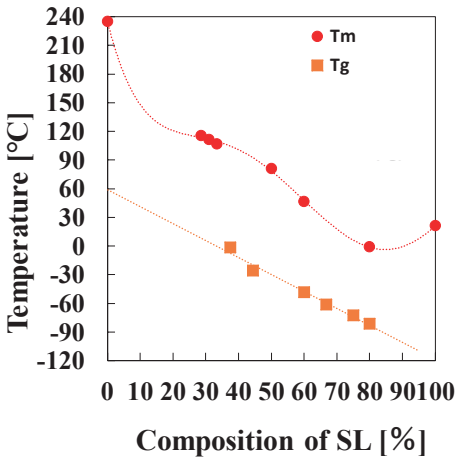

Fig. 3 Phase diagram created from differential scanning calorimeter (DSC) result.

References:

[1] K. Yoshida et al, J. Am, Chem. Soc. 2011, 133, 13121.
[2] Y. Yamada et al, J. Am. Chem. Soc. 2014, 136, 5039.

Study on wavelength matching for optical wireless power transmission for visible light

Hiroki Hirukawa[1)], Tomohiro Yamaguchi, Takeyoshi Onuma, and Tohru Honda

[1)]Department of Electrical Engineering and Electronics, Undergraduate School of Engineering, Kogakuin University, Tokyo, Japan

E-mail: s415035@ns.kogakuin.ac.jp

Abstract

Wireless power Transmission (WPT) system has been attracted much attention for realizing the life in the society where all electric appliances have no cables for supplying electricity. Optical Wireless Power Transmission (OWPT) is one of the methods in WPT, and it has several advantages such as long-distance transmission and no electromagnetic interference [1]. However, there are few repots on OWPT compared to other methods such as electromagnetic induction, magnetic field resonance and microwave. Therefore, it is important to grasp problems of the entire system.

OWPT has a simple setup, which consists of light source and light receiver, as same as solar light and solar cell in photovoltaic system. The candidates of light source are laser diode (LD) and light-emitting diode (LED). The candidate of light receiver that we can prepare at present is solar light. Since blue light has a short wavelength and high energy, high power transmission efficiency can be expected. However, there are no suitable light receivers.

Figure 1 shows the prototype system setup we fabricated in this study. As a light source, blue LD with a wavelength of 450 nm and an output power of 2.0 mW was used. As a light receiver, LEDs with different emitting wavelengths, that is, different absorption wavelengths, are used.

Figure 2 shows the short-circuit currents as a function of emitting wavelength of LEDs. As can be seen in Fig. 2, a few mA of the short-circuit currents were observed in whole LEDs. This indicates that OWPT is possible in the combinations of LD and LED for light source and light receiver, respectively. As can be also seen in Fig. 2, the highest short-circuit current was obtained when the LED with an emitting wavelength of 520 nm was used as light receiver. The relationship between spectral sensitivity of LED and short-circuit currents is discussed.

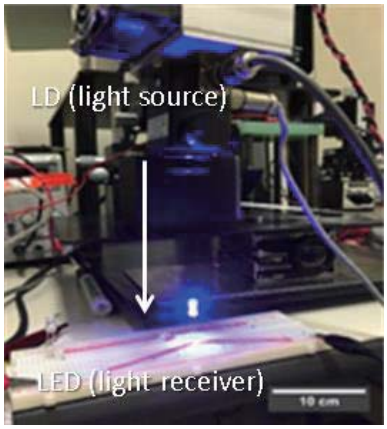

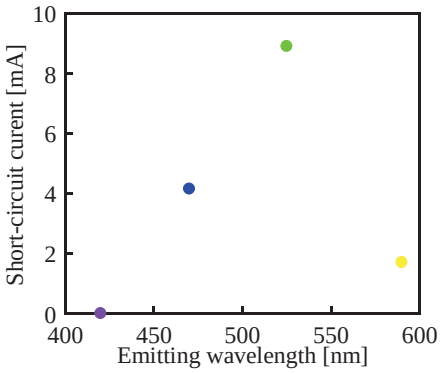

Fig. 1 *(left)* Prototype system setup we fabricated for OWPT.
Fig. 2 *(right)* Short-circuit currents as function of emitting wavelength of LEDs.

References:

[1] Y. Katsuta and T. Miyamoto, Jpn. J. Appl. Phys. 57, 08PD01 (2018).

Accelerating IPSec communication using Hardware & Software Co-Design technique on the Xilinx Zynq-7000 ARM/FPGA SoC platform

Assoc. Prof. Viet-Thang Huynh[1)], Hoang-Viet Ho[2)*], and Nguyen-Hoang-Phuc Ly [3)]

[1)]Faculty of Electronics and Telecommunication, Danang University of Science and Technology, The University of Danang, Danang, Vietnam
E-mail: thanghv@dut.udn.vn
[2)]Faculty of Advanced Science and Technology, Danang University of Science and Technology, The University of Danang, Danang, Vietnam
E-mail: hoangviet4796@gmail.com
[3)]Faculty of Advanced Science and Technology, Danang University of Science and Technology, The University of Danang, Danang, Vietnam
E-mail: lynhphuc@gmail.com

Abstract

In this paper we present a practical embedded system solution for Internet Protocol Security (IPSec) implemented on the Field Programmable Gate Array (FPGA) device in the Zynq7000 family. The proposed solution supports the three main IPSec protocols: Encapsulating Security Payload (ESP), Authentication Header (AH), and Internet Key Exchange (IKE). This system uses efficiently hardware-software co-design. Thanks to utilization of both methods we were able to enhance the performance of IPSec. In this work we propose a division of the basic mechanisms of IPSec protocols, namely cryptographic algorithms and their modes of operation to be implemented either in software or hardware (AES-CBC HMAC(SHA256)). Through this, we were able to combine the high performance offered by a hardware solution with the flexibility of a software implementation

The security services provided by the Internet Protocol Security (IPSec) include:

- Confidentiality - Prevents unauthorized access to the transmitted data.
- Data integrity - Ensures data was not altered during transmission.
- Authentication - Enables the identification of the information source.

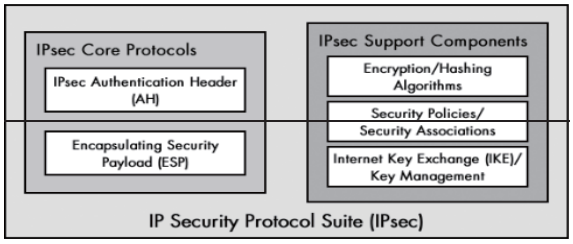

Fig. 1 Over view of IPsec protocols and components

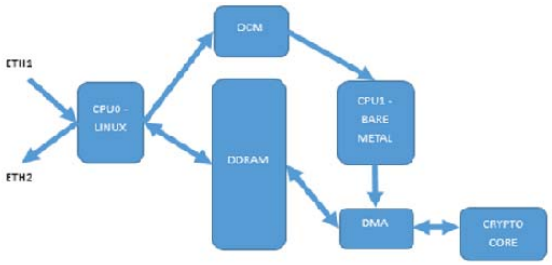

Fig. 2 Dataflow Diagram

The Internet Key Exchange must be used to establish secure connections. The Encapsulating Security Payload (ESP) protocol provides mechanisms for confidentiality and data integrity services. It uses AES cipher in Cipher-Block-Chaining (CBC) mode of operation. The Authentication Header (AH) protocol provides connectionless integrity and data origin authentication. AH uses Hashed Message Authentication Code (HMAC) with Secure Hash Algorithm (SHA). Due to the broad use of IPSec, it has been implemented in hardware and software with various designs and parameters to suit different platforms and provide better solutions. Among popular implementations of IPSec in hardware are those that target FPGA platforms because of the flexibility they offer the designer, ease of programming and high speeds that cannot be achieved through software.

Ipsec	speed
Software implementation	6.4 MB/s
Hardware implementation	8.4 MB/s
Hardware implementation With XAPP1078 architecture	9.4MB/s

Fig. 3 Result Table

References:

[1] Internet Protocol Security (IPSec): http://www.ciscopress.com/articles/article.asp?p=24833&seqNum=3
[2] Secure Hash Standard (SHS) FIPS 180-4: https://csrc.nist.gov/csrc/media/publications/fips/180/4/final/documents/fips180-4-draft-aug2014.pdf
[3] Advanced Encryption Standard (AES), FIPS 197: https://nvlpubs.nist.gov/nistpubs/fips/nist.fips.197.pdf

Implementing an Energy Efficient OpenFlow Switch on the Xilinx Virtex-6 FPGA ML605 Platform

Assoc. Prof. Van-Cuong Nguyen[1)*], Nguyen-Hoang-Phuc Ly [2)*], and Hoang-Viet Ho[3)]

[1)]Faculty of Electronics and Telecommunication, Danang University of Science and Technology, The University of Danang, Danang, Vietnam
E-mail: nvcuong@dut.udn.vn
[2)]Faculty of Advanced Science and Technology, Danang University of Science and Technology, The University of Danang, Danang, Vietnam
E-mail: lynhphuc@gmail.com
[2)]Faculty of Advanced Science and Technology, Danang University of Science and Technology, The University of Danang, Danang, Vietnam
E-mail: hoangviet4796@gmail.com

Abstract

Current network architecture is static and non-programmable. Recently, SDN is appealed to make network programmable. OpenFlow is a typical protocol for SDN, which has gained attention because of its flexibility and consistency in managing networks by making control function independent of the hardware it is intended to control. Many OpenFlow switch implementations have already been done on different platforms, but few works of energy efficient analysis are available. Thus, this project is meant to implement both data plane and control plane of an OpenFlow switch on FPGA and then develop a power saving extension for the switch.

We proposed an architecture of the data plane for the switch and successfully implemented it on the Xilinx Virtex-6 FPGA ML605 Platform. Each input queue connects to each port and buffers the received packets. When new packets stream into the OpenFlow switch, important header information is extracted and then composed into fixed format which is compared with the flow table entries in flow tables. Then the matching results associated with forwarding action are sent to the action processor in order to tell the action processor how to deal with the packet. The policy of the controller policy module is to add flow entry information including the flow entry, the flow mask and the action.

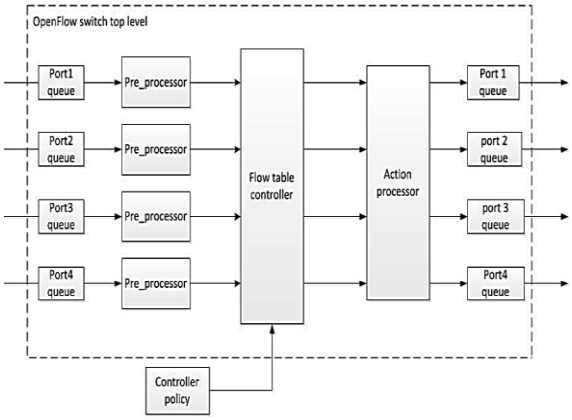

Fig. 1 OpenFlow switch top level hardware architecture

We also proposed an architecture, implemented the power saving extension for the switch and measured the dynamic power consumption. The controller unit will check the state of the ethernet PHY to change the operation state of the corresponding input ports between off and on.

Table 1 Measurement of power consumption

No.	Measurement	Power of switch (Dynamic power)
1	No port is off	180mW
2	Turn off 1 port	160mW
3	Turn off 2 ports	120mW
4	Turn off 3 ports	100mW
5	Turn off 4 ports	80mW

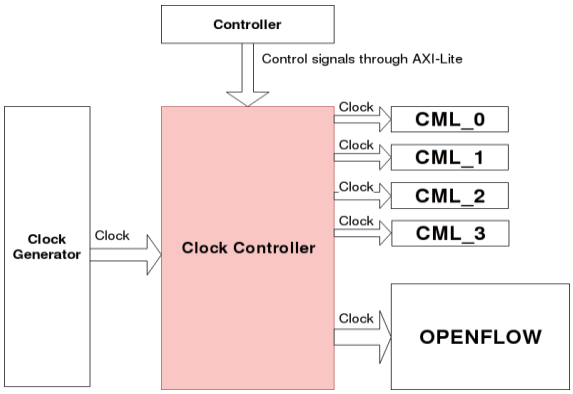

Fig. 2 Power saving extension architecture.

References:

[1] Tran Hoang Vu, Tran Thanh, Vu Quang Trong, Pham Ngoc Nam, Nguyen Huu Thanh, *NetFPGA Based OpenFlow Switch Extension for Energy Saving in Data Centers*, REV, 1−7 (2013).

[2] J. Naous, D. Erickson, G. A. Covington, G. Appenzeller, and N. McKeown, *Implementing an OpenFlow switch on the NetFPGA platform*, Proc. ANCS, 1-9 (2008).

DEVELOPING THE OVERTURNING WARNING SYSTEMS FOR MOTORCYCLES TRAVELLING IN STRONG WIND CONDITION

VU Anh Do[1)], TRUNG Van Ngo[2)], HUNG Duy Vo[3)*], THUONG Nhat Huynh Nguyen[4)]

[1)] B.Eng. Faculty of Road and Bridge Engineering,
University of Science and Technology – The University of Danang, Danang, Vietnam
E-mail: doanhvu.bkdn@gmail.com
[2)] Faculty of Electronic and Telecommunications Engineering,
University of Science and Technology – The University of Danang, Danang, Vietnam
E-mail: vantrung1001@gmail.com
[3)]PhD, Faculty of Road and Bridge Engineering,
University of Science and Technology – The University of Danang, Danang, Vietnam
vdhung@dut.udn.vn
[4)]B.Eng., Faculty of Electronic and Telecommunications Engineering,
University of Science and Technology – The University of Danang, Danang, Vietnam
nhnthuong@dut.udn.vn

Abstract

Motorcycle is a typical transportation mean in Vietnam. In present, motorcycles travel in strong wind conditions is always difficult and can lead to unacceptable accidents, that may have an adverse effect on people who ride the motorbike. In this case, so many accidents are in relation to motorcycle because of strong wind when the resident move on the bridges. In general, there are various researches about car overturning in development country (ex: Japan, America, France…) but the overturning of motorbikes is quite new and not so much researches mentioned about this. In this study, the authors give an overview of the effects of motorcycles when subjected to win. Furthermore, authors try to build the risk curves, analyze the data and provide a regulation system for motorcycle in strong wind conditions. The warning work is based on wind speed and wind direction. Specifically, this paper also used the basic system for measuring the wind speed and wind direction. Then, based on the relationship of the wind speed and wind direction with motorbikes velocity, the system will send the warning messages for motor-riders. Especially, the renewable power also uses to operate the warning system which can make it become more efficiency and sustainable.

Keywords: *Motorcycle, overturning, warning system, wind speed, vehicle velocity, wind direction…*

References:

[1] Simiu E., Scanlan R.H: *Wind Effects on structures – Fundamentals and Application to Design*. New York, John Wiley & Sons, 3rd ed., 1996
[2] ASCE: *Minimum Design Loads for Buildings and Other Structures* – ASCE/SEI 7 – 10, 2010.
[3] Nakaguchi H., Hashimoto K. & Muto S.: *An experimental study on aerodynamic drag of rectangular cylinders*. Journal of Japan Aeronauics Space Science, Vol. 16(168), 1968.
[4] Davenport A.G: *The Dependence of Wind Load upon Meteorological Parameters*. Proceedings of the International Reasearch Seminar on Wind Effects on Buildings and Structures, 1968.

Research in transmission of sound in human body – bone conduction devices

Vo Hoang Chuong, Pham Le Minh Hoang, Le Quang Dao and Ho Ba Trung

Faculty of Advanced Science and Technology, Electronics and Telecommunication Engineering, the University of Danang – University of Science and Technology, Danang, Vietnam
E-mail: vhchuong1997@gmail.com
Faculty of Advanced Science and Technology, Electronics and Telecommunication Engineering, the University of Danang – University of Science and Technology, Danang, Vietnam
E-mail: mhdstudiodng@gmail.com
Faculty of Advanced Science and Technology, Electronics and Telecommunication Engineering, the University of Danang – University of Science and Technology, Danang, Vietnam
E-mail: quangdao215@gmail.com
Faculty of Advanced Science and Technology, Electronics and Telecommunication Engineering, the University of Danang – University of Science and Technology, Danang, Vietnam
E-mail: onimenokyo145@gmail.com

Abstract

The skull conducts lower frequencies better than air so people perceive their own voices to be lower and fuller than others do, and a recording of one's own voice frequently sounds higher than one expects it to sound. [1][2] Bone conduction allows users to hear sound through the vibration of the bones of their faces (jaw bones and cheek bones). This means that the sound waves are bypassing the outer and middle ear (where the eardrum is located) and directly stimulating the inner ear (hearing organ).

The bone conduction headphones would deliver sound signal to the audiences' cochlear, bypassing the eardrums. This mechanism is extremely important to the people who are already wearing hearing aids but want to enjoy music privately or the ones that need to continuously hear sound from the surrounding space. M

Normal sound waves are actually tiny vibrations in the air. The vibrations travel through the air to our eardrums. The eardrums in turn vibrate, decoding these sound waves into a different type of vibrations that are received by the Cochlea, also known as the inner ear. The Cochlea is connected to our auditory nerve, which transmits the sounds to our brain.

The basic idea is illstrated in figure 1. Bone Conduction bypasses the eardrums. In bone conduction listening, the bone conduction devices (such as headphones) perform the role of your eardrums. These devices decode sound waves and convert them into vibrations that can be received directly by the Cochlea so the eardrum is never involved. The "sound" reach the ears as vibrations through the bones (or skull) and skin.[3]

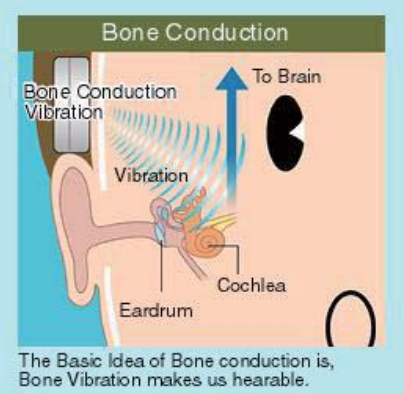

Fig. 1. Basic idea of bone conduction

References:

[1] Zhi Cai; Alan G. Madsen; Douglas G. Richards; Martin L. Lenhardt, Virginia Commonwealth University, *Response of Human Skull to Bone Conducted Sound in the Audiometric to Ultrasonic Range.* (2002)

[2] Brent Zupp. *"Why Does Your Voice Sound Different on a Recording?", Wanderings.* (2003-2012)

[3] Goldendance, *Bone Conduction: How it Works*. (2008).

Robotic Hand Controlled by Glove

Hoang-Khoi Dang[1)], Minh-Vu Nguyen[1)], Tuan-Anh Le[1)], Duc-Huy Dang[1)], Duc-Thinh Nguyen [1)], Van-Lic Tran[2)]

[1)] Faculty of Advanced Science and Technology, The University of Da Nang - University of Science and Technology (UD-DUT)
E-mail: khoihoangdang97@gmail.com
[2)] Faculty of Advanced Science and Technology, The University of Da Nang - University of Science and Technology (UD-DUT)
E-mail: vanlic.dn@gmail.com

Abstract

Working in the dangerous conditions, such as radioactive contamination of the environment, conflagration, etc. may affect to the human health. Finding effective solutions in that situations is extremely important. In this work we aim at designing and building a Remote-Controlled Robotic Hand which can be controlled by a remoted glove to help people is such cases.

The system consists of two basic blocks in ***Fig.1***: control block and implementation block. Two blocks use the radio wave at 2.4GHz, using the NRF24L01 modules, to communicate. The control block includes an Arduino board (Arduino R3, Arduino nano), five flex sensors and NRF24L01 transfer. The implementation block includes: Arduino board, servo motors, robotic hand and NRF24L01 receiver.

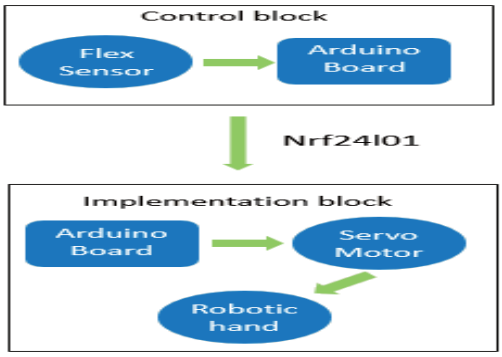

Fig.1 Block diagram.

The sensor bends in one direction, the more it bends, the higher the resistance gets [1].
Five flex sensors stick on the glove, sensors change in resistance on the amount of bend on they, therefore, by the voltage divider [2] in ***Fig. 2***, the flex sensor can change the output voltage in range from 0 to Vcc (5V).

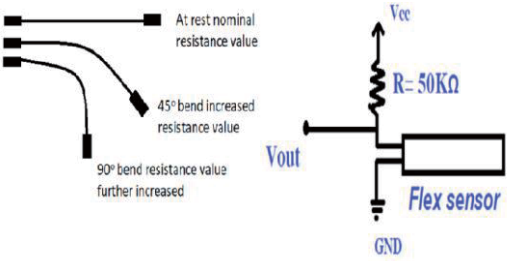

Fig.2 *Voltage divider circuit.*

In the future, we address the problems of flex sensors, moreover, we develop the control block by using other ways such as: voice or brainwaves that can help the disabled people.

Fig.3 *Robotic Hand and Glove.*

References:

[1] http://tinkerfest.in/bending-detection-flex-sensor/
[2] https://learn.sparkfun.com/tutorials/voltage-divider

Design and Build a Self-study Space Management System for Smart Campus using Image Processing and LoRA Wireless Communication

Loc-Minh-Phuc Le [1)], Van-Khoi Bui[1)], Tan-Hien Van[1)], Nguyen-Phu-Hien Pham[2)], Thai-Hoang Nguyen[2), *], Dinh-Thanh Ngo[2)]

[1)] Faculty of Advanced Science and Technology, The University of Danang - University of Science and Technology

[2)] Department of Electrical Engineering, The University of Danang - University of Science and Technology

Email: hoangchuyenli@gmail.com

Abstract

The University of Danang - Danang University of Science and Technology (UD-DUT) is one of the leading universites in technical training in Central of Vietnam. There are 8 lecture halls with 200 classrooms and the total area is 240,900 m^2. However, it is difficult for students when they would like to find the shortest to their classrooms, cafeteria or self-study places.

In order to solve this challenges, we have designed a self-study management system allowing students to find a self-study location with available space through an application on smartphone. Students can use the GPS function on their smartphone to locate their position, then choose the place they want to come, the app will show the shortest path and guide the way. This application can remind students schedule and time to return borrowed books to the library. The most important point is the application can run on both Android and iOS so that everyone can use our system.

Figure 1 describes a summarized block diagram of the system. Each self-study place is monitored in realtime by a node consisting of an embedded computer Raspberry Pi 3 connected to a camera. The frame then will be processed using an background subtraction algorithm [1-3] which is embbeded in the node's computer. Information from each node is then fowared to a gateway using LoRA wireless communication. The gateway then sends data to the cloud server by MQTT protocol. A smartphone application is developed to connect to the server and get data, then illustrate it in the app [4]. There is a menu with options to monitor self-study places, use a service map or book return reminder. The application is optimized to run in as many smartphones as possible with small lag as possible.

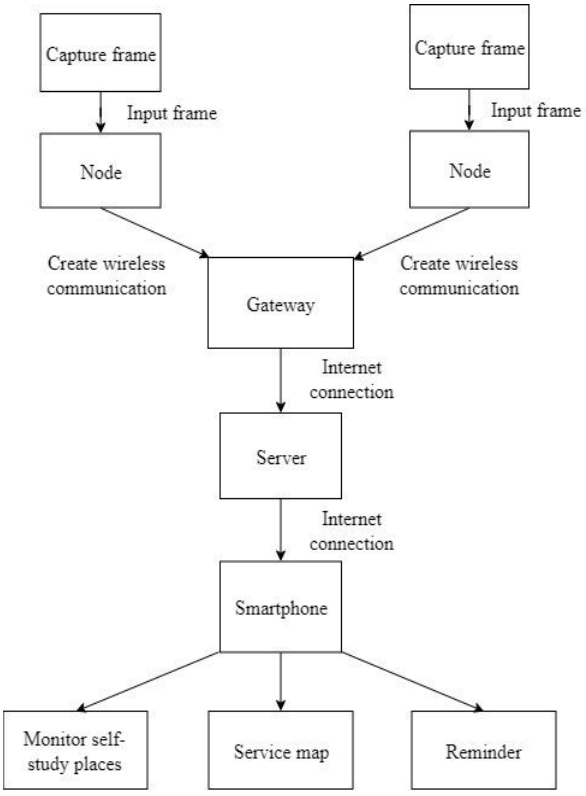

Figure 1: System block diagram

Experimental results show that when the internet is not stable, there will have a considerable delay in the application and users will have false information. Further work should solve this problem and to ensure the stability of the whole system. Feedback from users would help us to improve the user interface of the application. Deep learning algorithm will be applied to increase the accuracy of human detection at faster speed.

References:

[1] T. Bouwmans. "Recent Approaches in Background Modeling for Static Cameras", Chapter 2 in Handbook on "Background Modeling and Foreground Detection for Video Surveillance", CRC Press, Taylor and Francis Group.

[2] M. Piccardi, "Background subtraction techniques: a review", in IEEE International Conference on Systems, Man and Cybernetics, October 2004, p. 3099–3104

[3] Pulli, Kari, Baksheev, Anatoly, Kornyakov, Kirill, Eruhimov, Victor, "Realtime Computer Vision with OpenCV" in Queue, 1 April 2012, pp. 40:40–40:56.

[4] Google developers. Introduction to Android Studio, Google Developers, 23 Feb. 2015

Self-driving car – Traffic signs recognition

Thi-Thanh-Hoa Tran [1)*], Duy-Hung Phan [1)], Gia-Khang Tran [1)], Quang-Huy Tran [1)]

[1)] Faculty of Advanced Science and Technology (FAST), The University of Danang - Danang University of Science and Technology

Email: [*)] *tthithanhhoa@gmail.com*

Abstract

Self-driving car is a popular trend in the world. This research proposes a PID (proportional–integral–derivative) algorithm and implemented controller to drive a car and Convolutional Neural Network (CNN) to detect traffic signs.

The PID control uses closed-loop control to drive the car along the lane. It minimizes difference between the set value (car's position) and actual value by modifying parameters (speed, steer angle).

In machine learning, a network (CNN, or ConvNet) is a class of deep, feed-forward artificial neural networks, most commonly applied to analyzing visual imagery. In our work the proposed CNN comprise of:

+ Convolution layer
+ Pooling layer
+ Fully-connected Layer

We applied CNN to recognize traffic signs through these steps:

+ Pre-processing and feature extracting dataset
+ Training
+ Detecting and classifying

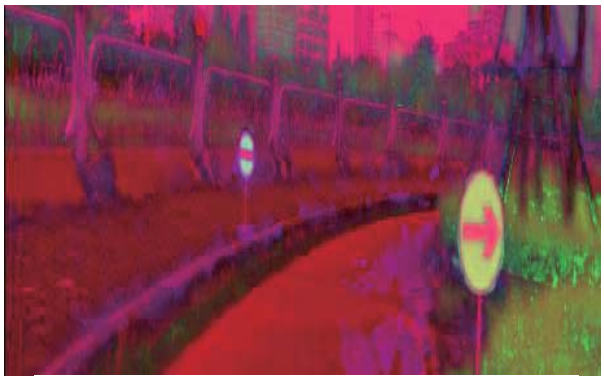

Fig 1 : Image in HSV

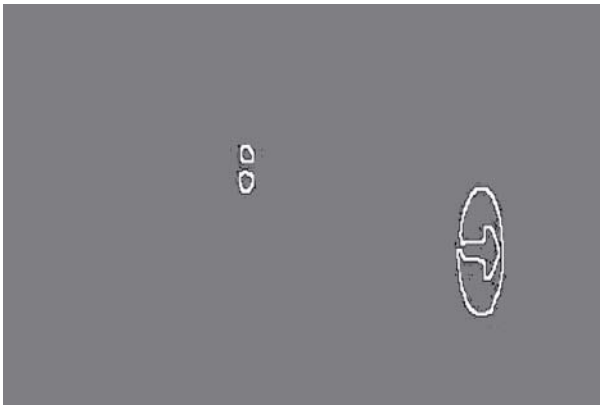

Fig 2 : Segmenting and binarizing

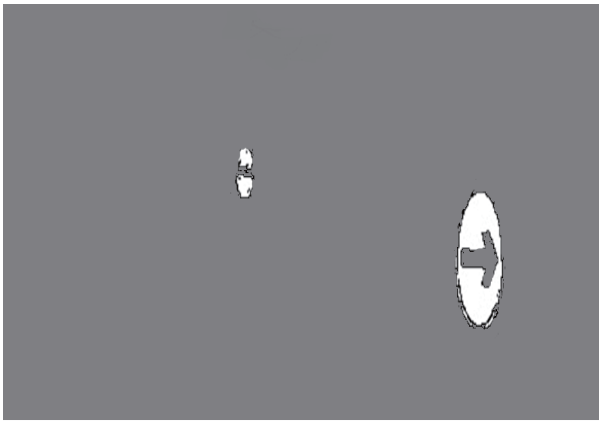

Fig 3 : Find contours, shape and traffic region

References:

[1] Bennett, Stuart (1993). *A history of control engineering, 1930-1955*. IET. p.48

[2] https://en.wikipedia.org/wiki/Deep_learning

[3] https://www.tensorlfow.org

3D Printing Technology- A Model of Lattice Structure in CAD Environment

T.H. Tuan Tran[1)], D. Kien Le[1)], V. Than Le[1)], D. Son Nguyen[2)]

[1)] Faculty of Advanced Science and Technology, The University of Danang - University of Science and Technology, Danang, Viet Nam
E-mail: haituandn2010@gmail.com, ldkien96@gmail.com, than1996969@gmail.com
[2)]Faculty of Transportation Mechanical Engineering, The University of Danang - University of Science and Technology, Danang, Viet Nam
E-mail: ndson@dut.udn.vn

Abstract

Lattice structures include a network of truss including struts or plates interconnected to each other [1]. Lattice structures created by additive manufacturing have many advantages thanks to their ability to reduce the product weight but at the same time to ensure high specific strength and stiffness of materials. There are different studies on how to generate lattice structures for additive manufacturing but they do not have the ability to generate automatically lattice structure in CAD environment. This research will present a method to create automatically a model of lattice structure in CAD environment.

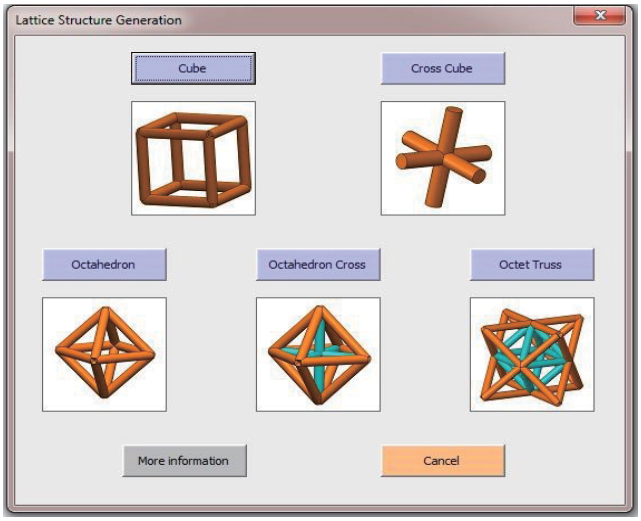

Fig. 1 The interface of the library of unit cells.

Table 1 Percentage of material reduction of the lattice structure.

Type of unit cell	Reduction of materials
Cube	87.9 %
Cross-Cube	91.7 %
Octahedron	79.3 %
Octahedron-Cross	74.4 %
Octet-truss	57.4 %

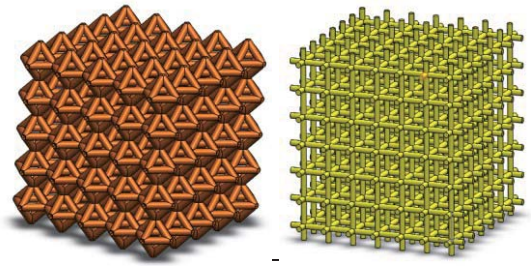

Fig. 2 Some models of lattice structures created by the interface in SolidWorks® software.

The result of the research is an interface in SolidWorks® software shown in Fig. 1. By using this interface, we can create automatically models of lattice structure and then send them to the 3D-printer to make reality parts (Fig. 2). It helps us to reduce a significant amount of material shown in Table 1 as well as time-consuming in design and fabricate the products.

By applying Visual Basic programming language based on the API functions in SolidWorks® software, an interface to generate a model of lattice structure has been developed. The interface helps us generating automatically a model of lattice structure in CAD environment. Besides, the interface allows us to select different types of unit cell, to change the parameters of unit cell and the volume size of lattice structures flexibly. In the future, it is very essential to focus on generating new types of lattice structure and testing the strength of lattice structure intergrated in products.

References:

[1] L. J. Gibson, and M. F. Ashby, *Cellular Solids Structure and Properties*: Cambridge Solid State Science Series, 1999.S. A. M. Tofail, E. P. Koumoulos, A. Bandyopadhyay, S. Bose, L. O'Donoghue, and C. Charitidis, *"Additive manufacturing: scientific and technological challenges, market uptake and opportunities"*, Materials Today, 2017/07/29/ 2017.

Development of Automatic Washing and Selecting Fruit System Applying Image Processing Technology

Vo Nhu Thanh, Pham Duy Thong

Faculty of Mechanical Engineer, University of Science and Technology, The University of Da Nang
Email: vnthanh@dut.udn.vn

Abstract

The automatic system for agricultural production as well as the system of washing and sorting fruit in particular is the indispensable trend of modern agricultural production. New technologies are and will be used extensively to replace human labor, improve labor productivity and reduce product costs.

Many systems are developed and applied in developed countries. In Vietnam, the system is applied only to companies and factories processing agricultural products with machines and technologies imported from developed countries. Small-scale producers still have to use human labor for washing and sorting, so the productivity is not high and the price of the product increases.

With the attention to help the small-size factory, we develop an automatic washing and selecting fruit system. Throughout the design process, the system consists of three main components: the fruit conveyor, the fruit wash and the photo-processing unit. At the same time, the system must meet the technical criteria such as flexible control, easy operation and maintenance, ensuring safety, longevity for the system and economic-art such as reasonable price, productivity, well functional, and friendly interface. The overview of the system is shown in figure 1.

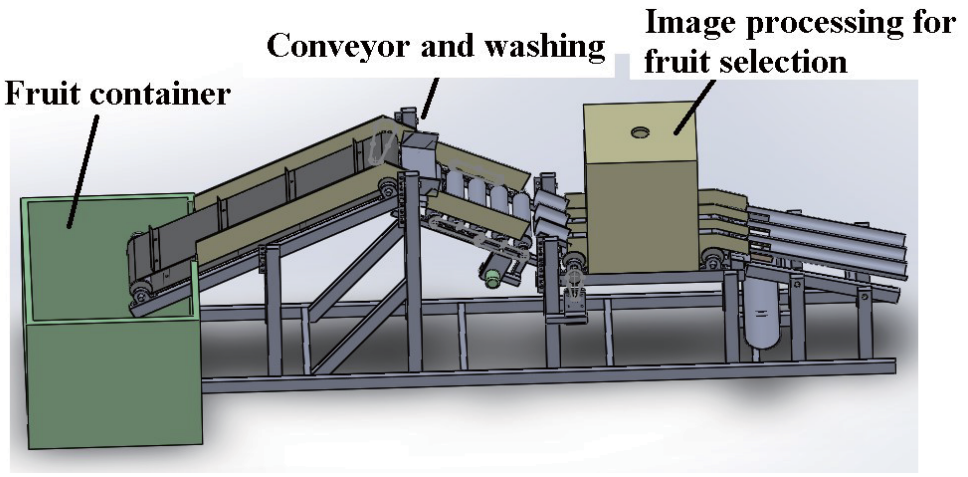

Fig.1 System overview

An automatic washing and selecting fruit system using image processing technology has been developed and tested. The test results are as follow:

- Ability to clean fruit well.
- Stable fruit classification and high accuracy.
- Mechanical design meets the actual requirements such as fruit weight, engine speed, image processing speed, etc.
- Intuitive interface, ensuring the full functionality of a basic system.
- The system is firmly built, ensuring long-term working requirements.

References:

[1] Robert H. Bishop, *The Mechatronics Handbook*, CRC Press; 2 edition (2007).
[2] Ha Van Vui , Nguyen Chi Sang. *Sổ tay thiết kế cơ khí (Mechanical Design Handbooks)*, Scientific Publishing House (2006)
[3] Naoshi Kondo, "Automation on fruit and vegetable grading system and food traceability", *Trends in Food Science & Technology*, Volume 21, Issue 3, Pages 145-152, March 2010

Development of Restaurant Serving Robot Using Line Following Approach

Vo Nhu Thanh, Vuong Dinh Nhan

Faculty of Mechanical Engineer, University of Science and Technology, The University of Da Nang
Email: vnthanh@dut.udn.vn

Abstract

In today's industrialized world 4.0, robots replace most of the human work in industry; however, the life supporting robot for human still very limited. Restaurant serving robot has been developed and used in many countries like Japan, China and America. The serving robots attract the attention of customers and they want to experience being served by these robots. In fact, many restaurants want to have this type of robot for serving their customer and also for advertising purpose. This is a robot that can be used to serve in different restaurants.

This paper focuses on a Line Following approach to develop the movement for the robot. The working principle of this robot is based on the mapping of tables with color lines on the floor. Based on the line reading algorithm the robot follows the line to move to the desired table position and returns to the service counter after completing the task. The robot is also equipped with ultrasonic sensor that helps it detects obstacle (e.g. customers, other robot …) and stops moving before collision. The robot is also programmed to speak to customers in English, Korean and Vietnamese some common phrase such as "Welcome to restaurant", "Please enjoy your food", "Please take your food"

Through surveys and inquiries at restaurants in the city, the team has launched a human-shaped robot model with two separate trays. The main parts of the robot consist of robot wheels (1,2), motors (3,4) Robots guide rotors (5,6), bearing (7), joints (8), robot base (9), food trays (11,12), control panel (13), Lcd display (14), and Ipad holder – for taking order (15) . The design of the restaurant robot shown in figure 1

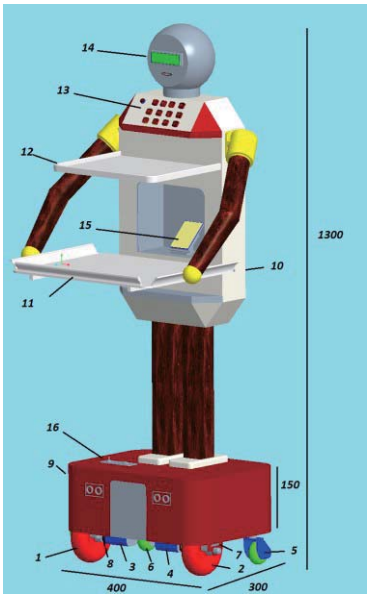

Fig.1 Design of the restaurant serving robot

The controller of the system consists of Pic18F4550 microcontroller for controlling the whole process, line sensor for detecting and following line, 30W DC motor, 12V-12Ah power source for the robot continuously work in 12 hours, speakers for speaking to customer, and recharge system for fully restore the robot battery within 5 hours . The machine is on testing phase and give very promising results.

References:

[1] Robert H. Bishop, *The Mechatronics Handbook*, CRC Press; 2 edition (2007).
[2] Pakdaman, M., (28-30 December 2009), Design and Implementation of Line Follower Robot, Tabari Inst. of Babol, Iran, page(s): 585, Conference Location: Dubai, E-ISBN: 978-0-7695-3925-6, Print ISBN: 978-1-4244-5365-8.

Development of Vietnamese Banana Leaf Cake Maker Machine

Vo Nhu Thanh, Vo Minh Nhat

Faculty of Mechanical Engineer, University of Science and Technology, The University of Da Nang
Email: vnthanh@dut.udn.vn

Abstract

Automatic machine for food industry and home appliance is one of the needs and trends that are applying around the world. There are many machines that are designed, manufactured and put into practice. However, some fields are not fully exploited. The banana leaf cake is one of the specialty food of Central Vietnam and is enjoyed by many Vietnamese and foreign tourists. However, Vietnamese banana leaf handmade cakes with disadvantages like all the steps are handmade include making powder, fillings and package that can take a lot of time, effort and employees. Recognizing the disadvantages, our team decide to design and manufacture the "Vietnamese banana leaf cake maker machine" with the desire to improve efficiency and reduce the cost of employees. This machine is developed from the order of a local restaurant that can completely put all the ingredient in a banana leaf and fold it to make the final product. With this machine, the restaurant can save labors and cost of making the banana leaf cake. This is important for development of local products that serve for tourism purpose.

The main parts of the system consist of conveyor, powder and core feeder, folding mechanism and controller. Banana leaves are placed on the conveyor belt to the level of powder and the kernel is then folded using a folding mechanism. The design of this system is shown in figure 1.

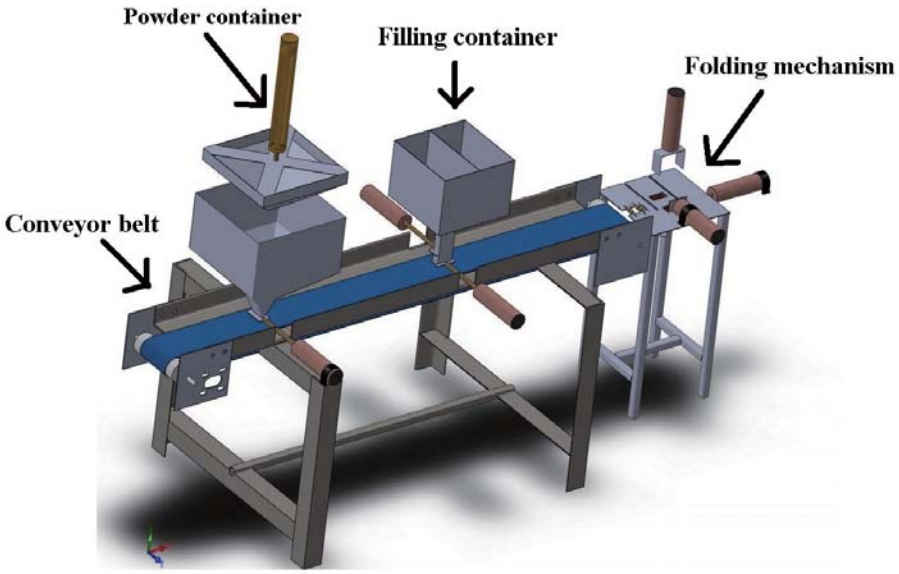

Fig.1 Design of the Vietnamese banana leaf cake maker machine

The controller of the system consists of Arduino Mega microcontroller for controlling the whole process, optic sensor for detecting banana leaf, and relays in combination with valves for controlling the pneumatic pistons. The machine is on testing phase and give very promising results.

References:

[1] Robert H. Bishop, *The Mechatronics Handbook*, CRC Press; 2 edition (2007).
[2] Ha Van Vui , Nguyen Chi Sang. Sổ tay thiết kế cơ khí (Mechanical Design Handbooks), Scientific Publishing House (2006)